

**Design and Analysis of Series Elasticity in Closed-loop
Actuator Force Control**

by

David William Robinson

B.S., Mechanical Engineering
Brigham Young University
April 1994

S.M., Mechanical Engineering
Massachusetts Institute of Technology
June 1996

Submitted to the Department of Mechanical Engineering
in partial fulfillment of the requirements for the degree of

Doctor of Philosophy in Mechanical Engineering

at the

MASSACHUSETTS INSTITUTE OF TECHNOLOGY

June 2000

© Massachusetts Institute of Technology 2000. All rights reserved.

Author
Department of Mechanical Engineering
May 11, 2000

Certified by.....
Gill A. Pratt
Associate Professor of Electrical Engineering and Computer Science
Thesis Supervisor

Certified by.....
David Trumper
Associate Professor of Mechanical Engineering
Thesis Committee Chair

Accepted by.....
Ain A. Sonin
Chairman, Department Committee on Graduate Students

Design and Analysis of Series Elasticity in Closed-loop Actuator Force Control

by
David William Robinson

Submitted to the Department of Mechanical Engineering
on May 11, 2000, in partial fulfillment of the
requirements for the degree of
Doctor of Philosophy in Mechanical Engineering

Abstract

Series elastic actuators have a spring intentionally placed at the actuator output. Measuring the spring strain gives an accurate measurement for closed-loop actuator force control. The low spring stiffness allows for high control gain while maintaining actuator stability. This gives series elastic actuators many desirable properties including high bandwidth at moderate force amplitudes, low output impedance, large dynamic range, internal error rejection and tolerance to shock loading. However, as a consequence of the elasticity, the large force bandwidth capabilities of the actuator are reduced when operating at power saturation limits.

Series elasticity is examined with three models. First, it is generalized by using a minimal actuator model. This mathematical model consists of an ideal velocity source actuator, linear spring and proportional controller. Series elasticity is then demonstrated in two case studies of physical actuator systems. The first is a linear hydraulic piston with a servo valve and the second is an electric motor with a geared linear transmission. Both case studies have a linear spring and low complexity control systems. The case studies are analyzed mathematically and verified with physical hardware.

A series elastic actuator under simple closed-loop control is physically equivalent to a second order system. This means that an equivalent mass defined by the control system and physical parameters, is effectively in series with the physical spring connected to the actuator load. Non-dimensional analysis of the dynamics clarifies important parametric relationships into a few key dimensionless groups and aids understanding when trying to scale the actuators. The physical equivalent abstractions and non-dimensional dynamic equations help in the development of guidelines for choosing a proper spring stiffness given required force, speed and power requirements for the actuator.

Thesis Supervisor: Gill A. Pratt

Title: Associate Professor of Electrical Engineering and Computer Science

For Sarah

Acknowledgments

MIT has given me an incredible education the last four years. It has stretched me academically and personally. I am very grateful to the people that have been with me to share this whole experience.

I want to thank my advisor Professor Gill Pratt for his advice, guidance, help, time, and enthusiasm. I appreciate all that I have learned from him as an advisor, teacher, mentor and especially as a friend.

I also want to thank the other members of my doctoral thesis committee: Professor David Trumper, Professor Haruhiko Asada, and Dr. J. Kenneth Salisbury. They have all made significant contributions to this thesis. Their direction and encouragement as a group and as individuals has been tremendous.

The Leglab is a great place to work because of the people. Dan Paluska, Ben Krupp, Jerry Pratt, Chris Morse, Andreas Hofmann, Greg Huang, Robert Ringrose, Mike Wessler, Allen Parseghian, Hugh Herr, Bruce Deffenbaugh, Olaf Bleck, Ari Wilkenfeld, Terri Iuzzolino, Joanna Bryson, Jianjuen Hu, Chee-Meng Chew, and Peter Dilworth have been great friends and colleagues. They have filled this experience with wonderful camaraderie in both work and fun.

I especially appreciate my good friends Brandon Rohrer, Sean Warnick, and Rick Nelson with whom I have shared the MIT engineering Ph.D. road. The time I spent working and in counsel with these men has been choice. They have each been marvelous examples to me in the ways that they balance family, service, work, school, and fun.

I thank my parents, brothers, sisters, and their families for their constant support, encouragement, and words of confidence. Mom and Dad are the ones who made it possible to start this journey and the whole family have always been there to see me through.

I particularly appreciate the support of my two daughters. Hannah's smiles, hugs and clever wit have kept me going. MaryAnn's recent arrival gave me the desire and motivation finish up quickly. They have both helped me to keep life in its proper perspective.

Finally, I give deep appreciation to my eternal companion Sarah. Our experience together has been full to overflowing. I am thankful for her faith, consistency, gentleness, kindness, and love. When you are with Sarah, how can your experience be anything but great! 143, always.

This research was supported in part by the Defense Advanced Research Projects Agency under contract number N39998-00-C-0656 and the National Science Foundation under contract numbers IBN-9873478 and IIS-9733740.

Contents

1	Introduction	17
1.1	Thesis	17
1.2	Motivation	18
1.2.1	Actuation and Force Control	18
1.2.2	Series Elastic Actuators	19
1.3	Highlights of thesis results	20
1.3.1	Actuators	20
1.3.2	Bandwidth	21
1.3.3	Output Impedance	23
1.3.4	Load Motion	25
1.4	Thesis Contributions	26
1.5	Thesis Contents	26
1.6	Note on thesis data	27
2	Background and Related Work	29
2.1	Force Control	29
2.1.1	Passive Compliance	30
2.1.2	Active Control	31
2.2	Applications of Force Control	32
2.3	Robot Actuators and Active Force Control	33
2.3.1	Electro-Magnetic	34
2.3.2	Hydraulic	35
2.3.3	Pneumatic	36
2.3.4	Others	36
2.4	Intentionally Compliant Robot Actuators	37
2.4.1	Series Elastic Actuators	37
2.4.2	Other Electro-mechanical Compliance	38
2.4.3	Hydraulic Compliance	41
2.5	Summary	42
3	Linear Series Elastic Actuators	43
3.1	General Model	43
3.1.1	Elasticity	44
3.1.2	Control System	44
3.1.3	Motor	45
3.1.4	System Inputs	46
3.2	Minimal Linear Model Derivation	47
3.2.1	General Power Domain Open-Loop Model	47
3.2.2	General Closed-Loop Model	48
3.3	Minimal Model Analysis	48
3.3.1	Case 1: Fixed Load – Closed-loop Bandwidth	49
3.3.2	Case 1: Fixed Load – Large force bandwidth	52

3.3.3	Case 2: Forced Load Motion – Output Impedance	54
3.3.4	Impact Tolerance	57
3.4	Mass Load	58
3.4.1	Forces on the load	58
3.5	Dimensional Analysis	61
3.6	General Model Summary	63
4	Hydro-Elastic Case Study	65
4.1	Model Derivation	65
4.1.1	Model Definition	65
4.1.2	Power Domain Model	68
4.1.3	Closed-loop Model	68
4.1.4	Two input cases	69
4.2	Model Analysis	69
4.2.1	Saturation and Large Force Bandwidth	70
4.2.2	Case 1: Closed-loop Bandwidth	72
4.2.3	Impedance: Case 2	74
4.2.4	Proportional Control	75
4.3	Effect of Load Mass	76
4.3.1	Load Forces	76
4.3.2	Load Motion	78
4.4	Physical Actuator	78
4.4.1	Component Selection	78
4.4.2	Choosing the Spring Constant	79
4.4.3	Physical Actuator Characteristics	80
4.5	Hydro-Elastic Summary	89
5	Electro-Magnetic Series Elastic Case Study	91
5.1	Model Derivation	91
5.1.1	Model Definition	91
5.1.2	Power Domain Model	93
5.1.3	Closed-loop Model	94
5.1.4	Two input cases	94
5.2	Model Analysis	95
5.2.1	Saturation	96
5.2.2	Bandwidth	100
5.2.3	Impedance	101
5.2.4	Force Error Rejection	103
5.3	Effect of Load Mass	104
5.3.1	Load Forces	105
5.3.2	Load Motion	107
5.4	Physical Actuator Prototype	107
5.4.1	Component Selection	107
5.4.2	Choosing Sensor Spring Constant	108
5.4.3	Actuator Characteristics	108
5.5	Case Study Summary	112
6	Conclusions	115
6.1	Further Work	116
6.1.1	Actuator Scaling	116
6.1.2	Springs	116
6.1.3	EM velocity mode control	117
6.1.4	Control system design	117
6.2	Summary	117

List of Figures

1-1	Series elastic actuator. The closed-loop actuator is topologically identical to any motion actuator with a load sensor and closed-loop feedback controller. The major difference is that the sensor is very compliant. Low spring stiffness removes gain from the power domain and thereby allows for increased controller gain in the signal domain while still maintaining desired stability margins.	20
1-2	CAD models of the hydro-elastic actuator (left) and EM series elastic actuator (right) developed and analyzed in this thesis. Both actuators have a force output range on the order of 400–600 lbs. The power output for the hydro-elastic actuator is 1.5 kW and 430 W for the EM actuator. The minimum resolvable force of both actuators is approximately 1 lb due to the noise floor in the sensor. This gives the actuators a dynamic range of the order 500:1.	21
1-3	REAL Experimental bandwidth of the two prototype actuators. The hydro-elastic actuator is on the left and the EM actuator is on the right. The magnitude of oscillation for the actuators is 40 lbs. The bandwidth of both actuators is in the range of 30-35 Hz.	22
1-4	REAL Experimental large force bandwidth. The actuators ability to sinusoidally oscillate at the maximum force, F_{sat} , at steady state is limited in frequency due to the spring compliance and motor saturation in force and velocity. The frequency at which that maximum force capabilities of the actuator begin to fall off is defined as ω_o . $\omega_o = 25$ and 8 Hz for the hydraulic and EM prototype actuators respectively.	23
1-5	SIM The EM actuator’s output impedance as a function of load motion input frequency under PD control. The plot comes from the dynamic equation derived in Chapter 5. The figure has been normalized in frequency by ω_o and in magnitude by the stiffness k_s of the physical spring. At low frequency the impedance is small. The impedance increases with increased frequency in the limit is equal to k_s , the physical spring stiffness.	24
1-6	Physical equivalent of output impedance. As x_l drives at different frequencies, the impedance of the actuator changes. At low frequency, the impedance looks like an equivalent mass, m_{eq} . At high frequencies, the impedance looks like the physical elasticity of the spring in the actuator. Even though damping is not shown it is assumed present to limit uncontrolled oscillations at the natural frequency.	24
1-7	Series elastic actuator connected to an inertial load. Ideally the actuator is a perfect force source (left). However, when moving and inertial load, the actuator has its physical equivalent impedance. Typically, m_{eq} is very small in comparison to the load mass, m_l . Nevertheless, understanding the relative magnitude of m_{eq} is important.	25
1-8	REAL Hydro-elastic actuator forces on an inertial load. The inertial load mass and the actuator equivalent mass are 18 kg and 20 kg respectively. Since the two are so close, at low frequency the actuator displays a significant non unity magnitude under PI control. The response magnitude rises as frequency increases and then drops at the closed-loop bandwidth of the actuator.	25

2-1	<i>P3</i> . A commercial walking robot built by Honda Research and Development. It uses a combination of passive compliance in both its actuators and feet as well as active force control at the ankles. Reprinted with permission of Honda Motor Co., LTD. . .	31
2-2	Series Elastic Actuator. A spring is intentionally placed in series with an eletromagnetic motor, transmission and actuator output. The spring deflection is controlled thus inferring force control.	38
2-3	COG is a humanoid robot with upper torso, arms and head. There are series elastic actuators for each of the six degrees of freedom in each arm. Here COG is turning a crank using a dynamic oscillating controller [76].	39
2-4	Spring Flamingo is a planar bipedal walking robot. It uses series elastic actuators to actuate its six joints. Its top walking speed is 1.25 m/s [50].	39
2-5	Corndog is a planar running robot representing half of large dog. It uses the electromechanical series elastic actuators developed as part of this thesis to actuate its four joints [34].	40
2-6	M2 is a 3D bipedal walking robot. It has 12 degrees of freedom: 3 at each hip, 1 at each knee and 2 at each ankle. The goal of M2 is to extend work done on Spring Flamingo to 3 dimensions.	40
2-7	Sarcos Dextrous Arm. It is a hydraulic force controlled teleoperated manipulator that has been used for many applications including production assembly, undersea manipulation and hazardous material handling. The manipulator actuators have accumulators on either side of the hydraulic fluid chambers. This gives the actuators intrinsic compliance. Reprinted by permission of Sarcos.	41
3-1	Minimal model for a series elastic actuators. There are four parts to a series elastic actuator: elasticity, control system, motor, and system inputs. The compliance is a simple linear spring with a stiffness of k_s . The force in the spring, f_l , is equal to the spring deflection times the stiffness. The control system consists of a simple proportional controller with gain K . The motor is modeled as a high impedance velocity source. The position output of the motor, x_m , is the time integral of the motor velocity. The system inputs or boundary conditions are the desired force, f_d and the load position, x_l	44
3-2	Graphical representation of the minimal motor model. The minimal motor model is a high impedance velocity source. It neglects inertia and has an instantaneous limit of force and velocity. It represents idealized models of both a hydraulic piston as well as an EM motor with a transmission.	45
3-3	General motor saturation model. All motors have limits to the instantaneous force and velocity output capabilities. The line connecting the maximum load force, F_{sat} , and the maximum actuator velocity, v_{sat} , defines the envelope in which the motor can operate. The slope of the saturation line is $K_{sat} = \frac{v_{sat}}{F_{sat}}$	46
3-4	Minimal model and block diagram for a series elastic actuator. The figure on top is a time domain graphical representation of the the minimal series elastic actuator. The bottom figure shows a block diagram representation of the actuator.	47
3-5	Fixed load model and block diagram – case 1. (Top) A fixed load constraint defines the closed-loop bandwidth of the system by isolating the relationship between desired force and load force. (Bottom) A block diagram of case 1 shows that the model is a simple first order system.	50
3-6	Zero order model for moving the gain from the power domain to the signal domain. A series elastic actuator removes gain from the stiffness of the spring. The control system can then increase control gain while maintaining actuator stability. The stiffness of the spring is <i>not</i> a limiting factor in the closed-loop stability of the actuator.	51
3-7	Zero order model for reducing sensitivity to internal position noise. With sensor stiffness gain and increased control system gain, internal position noise due to the transmission are greatly reduced. The provides for a very clean force output from the actuator.	52

3-8	Large force equals large elastic deformation. In order to create a large force, there must be a large elastic deformation. This requires the motor must move. In order to oscillate at high force amplitude, the motor must move very quickly.	53
3-9	SIM Small force and large force bandwidth. The small force closed-loop bandwidth is unaffected by the large force saturation constraints. However, as the magnitude of oscillation increases, the motor saturation dominates the large force output capabilities of the actuator. The more compliant the spring, the smaller the large force bandwidth. This is the key engineering tradeoff for series elastic actuators.	55
3-10	Forced load motion model and equivalent block diagram. (Top) The desired force is fixed constant, $F_d = F_o$, and the load motion is defined externally. The relationship between load motion and output force is defined as the output impedance. (Bottom) The block diagram shows that the feedback system and actuator dynamics are in the feedback loop.	56
3-11	Equivalent impedance for the general series elastic actuator. The active impedance of the actuator can be thought of as an equivalent damper in series with the physical spring. At low driving frequencies, the actuator appears to be a damper. At high frequencies, the impedance is the stiffness of the spring.	57
3-12	General series elastic actuator with load mass moving in free space. In this particular case, the load motion, x_l , is explicitly defined as a function of the loads mass, m_l , and the force in the spring, F_l	59
3-13	Equivalent model of the general series elastic actuator with load mass. The desired force is seen through a damper before the spring. A simple proportional controller does not make the actuator a force device.	60
3-14	SIM General closed-loop forward transfer function (left) and output impedance (right). These figures are normalized to the saturation frequency ω_o and have $\kappa = 3$	62
3-15	SIM General large force saturation bandwidth. The ability of an actuator to output its full steady state force level is compromised by the introduction of a very compliant spring. ω_o is the break frequency and is defined by the open loop dynamics of the actuator. The large force bandwidth is typically less than the controlled bandwidth of the actuator. Even though the actuator cannot achieve full force output at high frequency, it can and does operate above ω_o	63
3-16	SIM General force bandwidth profile with load inertia moving in free space. The variables in the figure are $\kappa = 2$ and $L = 0.2$. Any finite load inertia causes the system to have damper like qualities at low frequency as well as the bandwidth reduction at higher frequencies. As $L \rightarrow 0$, the system behaves as if it has a fixed load end.	64
4-1	Prototype Actuator CAD model. A 20MPa pressure source is connected to a MOOG series 30 flow control servo valve (not shown) that directs flow to the two chambers of the hydraulic cylinder. The piston is coupled to the output through four die compression springs. The spring compression is measured with a linear potentiometer which implies force. A closed-loop controller actively moves the piston to maintain a desired spring deflection.	66
4-2	Hydro-elastic actuator model. The servo valve directs fluid flow into the hydraulic cylinder which moves the piston and thus compresses the elastic element. The strain in the spring is measured and used in a proportional-integral feedback control system.	66
4-3	Power domain model for the hydro-elastic actuator. The force output of the actuator is determined by the compression of the spring. There are two inputs to the power domain. Q is the fluid flow from the servo valve and is a function of the input current i . x_l is a motion input from the environment.	67
4-4	SIM The power saturation profile for a hydraulic servo valve is a square root relationship between flow and pressure. In order to understand the effects of saturation on the actuator through linear analysis, a linear saturation relationship is assumed. The linear profile is a worse case than the square root saturation.	70

4-5	SIM This is a bode plot of the dimensionless closed loop system scaled to ω_o . Values for the plot were calculated from real parameters on the device: $\omega_o = 152$ rad/sec (25 Hz), $\kappa = 2$, $I = 0.3$ and $V = 4.4$	72
4-6	SIM The impedance of the actuator at low frequency is zero and is k_s at high frequency. The plot represents equation 5.14. It uses values $\omega_o = 152$ rad/sec (25 Hz), $\kappa = 2$, $I = 0.3$ and $V = 4.4$ which were calculated from the prototype actuator. . . .	74
4-7	Rough characterization of hydro-elastic impedance. As shown in the simulation, the impedance at low frequencies is equivalent to a mass and is equal to the spring constant of the sensor at high frequencies.	75
4-8	Hydro-elastic actuator model with load inertia moving in free space. Unlike the previous model where x_l is a system input defined by the environment, in this model the load inertia defines the motion of x_l as a function of the force in the spring. The load mass is part of the power domain and stores and releases kinetic energy as it moves.	76
4-9	Control abstraction for the hydro-elastic actuator pushing on an inertial load. Ideally, the actuator produces the desired force directly on the load. However, the dynamics of the actuator turn out to be an equivalent mass and spring. The equivalent mass is defined by the control system and power domain characteristics. The spring is the actual physical spring in the actuator.	78
4-10	Prototype hydro-elastic actuator. The actuator has a piston with $0.2in^2$ area in one direction and $0.15in^2$ in the other. The piston pushes on precompressed die compression springs. Spring deflection is measured with a linear potentiometer. Although not shown, fluid is directed into the piston via a servo valve with a 3000psi pressure source.	79
4-11	REAL Open-loop response for the servo, piston, spring and sensor. The solid line represents the mathematical model and the dashed line is experimental data. The simulation model uses a full third order servo valve. The model captures all important features except the light damping on 800 Hz resonance of the real servo valve. . . .	81
4-12	REAL Closed loop response for the hydro-elastic actuator under PI control. The solid line represents the mathematical model and the dashed line is experimental data. As in figure 4-11, the simulation model uses a full third order servo valve. The two models match very well in both magnitude and phase for the useful frequency range. . . .	82
4-13	REAL PI control step response without and with servo valve dither. The integrator in the controller keeps working on the errors in the system. Given that there is a small amount of stiction on the piston-cylinder interface, the integrator keeps hunting around the desired force. I add a small amount of dither on the to the servo valve and the hunting behavior disappears. Regardless of the dither, notice the fast response time of the actuator. The rise time is ≈ 10 msec and the system is settled in 50 msec. . . .	83
4-14	REAL Large force saturation for the hydro-elastic actuator. This is the response of the actuator when it is oscillating at its maximum force for different frequencies. The large force performance begins to drop off near the predicted saturation point of 25 Hz. After the response starts to die off, the first order bandwidth limitations of the servo valve begin to come into effect. This effect is not accounted for in the simulation. Therefore, there is a difference in the experimental and simulated responses at frequencies above the saturation point.	84
4-15	Risky testing the hydro-elastic actuator. The author is suspended under the hydro-elastic actuator. The actuator is supporting the load by a commanded force 1 lb above the downward force of gravity ($\sim 250lbs$). The author is holding a 2lb weight which drops the actuator. Releasing the weight causes the actuator to rise. The minimum resolvable force is 1 lb and is due to the noise floor of the sensor.	85
4-16	The hydro-elastic actuator rigidly connected to a hanging mass. The mass is 18kg. By commanding desired force on the mass oscillating and different frequencies, the effect of the load mass can be verified.	85

4-17	REAL Actuator force output with an inertial load. The inertial load mass and the actuator equivalent mass are 18 kg and 20 kg respectively. Since the two are so close, at low frequency the actuator displays a significant non unity magnitude under PI control as expected. The response magnitude rises as frequency increases and then drops at the closed-loop bandwidth of the actuator. Proportional control shows that the damper characteristics are significant for this actuator and inertial load combination. Using a proportional controller dramatically decreases low frequency force magnitude far beyond that of the PI controller.	86
4-18	REAL Results of drop testing an 18kg (40lb) mass attached to the actuator. At time $t = -0.2$, the actuator is pulling the mass with an upwards force (force up is defined negative). At about $t \approx -0.15$, the mass is released to drop. Even though the desired force of the actuator is set to zero, the impedance is not perfect and keeps pulling upwards with a 20lb force. At $t = 0$, the mass hits the end stop and the force spikes. The mass actually bounces a few times but the peak impact power is just after $t = 0$.	87
4-19	Model of the load mass during the drop test. Ideally, the load mass only feels the force of gravity, $F = m_l g$, since the actuator is set to output zero force (left). However the actuator still has impedance. The gravity pull only affects the load mass. The equivalent mass of the actuator does not feel the gravity. Therefore, in order for the load to drop, the gravity force on the load must be distributed between the two masses, one real, one apparent (right). In the drop test case, the $m_{eq} \approx m_l = 20\text{kg}$ and the gravity force is distributed equally between the two inertias.	88
4-20	REAL Close-up of drop test impact forces. This shows the first impact of the load mass. The impulse or change in momentum of the mass, J , is the area under the force curve. A numerical integration shows that $J = 12\text{kg} \cdot \frac{\text{m}}{\text{s}}$	88
4-21	REAL Impact power. The top figure shows the force in the spring on the first impact. By taking the area under the force curve, we can calculate the impulse, J , of the impact. $J \approx 12\text{kgm/s}$. The middle figure shows the energy stored in the spring. It is $E = \frac{1}{2} \frac{F_l^2}{k_s}$. Finally, the impact power is estimated in the bottom figure by looking at the rate of energy change $P = \frac{\Delta E}{\Delta t}$. The series elasticity spreads the impact time out so that the required power is well within the actuator's output power capabilities. .	90
5-1	The prototype actuator has a brushless DC motor rigidly connected to a ballscrew which drives the linear motion. The ballscrew nut is coupled to the output through four die compression springs. The spring compression is measured with a linear potentiometer. The actuator can output over 1350 N and move at 25 cm/second. . . .	92
5-2	Electro-magnetic series elastic actuator model. The motor mass has a driving force and viscous friction. The controller drives the motor mass to compress the spring which gives the desired force output.	92
5-3	EM series elastic actuator power domain model. The motor mass has a driving force and viscous friction. The F_l is the force output through the spring.	94
5-4	Electro-magnetic series elastic actuator model with a fixed load. This configuration helps to define the saturation limits of the actuator.	96
5-5	Velocity saturation model for the EM series elastic actuator. Simple velocity saturation limits the ability of the amplifier to produce high forces. This model is slightly different than the force saturation model described in the previous chapters but has very similar results. Here $K_{sat} = \frac{F_{sat}}{v_{sat}}$	98
5-6	SIM EM large force bandwidth due to force and velocity saturation. The motor mass spring resonance ω_o defines the large force bandwidth of the actuator. The B group (generalized damping) defines the shape of the profile around the saturation frequency. The three lines represent underdamped, critically damped, and overdamped frequency response. This plot only represents the large force capabilities of the actuator with the load fixed.	99

5-7	[SIM] Closed-loop bode plot of the EM series elastic actuator with PD control. This is a bode plot of the closed loop system with $\kappa = 3$ and $\zeta_c = 1$. The zero from the controller adds the apparent resonance near the controlled natural frequency.	101
5-8	[SIM] EM output impedance. The impedance of the actuator at small frequencies is low and is equal to k_s at high frequency. In this example $\kappa = 4$ and $B = 0.1$. For low frequencies, the actuator has an equivalent mass characteristic. The equivalent mass is, $m_{eq} = \frac{m_m}{\kappa}$. The higher the controller gain the lower the impedance. As Γ increases there is an effective reduction in the impedance at the controlled natural frequency.	102
5-9	Rough characterization if EM impedance. As shown in the simulation, the impedance at low frequencies is equivalent to a mass and is equal to the spring constant of the sensor at high frequencies.	103
5-10	[SIM] Inverse parabolic relationship of the force error due to stiction force. As control gain, K_p , increases non-linear friction forces are dramatically decreased. The two curves represent the estimate of κ^2 . The solid line includes the +1 and the dashed line does not. In the physical actuator, $K_p = 25$. As can be seen, at that level of gain there is very little difference between the two curves.	104
5-11	EM series elastic actuator model with load mass moving in free space. The load mass defines the load motion x_l	105
5-12	[SIM] Force on a load that is free to move. This plot shows that the actuator can output forces on a load mass even when it is free to move.	106
5-13	Control abstraction for the EM series elastic actuator. At frequencies below the controlled bandwidth, the actuator can be considered a pure force source. Above the controlled bandwidth, the dynamics of the equivalent mass m_{eq} (equation 5.25) and the spring come into play.	107
5-14	EM series elastic actuator used in testing. The actuator uses a brushless DC motor with a direct connection to a 2mm lead ball screw. The ball nut drives the springs in series with the load. The springs are precompressed die compression springs. A linear potentiometer measures the deflection of the springs and uses that signal for feedback to the controller.	108
5-15	[REAL] Open loop bode plot for electro-magnetic series elastic actuator with fixed end condition. This is a simple second order lumped mass spring system with a natural frequency of 7.5 Hz. The dynamic mass is the motor mass as seen through the transmission and the spring is the physical elasticity.	110
5-16	[REAL] Experimental maximum force saturation for the electro-magnetic series elastic actuator with fixed end condition. The actuator can only generate the maximum output force up to the ω_o , the mass-spring resonance frequency.	111
5-17	[REAL] Experimental closed-loop bandwidth for the electro-magnetic series elastic actuator with fixed end condition. The -3dB point is at 35Hz. The zero in the closed-loop equation causes the apparent resonance.	111
5-18	Risky testing. The EM prototype actuator is suspended from the ceiling and loaded with 300 lbs (me, seat and weights). The displacement of the spring is commanded so that it compensates for the gravity pull on the load mass. With small variations in the set point, the actuator moves the load up and down.	112
5-19	Fully loaded actuator demonstrating small force sensitivity. The actuator is fully loaded with 300 lbs and has a force equal to gravity pull on the load mass. Finger force of approximately 1 lb can get the actuator to move up and down. This shows that the dynamic range of the actuator is 300:1.	113

List of Tables

2.1	Flow and effort for different power domains. Every power domain has variables that define the flow and effort of the medium. The product of these two variables is the power transferred in the system.	30
3.1	Comparison of sensor stiffness. The top load cell is a standard off the shelf component. The bottom entry is the stiffness of the springs actually used in the prototype actuators of this thesis. The value shown is the one listed in the catalog. Experimentally, the springs were 12% more compliant.	56
4.1	Physical properties of Hydro-elastic prototype actuator. These properties are taken from component literature and from experimental tests.	80
4.2	Important physical properties for force saturation. The point at which the actuator begins to show signs of large force saturation is dependent upon these physical parameters.	82
5.1	Physical properties of EM prototype actuator. Some of the values are calculated from motor literature and others are measured.	109
5.2	Itemized mass distribution for EM series elastic actuator. This actuator is used in two dynamically stable robots described in Chapter 2. The table shows that over 50% of the mass is contained in the motor and magnet. In the design of series elastic actuators, it is important to keep the percentage power producing element mass high in comparison to the overall actuator mass.	113

Nomenclature

Force

- F_d — Desired output force.
- F_l — Measured output force in the spring.
- F_e — Error between the desired and measured forces.
- F_o — Constant desired output force.
- F_{sat} — Maximum actuator output force at steady state.
- F_{lmax} — Maximum force amplitude of oscillation any a desired frequency.

Motion

- x_m — Position of the motor before the spring.
- v_m — Velocity of the motor before the spring.
- x_l — Position of the load.
- v_l — Velocity of the load.
- x_p — Position of the piston.
- v_p — Velocity of the piston.
- x_n — Position noise in the motor.
- V_{sat} — Maximum actuator velocity.

Physical Parameters

- k_s — Actuator spring constant.
- m_m — Lumped motor mass.
- m_l — Load mass.
- b_m — Motor friction.
- A — Piston Area.
- τ_v — First order time constant of the servo valve.
- m_{eq} — Physical equivalent actuator inertia.
- b_{eq} — Physical equivalent actuator damping.

Frequency

- ω_o — Saturation frequency.
- ω_c — Controlled natural frequency.
- ω_l — Load mass (m_l) spring (k_s) resonant frequency.

Gain

- K — Controller gain.
- K_m — General model motor gain.
- K_v — Servo valve gain.
- K_a — Motor amplifier gain.
- K_i — Integral gain.
- K_p — Proportional gain.
- K_d — Derivative gain.

Chapter 1

Introduction

1.1 Thesis

Closed-loop control of series elasticity allows high-power density, high-impedance actuators to achieve low output impedance and good force sensitivity while maintaining good bandwidth. Intentional compliance in robot actuators is a deviation from traditional force control robot architecture. Nevertheless, series elastic actuators offer many advantages in force control tasks.

This thesis develops quantitative understanding of the effects, requirements and limitations for series elasticity in closed-loop actuator force control. The goals of the thesis are threefold:

1. Build a general framework for understanding series elastic actuators that is not dependent on a specific power domain.
2. Demonstrate and verify properties and limitations of series elastic actuators both mathematically and with physical prototypes.
3. Give guidelines for choosing spring stiffness given force, speed and power requirements for the actuator.

General Framework

The ideas of series elasticity can be applied generally to high impedance actuation systems. A hydraulic piston and an electro-magnetic motor with a large reduction transmission are two examples. This thesis develops quantitative measures for understanding and describing series elastic actuators. Regardless of an actuator's power domain, series elastic actuators exhibit good small force closed-loop bandwidth, reduced large force bandwidth and low output impedance.

Demonstration

This thesis demonstrates series elasticity both mathematically and physically with three models. First, a minimal actuator model generalizes the main ideas of series elasticity. This mathematical model consists of an ideal high-impedance velocity source motor, linear spring and proportional controller. Two case studies of physical actuator systems also demonstrate the principles of series elasticity. The first is a linear hydraulic piston with a servo valve and the second is an electric motor with a geared linear transmission. Both case studies have a linear spring and a low complexity control system, PI and PD respectively. The case studies include both mathematical analysis and physical hardware verification.

Choosing the Spring

The compliance of the spring in series elasticity is orders of magnitude less than traditional load sensors. Choosing a proper spring stiffness and designing an actuator that houses the elasticity

can prove challenging since the spring travel is so large. In this thesis, I explain the fundamental tradeoffs of spring stiffness in balancing the requirements for large force bandwidth and low output impedance. Through the use of non-dimensional models, a designer can also understand the effects of different spring stiffnesses in order to scale the actuator.

1.2 Motivation

The vast majority of commercial robot applications consist of tasks that control the position¹ or trajectory of each robot degree of freedom. Traditional robots can do this with great speed, endurance, precision and accuracy. Robots have been used in this commercial niche because repetitive tasks which require precision and accuracy are difficult and tedious for humans.

On the other hand, there are many tasks in which robot competence is inferior to that of biological counterparts. Despite extensive research, actions such as walking, running, swimming, catching, grasping and manipulation, considered easy to most able-bodied humans, are difficult for robots. These tasks all require interacting with the real world.

Since our world is kinematically and inertially constrained, it is important for a robot to be able to sense and control the interaction forces between itself and the environment. This is typically referred to as *Force Control*.² There are two aspects to successful force control. The first is to use an algorithm and sensory information to determine the desired robot joint torques in order to place the proper forces on the robot's environment. The second aspect of successful force control is to generate accurate forces at the robot joints. This thesis deals with the second aspect of force control and specifically on the actuators that create the forces.

Present-day actuation technology is typically poor at generating and maintaining accurate forces. Using local closed-loop control of actuator forces can improve the quality of force output by rejecting disturbances. Furthermore, it has also been shown that using a compliant load sensor in a configuration called *Series Elasticity*, increases an actuator's ability to generate accurate forces.

The focus of this thesis is to analyze and quantify the effects of load sensor compliance for closed-loop actuator force control. There are some unifying principles of series elasticity that can be captured in a general mathematical model. These general principles are further developed with specific models and physical prototypes for the hydraulic and electro-magnetic (EM) power domains.

This introductory chapter defines and outlines the qualities of good force control actuators. It also describes the first implementations of *Series Elastic Actuators* as a deviation from traditional actuator design. Finally, it gives a summary of the thesis results and contributions.

1.2.1 Actuation and Force Control

Actuation is the process of converting some form of energy into mechanical force and motion. An actuator is the device or mechanism that accomplishes this energy conversion process. An electro-magnetic motor with a gear transmission and a hydraulic piston are two examples of such actuators.

With few exceptions, standard robot actuation systems are poor at creating accurate forces in robot joints. The reasons for this inaccuracy include friction, stick-slip, breakaway forces on seals, backlash in transmissions, cogging in motors and reflected inertia through a transmission. All of these real phenomena induce force noise in the actuator. The effects of force noise are minimized when controlling the position or trajectory of the robot. The mass in both the robot and the actuators low-pass filter force noise on positional output. This is one reason why robots are so successful at trajectory control even in the face of force noise. However, for tasks requiring good force control, the force noise in the actuators can be problematic.

Good force-controlled actuators have several important measures: force bandwidth, mechanical output impedance, dynamic range, power density and force density. The first three measures are related to one another, and typically an improvement in one yields an improvement overall.

¹The term *position* is the generalized position/orientation vector.

²The term *force* denotes a generalized force/torque vector.

An increase in power or force density usually means that the other three characteristics suffer in performance.

The force **bandwidth** is a measure of how quickly the actuator can generate commanded forces. Bandwidth is the highest frequency at which the actuator creates a near one-to-one output force to desired force.³ The bandwidth must be sufficient to transmit accurate forces through the robot structure. Most force control tasks only require a few hertz bandwidth as demonstrated by the low bandwidth of human muscle. However, improving the bandwidth of the actuator above the minimal operational level can only improve the overall capabilities of the robot.

Mechanical output **impedance**⁴ is defined as the minimum amount of force an actuator outputs for a given load motion. In the simplest terms it can be thought of as the stiffness of the actuator output. Ideally, the impedance of a force controlled device is zero. Low impedance means that the actuator appears to the robot as a pure force source with negligible internal dynamics. An actuator with low impedance is sometimes referred to as being *backdriveable*.

Dynamic range is the maximum output force divided by the minimum resolvable output force increment of the actuator. It gives a measure for how sensitive the actuator is to small forces with respect to its full force output capability. A large dynamic range is desirable because it permits the actuator to be used in a versatile way in both very sensitive activities and in large force situations. Humans have very good dynamic range.

Force density and **power density** are not necessarily operational characteristics. Nevertheless, these qualities refer to an actuator's ability to generate force or deliver power to the robot per unit mass and unit volume of the actuator. Having high force and power density means that a small package can output a lot of energy. Lightweight actuators prevent over-burdening the robot structure with excess mass and allow for quick, responsive robot performance.

Electric motors with gear reductions and hydraulics are two present-day actuator systems that have high force and power density and can also achieve moderate to high bandwidth. Unfortunately, neither system possesses low impedance or large dynamic range qualities required for good force control.

1.2.2 Series Elastic Actuators

The force output capabilities of a standard actuator such as an electric motor with gear reduction or a hydraulic piston can be dramatically improved by using a load sensor as feedback for a closed-loop control system. This technique has been used for many years on both actuator closed-loop force control and robot endpoint force control.

Standard load sensors are designed to be as stiff as possible for a given load. This allows the sensor to transmit power interactions with no internal storage of energy. Unfortunately, a stiff load cell in series with an already stiff actuator means that the open-loop gain of the actuator is very high. This in turn implies that to maintain actuator control stability, control gains must be kept low. Low control gains typically indicate poor overall closed loop performance. Low control gains, high impedance actuators and stiff sensors make for a system that cannot handle shock loads from the environment or filter out friction and other transmission non-linearities inherent in real systems.

To overcome these deficiencies, several investigators including Howard [29] and Pratt and Williamson [46, 75] experimented with a closed-loop control of an electro-magnetic motor and gear reduction in series with a *compliant spring*. Information about force in the spring is obtained by measuring the spring strain or deflection. Pratt and Williamson named this actuator configuration a *Series Elastic Actuator*.

Figure 1-1 shows that series elastic actuators are topologically similar to any motion actuator with a load sensor and closed-loop control system. However, there are two significant differences resulting from the compliant element. First, there is increased energy storage in the spring that cannot be neglected. Second, integration of a compliant load-bearing sensor within a compact actuator can prove challenging. Nevertheless, compact designs have been successfully developed.

³A -3dB magnitude of output force to desired force is typically considered the bandwidth. -3dB is roughly 70%.

⁴Throughout this thesis mechanical output impedance is referred to as impedance or output impedance.

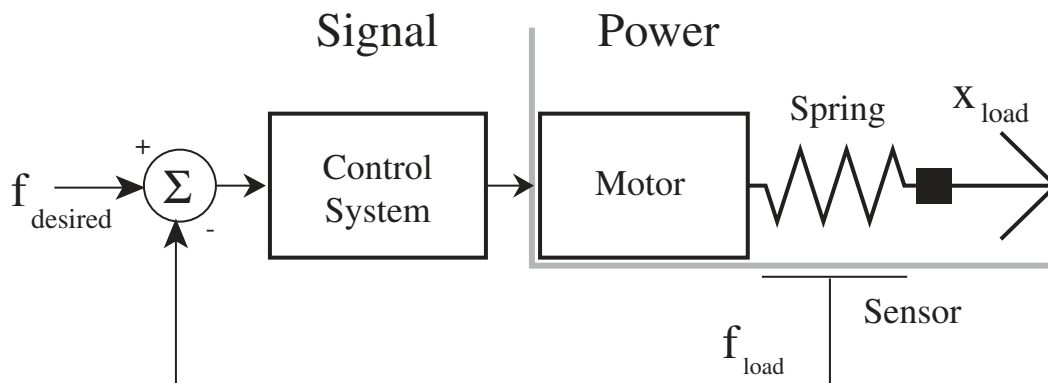


Figure 1-1: Series elastic actuator. The closed-loop actuator is topologically identical to any motion actuator with a load sensor and closed-loop feedback controller. The major difference is that the sensor is very compliant. Low spring stiffness removes gain from the power domain and thereby allows for increased controller gain in the signal domain while still maintaining desired stability margins.

The primary advantage of series elasticity is that the compliant load bearing sensor lowers the loop gain of the closed-loop system. The control gain can be proportionally increased to maintain the overall loop gain of the actuator at desired stability margins. This allows series elastic actuators to have low output impedance, be tolerant to shock loading and robust to changing loads. In addition, the increased controller gain greatly reduce the effects of internal stiction and other transmission non-linearities to give the actuators clean force output.

Many other research and commercial groups have recognized that purposeful compliance in actuators can be beneficial for force control. Several of these ideas and implementations in both stand-alone actuators and complete robots are described in Chapter 2. For the most part, in the past, the advantages of compliance in actuators, including series elastic actuators, have been explained with intuitive reasoning and not with mathematical demonstration.

In this thesis, I build quantitative understanding for closed-loop control of series elasticity. I also give performance measures for the actuator. These measures include closed-loop bandwidth, large force bandwidth, output impedance and inertial loading effects. These performance measures can be used to help guide actuator design, especially in choosing the stiffness of the elasticity. A brief summary of thesis highlights are given next.

1.3 Highlights of thesis results

The series elastic actuator shown in figure 1-1 is representative of the general model and the two physical actuators built for this thesis. Using minimal control the actuators achieve good bandwidth, low output impedance and large dynamic range.

As a brief summary of the thesis, I focus on results from the physical actuators. I first describe some of their general capabilities such as maximum force, power output and dynamic range. Then, by looking at specific cases of the actuators in operation, we can discuss other actuator measures: bandwidth, output impedance and the effects of an inertial load.

1.3.1 Actuators

Figure 1-2 shows CAD pictures of the two actuators designed, built and tested in this thesis. The left picture is of the hydro-elastic actuator and the right picture is the EM series elastic actuator. Both actuators have similar maximum force levels (400–600 lbs). The hydro-elastic actuator has

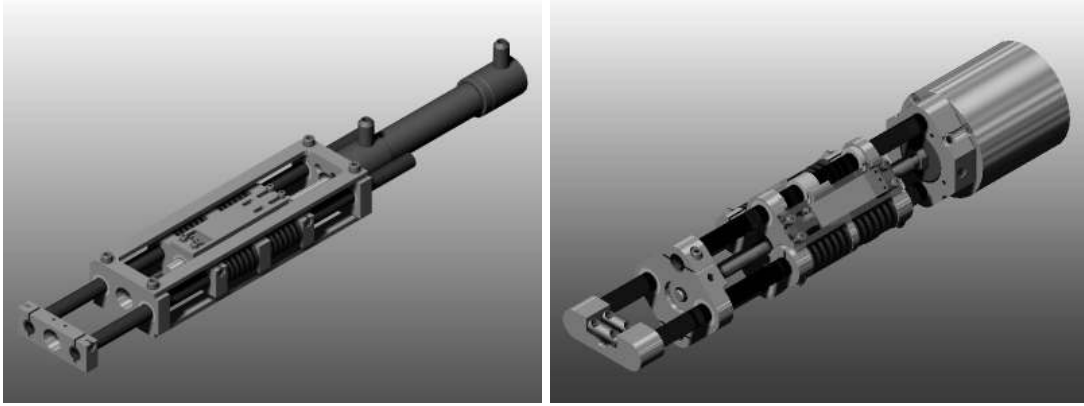


Figure 1-2: CAD models of the hydro-elastic actuator (left) and EM series elastic actuator (right) developed and analyzed in this thesis. Both actuators have a force output range on the order of 400–600 lbs. The power output for the hydro-elastic actuator is 1.5 kW and 430 W for the EM actuator. The minimum resolvable force of both actuators is approximately 1 lb due to the noise floor in the sensor. This gives the actuators a dynamic range of the order 500:1.

significantly higher power capabilities (1.5kW) compared with the EM actuator (430 W). The power density is also very high.

Without series elasticity, both actuators have high output impedance and are poor at open-loop force control. However, with series elasticity, the actuators are very force sensitive and can achieve high bandwidth at moderate force amplitudes. The closed-loop actuators have low output impedance. The lowest resolvable force, which is limited by the noise floor of the sensor, is approximately one pound, giving a dynamic range on the order of 500:1. The low output impedance also helps to significantly decouple the actuator dynamics from that of an inertial load.

1.3.2 Bandwidth

Bandwidth is a measure of how well the actuator can output a load force or force in the spring, F_l , given a desired output force, F_d . The closed-loop bandwidth, or the relationship between F_l and F_d , changes with frequency and can be written as a transfer function of the form

$$G_{cl}(s) = \frac{F_l(s)}{F_d(s)}.$$

The proposed bandwidth is measured with the load position of the actuator output held constant. This is analogous to when the actuator is in rigid contact with an unyielding environment or if the actuator is connected to an infinite load inertia.

I examine two cases of bandwidth. The first is the small force closed-loop bandwidth and the second is the large force bandwidth when the actuator is operating at full force and velocity saturation limits.

Small force bandwidth

The fundamental limits in small force bandwidth for series elastic actuators are *independent* of the spring stiffness that senses the force. The control system gain and the spring stiffness gain each contribute to the loop gain of the closed-loop system. With a lower spring stiffness the controller gain can be increased a proportional amount to bring the loop gain to the desired phase and gain stability margins.

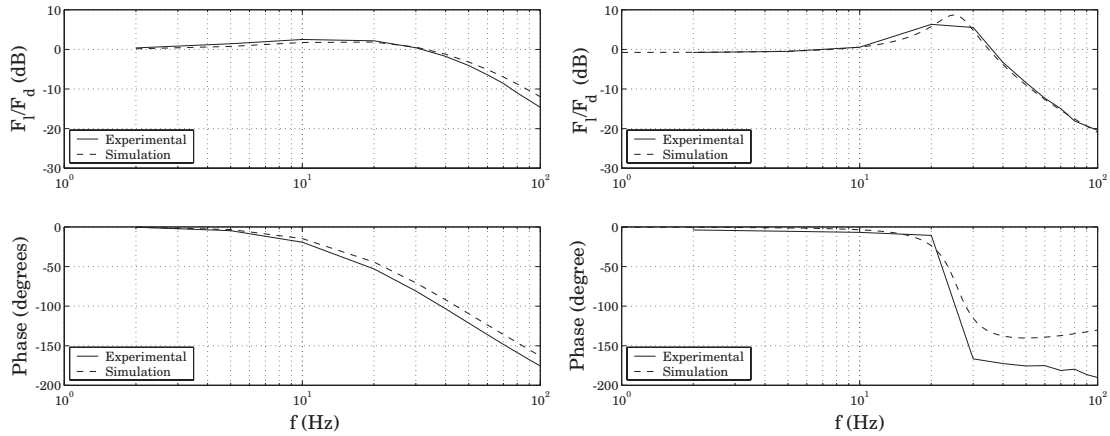


Figure 1-3: **REAL** Experimental bandwidth of the two prototype actuators. The hydro-elastic actuator is on the left and the EM actuator is on the right. The magnitude of oscillation for the actuators is 40 lbs. The bandwidth of both actuators is in the range of 30-35 Hz.

Assuming that the actuator is operating in a non-saturated state, we can measure the bandwidth. Figure 1-3 shows the closed-loop bode plots for both the hydro-elastic actuator (left) and the EM series elastic actuator (right). The force amplitude of oscillation for the test is 40 lbs. Each actuator has a bandwidth in the range of 30-35 Hz.

Large force bandwidth

Elasticity requires that there is a large elastic deformation in order to achieve a large force. High force amplitude oscillations require that the motor must move very fast. However, all motors have force and velocity saturation limits. Closed-loop analysis of the series elastic actuator does not apply when the actuator is operating at saturation levels. Motor saturation places a limit on the large force bandwidth. Large force bandwidth is defined as the frequency range over which the actuator can sinusoidally oscillate at a force amplitude equivalent to the maximum output force F_{sat} at steady state.

The large force bandwidth or saturation bandwidth, referred to as ω_o , is typically less than the closed-loop bandwidth when using a series elastic force sensor. The actuator can still produce force above ω_o but the maximum force capability decreases with increased frequency.

Figure 1-4 shows the large force bandwidth for the hydro-elastic actuator on the left and the EM series elastic actuator on the right. As with the small force closed-loop bandwidth, the large force bandwidth is tested with the load end of the actuator fixed. $\omega_o = 25$ and 8 Hz for the hydraulic and EM actuators respectively. It is important to note there that that the actuators are oscillating sinusoidally at full saturation force (over 400 lbs)!

The large force bandwidth, ω_o , for the hydro-elastic actuator is a function of the spring stiffness, piston area, maximum flow rate of the valve and the supply pressure. For the EM actuator, the large force bandwidth is defined at the natural frequency of spring and reflected motor inertia. Understanding and carefully defining an appropriate ω_o for a series elastic actuator is important in the actuator design process.

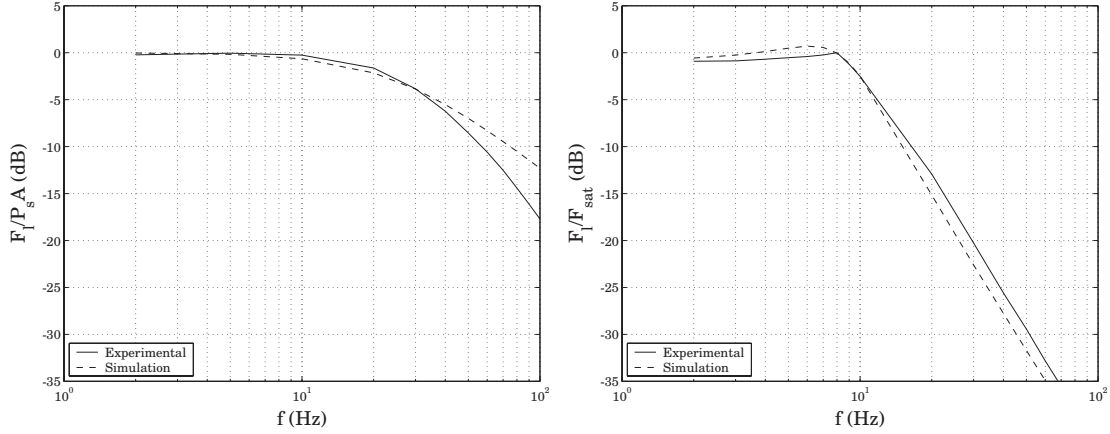


Figure 1-4: **REAL** Experimental large force bandwidth. The actuators ability to sinusoidally oscillate at the maximum force, F_{sat} , at steady state is limited in frequency due to the spring compliance and motor saturation in force and velocity. The frequency at which that maximum force capabilities of the actuator begin to fall off is defined as ω_o . $\omega_o = 25$ and 8 Hz for the hydraulic and EM prototype actuators respectively.

1.3.3 Output Impedance

As defined previously, output impedance is the amount of force at an actuator output given a moving load position. This can be written as a transfer function in the form

$$Z_{cl}(s) = \frac{F_l(s)}{x_l(s)}.$$

Ideally the actuator is a pure force source and has zero output impedance. If this were the case, the dynamics of the actuator would be completely decoupled from that of the load motion. However, since the actuator is a real system, it has some output impedance.

Figure 1-5 shows the calculated the EM actuator's output impedance as a function of load motion input frequency under PD control. The plot comes from the dynamic equations derived in the thesis. The impedance of the hydro-elastic actuator under PI control is almost identical to that of figure 1-5 and is therefore not shown. The figure has been normalized in frequency by ω_o and in magnitude by the stiffness k_s of the physical spring. The load motion is assumed to be a high-impedance position source. At low frequency the impedance is small. The impedance increases with increased frequency in the limit is equal to k_s , the physical spring stiffness.

The passive compliance in the spring and the active control system both contribute to the low impedance of the series elastic actuator.

The spring's stiffness can be more than two orders of magnitude lower than a standard load sensor. Even without closed-loop control, the spring lowers the impedance. This effect is most noticeable at high frequencies.

The second effect is due to the active control system. With a decreased sensor stiffness, the control gain is increased. This effect is noticeable at low frequencies. Notice that the impedance is rising at 40 dB per decade which means that the output impedance has two zeros at the origin in the dynamic equation. This implies that at low frequency

$$F_l = m_{eq}s^2X_l.$$

An equivalent impedance mass, m_{eq} , can be defined for both the hydro-elastic actuator and the EM

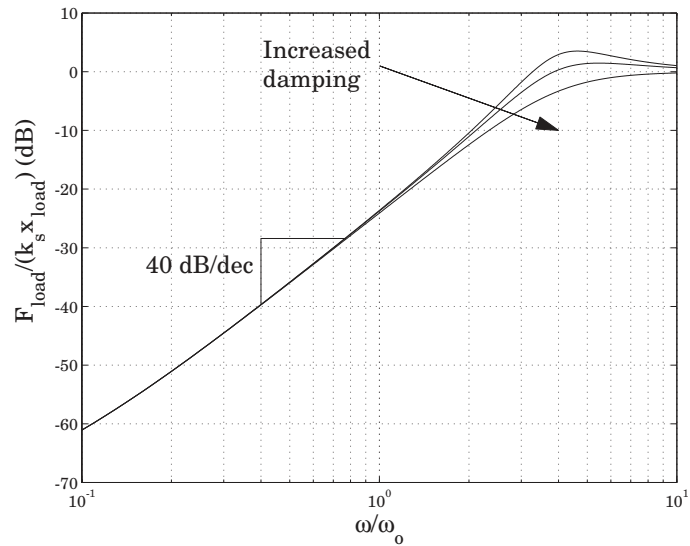


Figure 1-5: SIM The EM actuator’s output impedance as a function of load motion input frequency under PD control. The plot comes from the dynamic equation derived in Chapter 5. The figure has been normalized in frequency by ω_o and in magnitude by the stiffness k_s of the physical spring. At low frequency the impedance is small. The impedance increases with increased frequency in the limit is equal to k_s , the physical spring stiffness.

actuator. To give a sense of the equivalent mass, I define it for the EM series elastic actuator

$$m_{eq} = \frac{m_m}{K}$$

where m_m is the reflected motor inertia and K is the overall gain in the control system. In a series elastic actuator, the control system gain, K , is very large. Therefore, the equivalent inertial impedance, m_{eq} , is small relative to the reflected motor mass, m_m .

The output impedance is shown graphically in figure 1-6 as a physically equivalent mass in series with the spring driven by the load motion. Eventhough the impedance of the actuator is not zero, it is small.

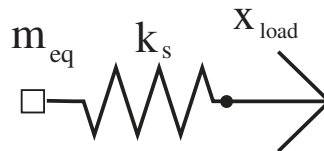


Figure 1-6: Physical equivalent of output impedance. As x_l drives at different frequencies, the impedance of the actuator changes. At low frequency, the impedance looks like an equivalent mass, m_{eq} . At high frequencies, the impedance looks like the physical elasticity of the spring in the actuator. Even though damping is not shown it is assumed present to limit uncontrolled oscillations at the natural frequency.

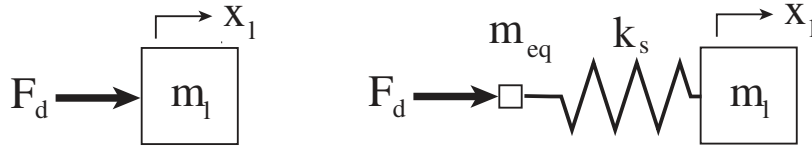


Figure 1-7: Series elastic actuator connected to an inertial load. Ideally the actuator is a perfect force source (left). However, when moving and inertial load, the actuator has its physical equivalent impedance. Typically, m_{eq} is very small in comparison to the load mass, m_l . Nevertheless, understanding the relative magnitude of m_{eq} is important.

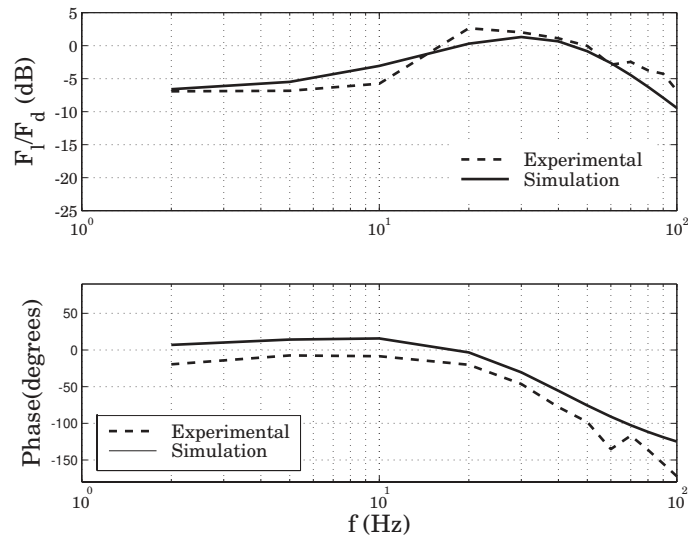


Figure 1-8: REAL Hydro-elastic actuator forces on an inertial load. The inertial load mass and the actuator equivalent mass are 18 kg and 20 kg respectively. Since the two are so close, at low frequency the actuator displays a significant non unity magnitude under PI control. The response magnitude rises as frequency increases and then drops at the closed-loop bandwidth of the actuator.

1.3.4 Load Motion

Series elastic actuators are meant to be used in real-world robots that contact the environment. However, there are many times when such a robot is simply moving an inertial load in free space. In this case, the load motion is defined by the mass of the load, m_l , and the force through the actuator.

Ideally, a series elastic actuator can be considered a pure force source within the controlled bandwidth independent of the load mass. However, as just explained, the impedance of the actuator is not perfectly zero. The actuator does have minimal dynamics that must be considered when looking at the force the actuator applies to a freely moving inertial load. Figure 1-7 graphically depicts the difference between the ideal force source (left) and with the impedance model (right).

When $m_l \gg m_{eq}$ then the dynamics of the actuator are negligible to within the actuator bandwidth and the actuator can be considered a force source. However, the closed-loop force transfer function changes at low frequency if the load inertia is close to or less than that of the impedance equivalent mass, m_{eq} . In the limit, if there were no load mass, the actuator has nothing to push on and produces no force.

Figure 1-8 shows the results of applying hydro-elastic actuator forces to a freely moving inertial

load. The inertial load and equivalent mass of the actuator are 18 kg and 20 kg respectively. At low frequency, the force on the load is a little less than half of the desired force. As force frequency increases, the response magnitude rises and then drops at the closed-loop bandwidth of the actuator.

In summary, series elastic actuators have many desirable properties as force controllable actuators. The high bandwidth, low impedance, shock tolerance, internal non-linear error rejection and large dynamic range are balanced with reduced large force bandwidth and reduced load force response. Understanding these tradeoffs is the key to successfully applying series elastic actuators in robot systems.

1.4 Thesis Contributions

The contributions of this thesis are:

1. A presentation of a minimal model for series elastic actuators that aids in understanding the fundamental principles of the actuators.
2. The design and construction of a linear hydro-elastic actuator that uses a linear piston and servo valve.
3. The design and construction of a modular electro-mechanical series elastic actuator that uses a brushless DC motor and linear transmission.
4. The development of linear models for both the hydro-elastic actuator and EM series elastic actuator.
5. The clarification between small and large force bandwidth and a discussion of bandwidth limits.
6. The development of intuitive physical equivalent models that represent actuator impedance.
7. The development of a linear model for the actuator connected to an inertial load moving in free space.
8. The demonstration and explanation of impact tolerance in series elastic actuators.
9. The reformulation of the linear models into dimensionless terms that aids in understanding important relationships in actuator scaling.
10. The explanation of choosing spring stiffness for actuator design and development.

1.5 Thesis Contents

The thesis is organized as follows:

Chapter 1 gives a brief introduction to the background and motivation of the thesis. It also includes a summary of the thesis objectives and covers the key results from the research.

Chapter 2 presents detailed background material and related work covering general ideas of force control, present-day actuator technology and actuators which use compliance.

Chapter 3 describes a minimal model of series elastic actuators. This model contains all of the key characteristics of a compliant load sensor used in closed loop force control.

Chapter 4 applies results of chapter 3 to a case study for a hydraulic piston, a hydro-elastic actuator. The theoretical model is compared with experimental results.

Chapter 5 applies results of chapter 3 to another case study of an electro-magnetic motor with a gear reduction. The theoretical model is compared with experimental results.

Chapter 6 gives concluding remarks and outlines future avenues of investigation.

1.6 Note on thesis data

This thesis includes data from both mathematical models and hardware. The figure captions indicate the source of the data. Simulated figures are marked $\boxed{\text{SIM}}$ and figures from hardware are marked $\boxed{\text{REAL}}$. $\boxed{\text{REAL}}$ is also used when both simulated and real data are compared in the same figure. This notation method is adapted from Williamson [76].

Chapter 2

Background and Related Work

Robots are very successful at performing tasks that require movement in free space or known environments under position control. Tasks such as spray painting vehicle exteriors, pick and place of IC chips, arc welding and spot welding fit very well into this paradigm. While many robotic applications that use position control have found their way into the commercial sector, robots that contact the surrounding environment and work within kinematic constraints have for the most part been limited to laboratory research. In fact, simple tasks such as driving a screw, turning a crank, assembling toys, and writing on a chalk board are extremely difficult for most robotic manipulators [5]. Instead of position control, these robots require force control. The robots themselves must be capable of accurately modulating and controlling actuator torques and forces.

This chapter explores the background of force control and force controllable actuators and provides explanations of applicable previous work. Some explanations of different techniques and algorithms to achieve robot compliance are outlined. The bulk of the chapter discusses capabilities of different actuator systems and how each performs with respect to force control. Actuators with intentional compliance, specifically series elastic actuators, are also discussed with examples of related work in both the electro-magnetic and hydraulic domains.

2.1 Force Control

Force Control is the term used to describe the necessary interaction between a robot and an external unknown environment. The robot must have the capability of sensing and controlling forces in addition to knowing where it is in its work space.

The necessity for force control deserves some discussion. Paynter gives a general explanation for maintaining proper causality when any two physical systems interact energetically [43]. The two systems' interaction is defined at the interface by a set of orthogonal variables: flow and effort. In a mechanical system, flow is the velocity or motion and effort is the force. In any power domain (such as mechanical, hydraulic, electric, thermal, etc.) there are equivalent flow and effort variables (Table 2.1). The product of these two variables is the power transferred across the system interface. Interestingly, one physical system cannot independently control both the flow and the effort at the point of interface. A system may define and control one of these variables or a relation between the two variables, but not both.

This explanation of general physical system interaction has direct application for why force control is necessary when a robot interacts with an unknown environment. Most workpieces and environments with which a robot will interact are inertially and kinematically constrained. A pallet has mass. A door swings on a hinge. A wall and floor are vertical and horizontal barriers respectively. Given these constraints the environment often defines the flow interaction. This leaves the robot with only the option to modulate the effort. In other words, while the robot can push on and give energy to the environment, it cannot specify how the environment will respond. If the robot tries to control the position at a constrained interface, there exists a basic incompatibility between the two physical systems. Therefore, whenever a robot interacts with an environment or workpiece and is

Power Domain	Effort	Flow
Mechanical	Force (N)	Velocity (m/s)
Hydraulic	Pressure (Pa)	Flow rate (m^3/s)
Electric	Voltage (V)	Current (A)
Thermal	Temperature (K)	Entropy rate (J/Ks)

Table 2.1: Flow and effort for different power domains. Every power domain has variables that define the flow and effort of the medium. The product of these two variables is the power transferred in the system.

not simply moving around in free space, it must use force control. While it is still important for the robot to understand its own sense of position, it also needs some capability of being compliant in order to effectively match the given constraints. As defined in the introduction, the robot must have low impedance. This allows the causality of the robot-environment interface to maintain a proper relationship.

It is important to point out that all environments do have some compliance. While most constraints have high stiffness, there are other environments which are very compliant such as sod or carpet. In fact some systems, like water, can exhibit variable compliance depending on the conditions. In these cases it may be necessary to control some linear combination of flow and effort. Nevertheless the robot must be capable of being compliant. It cannot be limited to high stiffness. Therefore, responsive force control is essential.

The following three subsections cover different techniques, ideas and algorithms that robot operators use in order to match compliance requirements with the environment. This includes passive methods as well as active control. The discussion also outlines some robotic applications where force control can be very useful.

2.1.1 Passive Compliance

A simple method to achieve pseudo force control and low robot output impedance is to have a robot use conventional position control but incorporate passive compliance. Passive compliance can be found in the robot structure, joints, and at the end effector. It differs from active force control in that passive compliance does not use force information for feedback to modulate the control algorithm. There are two major ideas behind passive compliance: low servo stiffness and passive end effectors.

By introducing passive compliance into the joints, the loop gain for the position control loop is effectively *softened*. A similar effect can be achieved by increasing the compliance in the robot structure (links). With a combination of low servo stiffness and low structural rigidity, the robot may be able to successfully interact with a work piece or environment simply by using position control schemes. However, the risk of adding too much compliance to a robot is that the robot may be *sloppy* in its task execution and may fail in its overall goal [16].

Successful examples of passive compliance in robot joints are the bipedal walking robots built by Honda Research and Development called *P2* and *P3* (figure 2-1 shows two views of *P3*). *P3* is slightly smaller than *P2*. Both robots use a compliant damping material as a coupling between the robot actuators and joints [17, 24]. The coupling protects the robot's actuators from the shock loads in each step and decouples the reflected inertia through the large Harmonic drive gear reduction. To compensate for *softened* servos, *P3* has active force sensors in the ankles which give feedback to the control system and are critical to its walking stability.

Passive end effectors are another successful strategy for helping robots interact with the environment. This is because many robots only touch the environment at the manipulator endpoint. A robot can use position control to approximately locate the endpoint properly in its workspace. The endpoint then performs its workpiece interaction task. For example, many end effectors have a soft rubber covering. This effectively decouples the robot from the workpiece through the compliance. Biological examples of passive compliance at manipulator end points are human hands and feet.

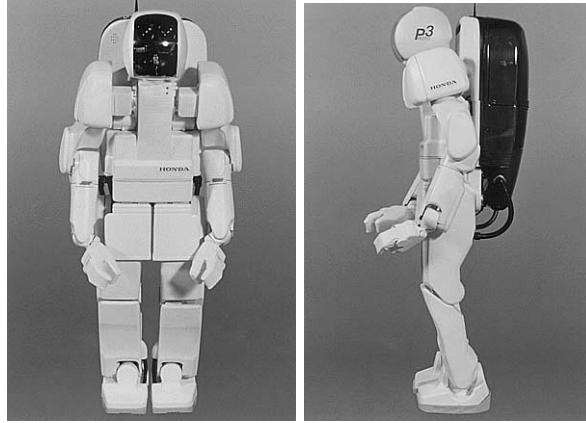


Figure 2-1: *P3*. A commercial walking robot built by Honda Research and Development. It uses a combination of passive compliance in both its actuators and feet as well as active force control at the ankles. Reprinted with permission of Honda Motor Co., LTD.

The soft compliant skin compensates for poor positioning accuracy of gross motions, allows for fine manipulation and also aids shock reduction in locomotion [3].

Interestingly, soft endpoint covering has also been shown to be an effective tool for active force control [16]. *P3* (figure 2-1) has a compliant foot in addition to compliance in the actuators. It helps to keep the supporting foot securely in contact with the ground during walking.

Besides a soft rubber covering, pneumatics are also common end effectors that effectively convert the end of the robot into a force control device. This is because pneumatics are inherently compliant. By controlling the pressure in a pneumatic piston, the piston converts gas pressure into a mechanical force. Pneumatics also maintain relatively low output impedance regardless of the pressure or force at the output.

Another clever passive end-effector is the remote center compliance (RCC) that is set up to automatically perform a peg-in-hole assembly [14]. The configuration of the RCC creates a compliance center at a certain point within its structure. Forces acting on the compliance center of the RCC result in pure translation and torques at that point cause pure rotation. By placing a peg tip right at the compliance center, it can be passively dropped into a hole without jamming.

2.1.2 Active Control

Passive methods have limits when trying to increase the capability of force controlled robots. Often passive techniques are task specific, such as RCC being applied to peg-in-hole assembly. In order for the robot to have the capability to perform more general tasks, there is a need for active control and task planning. This leads to the need for active feedback of measurements to modulate the control of forces on either the manipulator endpoint, joint actuators or both.

The vast majority of active force control techniques and algorithms have been developed to control and monitor the end point forces and torques via a force sensor at the robot tip. Mason [36] and Whitney [74] give good summaries of formalized compliance control and other active force control methods.

Even though this thesis deals with single degree of freedom force controlled actuators, I assume that a high level force control algorithm is used in the coordination and control of the entire robot system. Therefore, I present an overview of several force control methods and algorithms for multi-degree of freedom robots. Also included are a few general applications which require force control. More will be discussed about the physical capabilities of robots and actuators in the next section.

Various active force control methods include explicit force control, stiffness control and damping control, impedance control, hybrid position/force control and virtual model control.

- **Explicit Force Control** creates a virtual endpoint force *servo*. The controller input is the error between the desired force and actual measured endpoint force. The difficulty in this type of controller is that there is no positional feedback on the robot which means that there is no control on the absolute endpoint position. Therefore, this approach is somewhat difficult to apply to a multi-degree of freedom robot without a higher level control system modulating the forces.
- **Stiffness Control** [60] and **Damping Control** [74] create a virtual six degree of freedom *spring* or *dampner* in robot end point coordinates respectively. Both techniques are related because they measure the endpoint forces as well as the joint positions and velocities in order to generate a desired force output relating to the virtual spring or damper. Good torque control on the joints is helpful as the endpoint forces are created with the Jacobian transpose. However, no inverse kinematic calculations are needed.
- **Impedance Control** [26] generalizes the ideas of stiffness control and damping control. The position and velocity of the robot endpoint is commanded to follow some trajectory. In addition, the control system modulates a manipulator *disturbance response* which handles the control of dynamic interactions. The robot disturbance response is modeled after a second order mass-spring-damper behavior. In other words, the robot endpoint will behave as if it is a second order system. Therefore the endpoint forces, joint positions and velocities are used to generate actuator torques. The gain matrices which set the effective stiffness, damping and inertia of the manipulator endpoint correlate directly with stability and bandwidth criteria for the robot.
- **Hybrid Position/Force Control** [51] is a method that combines conventional position control and force control. The environment dictates natural constraints (such as being in contact with a surface) where only force control can be used. Similarly, position control is used in the directions where there are no constraints and the robot can move freely. The trajectory and path that the robot follow are called artificial constraints. A systematic method for understanding and defining natural and artificial constraints has been outlined in several places [5, 37, 67]. Once a task has been defined, actuator torques are then commanded to make the robot operate within the given constraints. This technique requires a new control system for each new task.
- **Virtual Model Control** [47, 49] is a motion control language that allows the control designer to use simulations of virtual mechanical and/or other components, linear or non-linear, to create reaction forces which are transmitted through the robot via joint torques. The robot behaves as if the virtual components are actually attached to the robot. This algorithm can be formulated into a state machine so that different virtual elements control the robot with each change of state. Virtual model control is different from impedance control in that it does not assume a fixed base and allows component connections between any two points on the robot, not just between base and endpoint. While this control language has been applied to legged robots that successfully accomplish their task of locomotion [48], there are currently no formal methods for quantifying stability.

2.2 Applications of Force Control

There are many applications that require real time force control. These applications include: teaching and skill acquisition both for people teaching robots and robots training people, telerobotics, haptics and biomimetic robots. While each application does not have a specific technique associated with it, the following are some of the applications to give emphasis to the importance of force control.

- **Teaching and Skill Acquisition** [7] – Off-line programming has had only partial success in applications in manufacturing such as grinding and deburring. In these cases, interaction forces for the task must be acquired or learned. These skills are often difficult to teach to

people, let alone robots. Often it is easiest to train force interaction skill with a teach-by-showing method. It is then possible to embed that information into one of the active control methods listed above such as hybrid force/position control or impedance control. In order for the robot to learn these skills, it must be compliant in the instructor’s hands. This requires good force control.

Conversely, robots can teach humans. Experiments are being done with robots helping in the rehabilitation process of upper limb control for people recovering from strokes [2]. These robots must be force-sensitive and inherently safe.

- **Telerobotics** [62, 63] places a human in the control loop of a robot. One standard form places a human on a master manipulator and the robot slave mimics the motion of the master. To add to the capabilities of the system, a controller will reflect the forces felt by the slave to the master. While it is not recommended that the slave manipulator have endpoint force control from the standpoint of stability, local force control on each individual joint is highly recommended (if not required) for proper teleoperation [41]. Advances in manipulator design and control algorithms have allowed for the development of a teleoperated micro-surgery robot [57].
- **Haptics** [58, 56] is closely related to teleoperation where the only difference is that there is no slave manipulator. A haptic interface will generate forces at its end point as it follows the users motion. The desired forces are created in a virtual environment rather than reflecting a remote real environment. However, the haptic interface gives the illusion that an environment actually exists. Good force control is critical in haptically representing a virtual environment.
- **Biomimetic Robots** are those that try to imitate motions and actions of humans and animals. Robots that walk[48], run[52], catch[28], grasp[58], swim[71], etc. are all currently inferior to their biological counterparts in both structure and technique. These robots interact with the surrounding environment and therefore good actuator force control is very beneficial.

2.3 Robot Actuators and Active Force Control

The above algorithms and applications, while using different methods of calculation, generate desired output forces for each of the joints in response to joint positions, endpoint forces, desired behavior, and/or the environment. Regardless of the application, algorithm or technique, there is often an assumption made in the control system that high level desired force equals actual force at the robot actuator. For the most part, this assumption is poor, particularly for very low forces when desired force is near zero. There are many reasons why this is the case. Friction, stick-slip, intermittent environment contact (impacts), transmission dynamics, actuator dynamics, actuator saturation, reflected inertia and noncolocated control are all limiting factors.

Although actuators are often assumed to be *black box* force devices, the limiting factors above make that assumption invalid.¹ It is important to understand how well various actuation methods generate clean and accurate forces or torques. Studies have been conducted that compare and contrast different actuation domains including internal combustion engines, electro-magnetics, hydraulics and pneumatics as well as other developing technologies such as shape memory alloys (NiTi), electro-active polymers and braided pneumatics (McKibbin muscles). In the comparisons, biological muscle is used as a benchmark. These studies focused on characterizing and generalizing different actuators by the shape of their flow-effort relationship [22] and on looking at the power density and force density of each actuation method [27].

This thesis considers only the traditional actuation methods of hydraulic and electric actuation. The following discussion focuses on how each method performs with respect to force control. Pneumatics and other actuation methods are mentioned for completeness.

¹It is interesting to note that many linear and non-linear position control methods and algorithms also assume accurate force generation from the actuators in order to prove proper operation [13, 65].

2.3.1 Electro-Magnetic

The vast majority of robotic actuators in use today consist of some form of electro-magnetic (EM) motor with a transmission. EM motors by themselves are well understood. They are fairly easy to model and control because they are linear for the most part. In the simplest model, motor torque is proportional to current. Transmissions, on the other hand, are not linear. They introduce several problems discussed below.

The purpose of having a transmission is to increase the force and power density of the actuator. This allows the EM motor to run at peak efficiency operating conditions (high speed and low torque) while output power is at the low speed and high torques good for robot operation.

While mathematically a transmission works wonderfully, physically it presents problems for both position as well as force control. Non-linearity in the form of backlash, increased dynamic mass and increased output impedance are all a function of the transmission.

Backlash and other non-linearities in the transmission are especially problematic at low forces. The actuator may hunt back and forth in the dead zone between gear teeth in an attempt to modulate zero force. It is possible to create and use non-backlash gears to create a stiffer transmission, however they correspondingly increase drive friction [19].

A gear reduction also increases the equivalent dynamic mass of the motor as seen after the transmission by N^2 , where N is the reduction. For geared motors, the large reflected inertia leads to broken gear teeth, damaged ball screws and ruined actuators when large unexpected loads appear as the robot interacts with an environment. This is because the large reflected inertia needs time to accelerate in order to store energy. Therefore, the impact energy goes directly into the compliance of the transmission elements until they yield or break. In addition, the motor inertia, as seen through the transmission, will typically be on the same order of magnitude as the robot link inertia and be coupled to the link, significantly altering its dynamic behavior.

EM motors by themselves are typically easy to backdrive and have low impedance. This means that a small external torque on the motor shaft will cause it to accelerate. However, with a large transmission, due to the increased real and apparent friction and increased reflected inertia, an EM motor becomes significantly more difficult to backdrive. With this increased impedance, the actuator becomes much more of a position causal system rather than a force causal one.

To overcome the difficulties associated with linking an EM motor to a transmission, many novel approaches have been tried. Three of these approaches are described below which include: direct-drive, cable transmissions and evoloid gear sets.

In an effort to make a clean, low-friction, low-impedance actuator, Asada et. al. created direct-drive actuators and robots [6]. Direct-drive eliminates the transmission and connects a DC brushless motor directly to a robot link. This construction eliminates friction and backlash and creates a very force sensitive actuator. Advanced torque sensors in the actuators have added to the capabilities of direct-drive robots [1].

From a modeling and control standpoint, direct-drive robots are simple systems. The motor (magnet) mass is included with the link inertia. Unfortunately, to compensate for the loss of transmission, direct-drive motors must be large in order to achieve high torques. High torque requires high current which in turn requires heavy wiring. In weight sensitive and power sensitive applications such as mobile robots, direct-drive actuators are often unacceptable. Nevertheless, for ground based robots with few degrees of freedom, direct-drive actuators have been very successful in both force control applications and position control, particularly in semiconductor manufacturing automation.

In order to improve the force and power density of EM motors without sacrificing force sensitivity, work has also been done to create stiff, low-friction, clean, light-weight cable transmissions [70]. These transmissions have zero backlash and high power efficiency due to high tensioning in the cables. Cable transmissions have been used on novel robots such as the *Whole Arm Manipulator* [59] used in robot catching [28] and digging, the *PHANToM* [38] used as a three degree of freedom haptic point interface, *Robotuna* used to study undersea oscillating foil propulsion [8, 71] and robots for minimally invasive telerobotic surgery [35, 57]. However, because of the size constraints of pulleys, cable transmission can only achieve moderate transmission ratios.

Force control with slightly higher ratio gearing has been achieved with very careful actuator

design and development in the construction of *Artisan*, a ten degree-of-freedom manipulator [72]. Instead of using single stage helical gears, Vischer and Khatib used *evoloid* [9] gear sets for each joint. Evoloid gears have a much coarser pitch than traditional spur gears. These gears have higher load capabilities than helical gears but are still backdrivable and have smooth torque transfer characteristics. This transmission used in conjunction with a novel torque sensor, helped *Artisan* to demonstrate compliant behavior.

2.3.2 Hydraulic

In contrast to electro-magnetic motors, hydraulic systems operate best at high force (high pressure) and low speed (flow rate), which is ideal for robotics. Hydraulic systems also have the highest power density of modern controllable actuation methods [27]. Systems often operate at 3000 psi and higher. Hydraulics can hold large loads indefinitely while consuming minimal power. This is something that would cause electro-magnetic systems to quickly overheat. Hydraulics are particularly useful in high force and high power density situations such as construction machinery, airplanes and automobile steering systems. Nevertheless, there are several downsides to hydraulics which have caused electro-magnetic servos to be favored in the robotics industry. These include potential messiness (catastrophic failure), system complexity, high impedance, sensitivity to contamination and non-linearity from a control perspective.

There is an inherent messiness with hydraulics especially when hydraulic oil is used. This is especially true for catastrophic system failure such as a tree falling onto hydraulic forestry equipment [40]. Modern system design has alleviated some concerns regarding leakage of hydraulic fluid but the threat is always there.

Since pressure and return lines must be run to hydraulic actuators, there is increased system complexity from a plumbing perspective. The hoses and pipes going to and from the actuator are non-trivial in size. They must be accounted for in robot design and can add significant mass to the robot structure.

Hydraulic systems also have high impedance. This is a result of the low compressibility of hydraulic fluid and the fact that servo valves control fluid flow. All fluids are compressible to some extent, but traditional hydraulic fluids, such as oil or water, can typically be modelled as incompressible. The only way to backdrive (backflow) a hydraulic system is to create a load pressure higher than the source pressure. In this case, fluid reverses flow direction because flow in an open servo valve is a function of pressure difference. Hydraulics are usually designed for motion control, not force control.

Hydraulics are very sensitive to contamination as foreign particles in the working fluid can cause system failure. In order to limit contamination in the working fluid, hydraulics require tight seals at the piston cylinder interface. Tight seals increase friction and stiction in the system.

The final downside to hydraulic systems is that they are highly non-linear from a control perspective. Null bias, null shift, hysteresis, threshold, internal leakage, square root flow-load characteristics and unequal piston areas are all non-linear effects in hydraulics. Depending upon the level of precision required by the robot, some or all of these effects need to be accounted for.

The advantages of hydraulics often outweigh the disadvantages. Therefore, hydraulics are used quite frequently in position controlling robots and heavy equipment. Hydraulic actuators typically consist of a pressure source and a flow control valve (i.e., spool valve). A small signal current deflects the spool valve which allows the high pressure fluid to flow. In the simplest linear model, the fluid flow rate through the valve is proportional to the small input current. The valve directs high pressure fluid into one of two chambers which drives a piston thus converting fluid flow into a mechanical motion. Thus, in this configuration hydraulics are very good at position control.

It may seem that it would be possible to modulate the piston chamber pressure in order to get good force control. Unfortunately, the pressure in the chamber is not a good representation of the force at the actuator output. A few reasons for this include friction and stiction in the piston and seals, supply pressure variations and non-linear flow characteristics, and high output impedance. The friction and non-linearity create force noise on the actuator output. High impedance comes from difficulty in back-flowing through a servo valve as well as the fact that hydraulic fluid has great

inertia. In general, force control of hydraulic actuators is a difficult problem [12].

There have been attempts to overcome some of the difficulties associated with hydraulics for use in robotic contact tasks. These include mechanically decreasing the seal tolerance of the piston and implementing advanced control algorithms.

In order to reduce the sliding friction and stiction, the seal tolerance can be lifted. However, that has a direct effect on system efficiency, not to mention the problems of keeping the hydraulic fluid and potentially the work environment clean. In Raibert's hopping robots, the legs had two sets of loose seals [52]. The first set allowed leakage flow from the pressure chambers. The second seals simply scavenged the leakage. This configuration helped the piston to slide very smoothly. Even so, using pressure as an estimate of actuator output force proved inaccurate.

Given the natural non-linearity of hydraulic systems, Alleyne created a non-linear Lyapunov based hydraulic piston force controller [4]. This controller also includes adaptive behavior for unknown or varying parameters since many parameters in the hydraulic system are either difficult to measure off-line or are time varying (with temperature).

Hydraulic impedance control has been implemented on an industrial hydraulic robot. The algorithm for control is a specialized one which recognizes that many robot actuators are position causal and is called position-based end-point impedance control [44]. While the implementation was somewhat successful, limitations in the positioning accuracy and the bandwidth of actuators caused the robot to exhibit a hunting or chatter behavior when in contact with a semi-stiff environment [23].

It is interesting to note that the hopping robots and the Lyapunov controller also included springs in their actuators. This effect of the compliance will be discussed in the section 2.4.

2.3.3 Pneumatic

Pneumatics typically consist of a piston and a valve connected to a gaseous pressure source. Pressure in a piston chamber converts the piston into a force compliant actuator. Pneumatic actuators have many features similar to hydraulics but with significant differences resulting from the operating fluid. Inherent compliance from the compressibility of gas make pneumatics useful as end effectors. Clever design configurations and control schemes have demonstrated that it is possible to achieve moderate positional bandwidths of 21-35 Hz [27].

There are several problems with pneumatics that limit applicability to robotics including safety, thermodynamic effects and potential resonance. First, unlike hydraulics, pneumatic systems run at relatively low pressures (100 psi) for safety reasons. They can operate at higher levels but compressed air stores large amounts of energy. If there is a rupture in the line, pneumatics become very dangerous. Thermodynamic effects of compressing and expanding air can heat and cool the system dramatically. Valves and seals can be designed to operate within temperature variations; however, it is usually not recommended. Finally, the natural compliance of pneumatics can also resonate with robot link inertias. Clever damping schemes are often required to maintain stability.

A variation on the standard configuration above is an inflatable elastic tube covered by a flexible braided mesh typically called McKibben muscles [27]. When pressurized, the elastic tube inside expands but is constrained by the mesh. The flexible mesh shortens or contracts like a muscle due to the expanding tube. It has been found that McKibben muscles can exhibit passive behavior very similar to biological muscle [33] since it has both series and parallel elasticity.

2.3.4 Others

There are many emerging actuator technologies with potential for use in macro scale robots such as shape memory alloy (NiTi), electro-active polymers, polymer gels, piezoelectric and dielectric elastomers [10, 27, 45]. Some of these systems demonstrate moderate force density and look very promising. However, there are some technical hurdles that must still be overcome. These include long actuation time, small scale, low power density and low efficiency.

Several of the systems have very long actuation time constants. This is the case for polymer gels as well as shape memory alloy. Specifically for shape memory alloy, actuation time is thermally

limited. The elongation time is fairly short because high current can be pulsed through the actuator. However, in order for shape memory alloy to return to its initial shape, the latent heat in the actuator must be removed which can take a long time.

For the most part, electro-active polymers, piezoelectric actuators and dielectric elastomers have current working prototype systems on a very small scale. This is ideal for actuation of micro robots. In order to work on macro robots, however, work must be done to scale the systems in size.

The final difficulty with many of these actuators is that they have low output power density and are very inefficient. The power density is orders of magnitude lower than electro-magnetic motors and hydraulics. Also, the input power to these systems is still quite high, which gives a poor efficiency rating. One would hope that future development of these systems will make them more competitive with current macro scale robot actuators.

2.4 Intentionally Compliant Robot Actuators

Each actuation method described above has strengths and weaknesses with respect to force control, force density and power density. The predominant theme for the actuators is that those with high force and high power density typically have high impedance. Therefore, as is, these actuators are difficult to use in force control situations regardless of sensory feedback information.

In an attempt to overcome this impasse, it is possible to decouple the dynamics of the actuator from that of the robot by placing a compliant element between the two. This gives passive compliance to the actuators. In addition, by measuring the deflection of the spring, an estimate of force in the joint is obtained and can be used for active feedback control.

Introducing compliance into the drive system is contrary to conventional machine design wisdom. Traditionally, machines and drive systems are built to be as stiff as possible to increase bandwidth. However, it is interesting to note that the actuator benchmark for force control applications, biological muscle, is connected in series to a link output through an elastic tendon [3]. There are many reasons why this is thought to be the case. Ideas include energy storage and increased efficiency, stability when contacting environments and filtering shock loads to the body. Even though muscles do not have many of the problems inherent to EM motors and hydraulics, elastic elements can be useful to actuation regardless of whether the system is biological or artificial.

Active measurement of a compliant element in an actuator was first applied to electro-magnetic motors with a transmission and called *Series Elastic Actuators*. This section presents a history of these actuators as well as other systems that use active compliance.

2.4.1 Series Elastic Actuators

Howard [29] built an actuator with a spring in series with an EM motor and transmission. He then measured the relative spring deflection by taking the difference between the motor rotation and output shaft rotation. By controlling this deflection he essentially was controlling the actuator output torque by Hooke's Law:

$$F = kx. \tag{2.1}$$

Unfortunately, use of a differential measurement between motor and output shaft misses the actual strain in the spring due to transmission compliance and is also noise prone. Nevertheless, he was able to show that by using a smaller motor and larger transmission ratio, the output force and power density increased while maintaining good control over force.

Pratt and Williamson [46, 75] also used elasticity and created an actuator similar to that of Howard's. They showed that to get a better force measurement for closed-loop control, the strain/deflection of the spring should be measured directly and not as the difference of the motor and output shaft. This actuator configuration is called a *Series Elastic Actuator* (figure 2-2). As in Howard's actuator, the series elastic actuator mechanically filters friction and backlash and other non idealities in high ratio transmissions drives. It also filters shock loading from the environment.

In addition to initial prototypes, versions of series elastic actuators have been demonstrated in a few robots.

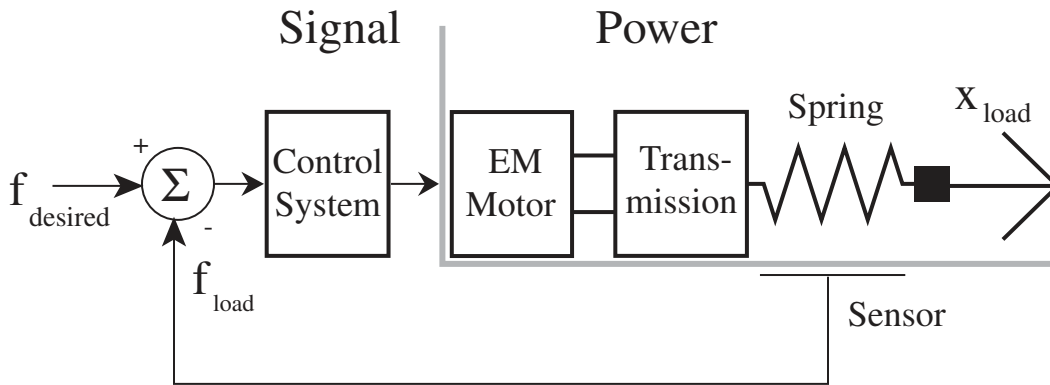


Figure 2-2: Series Elastic Actuator. A spring is intentionally placed in series with an eletro-magnetic motor, transmission and actuator output. The spring deflection is controlled thus inferring force control.

- *COG* (figure 2-3) [11] is a humanoid robot with upper torso and head. Series elastic actuators are used in its arms, which have 6 degrees of freedom. Using the natural dynamics of the arms, low noise force controllable actuators and dynamic oscillators for control, *COG* was able to do many tasks previously thought to be difficult for robots such as hammering and turning a crank [76].
- *Spring Flamingo* (figure 2-5) is a planar bipedal walking robot with series elastic actuators driving 6 degrees of freedom (three in each leg for hip, knee and ankle) [48]. It can walk at 1.25 m/s on flat terrain. It has also walked “blindly” over terrain of uphill and downhill 15 degree slopes.
- *Corndog* (figure 2-4) is a planar running robot with one fore and one aft leg [34]. It represents half of a large dog. The actuators used in *Corndog* are the electro-mechanical series elastic actuators developed as part of this thesis. These actuators are described in chapter 5.
- *M2* (figure 2-6) is a 3 dimensional bipedal walking robot. It has 12 degrees of freedom; 3 at each hip, 1 at each knee and 2 at each ankle. *M2* is an extension of the work started with *Spring Flamingo*. *M2* also uses the actuators characterized in this thesis described in chapter 5 [54]. At the time of writing this thesis, the robot could stand on its own.

Series elastic actuators work successfully over a moderate range of spring stiffnesses. Unfortunately no previous work gives design guidelines for choosing an appropriate spring constant in the actuator. The actuators in the robots were mostly designed through trial and error iterations. This thesis provides a more quantified understanding of the effects of the springs in the system and also provides direction to spring selection in actuator design.

2.4.2 Other Electro-mechanical Compliance

There are other examples in which springs have been used in series with transmissions. Elastic transmissions are an integral part of Morrell’s parallel coupled micro-macro actuators [39]. In this scheme, a small direct drive actuator is coupled in parallel with a larger geared motor through an elastic transmission. The large motor creates a force with gross sensitivity and the small direct drive motor accounts for the error. While increasing the complexity of the actuator, a substantial increase in dynamic range is achieved.

In the control and handling of arbitrary two dimensional objects, Hanafusa created a three finger gripper with springs at the end of each finger [21]. The fingers were driven by a single motor and by measuring the deflection of each spring, stable grasping forces were achieved.

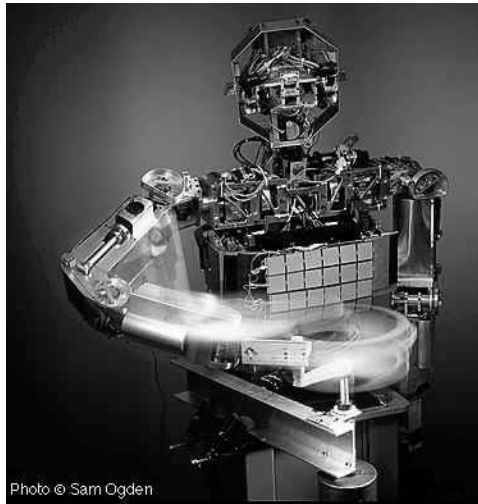


Figure 2-3: COG is a humanoid robot with upper torso, arms and head. There are series elastic actuators for each of the six degrees of freedom in each arm. Here COG is turning a crank using a dynamic oscillating controller [76].

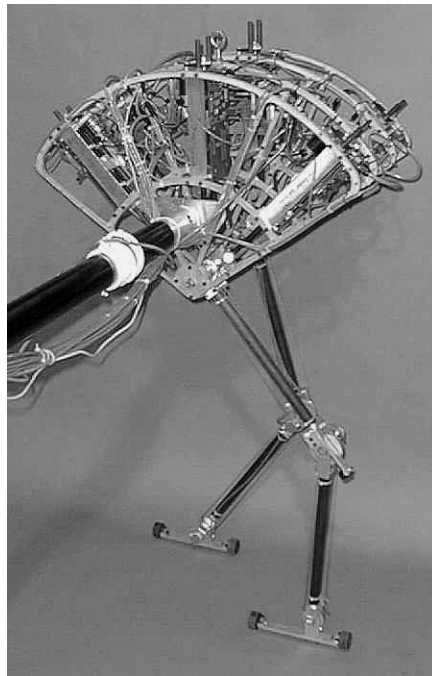


Figure 2-4: Spring Flamingo is a planar bipedal walking robot. It uses series elastic actuators to actuate its six joints. Its top walking speed is 1.25 m/s [50].

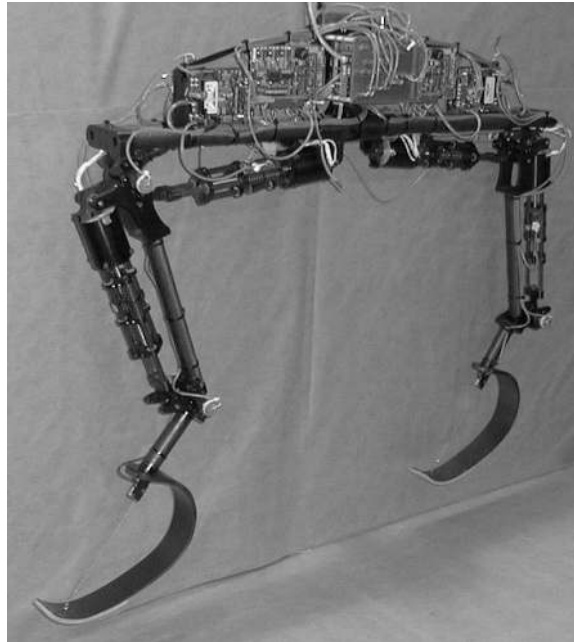


Figure 2-5: Corndog is a planar running robot representing half of large dog. It uses the electro-mechanical series elastic actuators developed as part of this thesis to actuate its four joints [34].

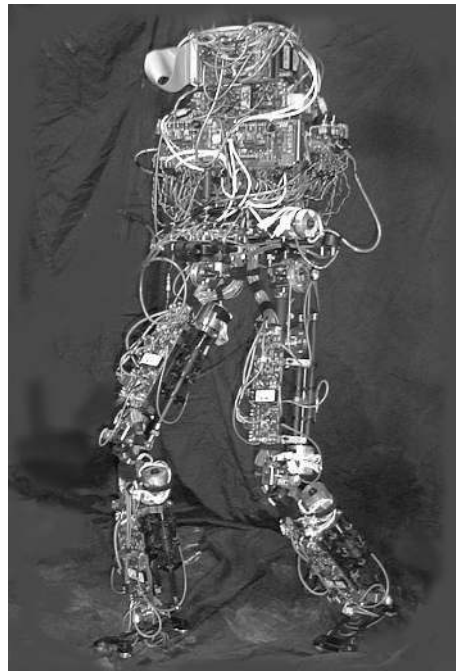


Figure 2-6: M2 is a 3D bipedal walking robot. It has 12 degrees of freedom: 3 at each hip, 1 at each knee and 2 at each ankle. The goal of M2 is to extend work done on Spring Flamingo to 3 dimensions.



Figure 2-7: Sarcos Dextrous Arm. It is a hydraulic force controlled teleoperated manipulator that has been used for many applications including production assembly, undersea manipulation and hazardous material handling. The manipulator actuators have accumulators on either side of the hydraulic fluid chambers. This gives the actuators intrinsic compliance. Reprinted by permission of Sarcos.

In the manipulator design for mobile robots to perform cooperative object handling, Sugar built a three degree-of-freedom parallel manipulator which could generate forces in the x and y directions and a moment in the z direction [69]. The actuators for the manipulator have springs between the transmission and load, and the force is controlled by measuring the deflection of the spring. This design is very similar to the series elastic actuators described above.

Sugano designed and build a compliant one degree-of-freedom finger [68]. The finger's compliance could be set by changing the effective length of a leaf spring which was in series with the motor and transmission. The actuator required three motors. One would drive the position and one would set the spring stiffness. An additional motor was required as a brake and used to damp out the residual vibration from the spring.

2.4.3 Hydraulic Compliance

Springs and other compliant mechanisms have also been used in conjunction with hydraulic actuators. Following examples from biological studies of running [3], Raibert's hydraulic legged robots use springs to recover impact energy from each step during locomotion [52]. Using the stored energy in the springs during stance, these robots were able to perform simple gymnastics such as a flip [25]. These robots were not under force control; however, the springs in the legs are necessary to maintain stability under high shock loading with each step.

As discussed previously, Alleyne designed and demonstrated a Lyapunov based controller for hydraulic piston force control [4]. The piston had a standard load cell attached to its output. However, rather than using an inertial load, the force sensor pressed on a spring fixed to ground. The spring compliance dominated over the sensor compliance and essentially lowered the loop gain and allowed the actuator to perform as well as it did.

The first force reflective teleoperated hydraulic manipulator was built by Sarcos, Inc. (Salt Lake City, UT) [30] (figure 2-7). Using one of the actuators for this robot, Wells characterized a hydraulic piston with accumulators which gives the actuator intrinsic compliance [73]. Instead of a mechanical spring at the actuator output, the piston has a fluid spring on the inside. Wells demonstrated that due to the compliance in the piston chambers, the actuator was much better able to tolerate external disturbances.

As with electro-mechanical series elastic actuators, little published work has been done to quantify the effects of compliance for hydraulic actuators. This thesis applies the ideas of series elastic actuators to the hydraulic domain. Similar ideas about the spring design tradeoffs and considerations are discussed as in the EM series elastic actuator. Initial work on hydro-elastic actuators done as part of this thesis has also been reported previously [53].

2.5 Summary

There are many applications for robotic force control, especially when the robot needs to interact with an external unknown environment. While there exist several types of algorithms and methods for implementing force control, there is a lack of actual robots than can achieve expected performance. One primary reason for this limitation is the robot actuators.

Robot actuators are especially poor at force control when high force and power density are required. In order to achieve the high power density, electro-magnetic motors require power transmission which introduces many problems including increased friction, large reflected inertia and high impedance. Hydraulic actuators achieve high force and power density requirements. However, force at the end of the hydraulic piston is difficult to control due to non-linearities, pressure variation and seal friction. Hydraulic and electro-mechanical actuators are much better suited for position control.

Closed-loop actuator force control has been shown to be improved with the introduction of compliance and controlling the deflection of the compliant element. The following chapters of the thesis describe and quantify this finding. I describe a general theory for series elastic actuators and give two case studies for implementing a series elastic design in the hydro-mechanical and electro-mechanical domains.

Chapter 3

Linear Series Elastic Actuators

This thesis focuses on understanding the effects of placing a significantly compliant spring in series between a motor output and load. By measuring the compression of the spring, the force in the spring and thus the force on the load can be inferred. Closed-loop feedback control then modulates the actuator system to obtain the desired output force. This technique has been termed *series elastic actuation*.

This chapter discusses the fundamental principles of series elasticity using a minimal complexity model which is not power domain specific. The general model demonstrates closed-loop bandwidth, internal error rejection, large force bandwidth, closed-loop output impedance and impact tolerance. It also discusses the effects on the actuator of an inertial load moving in free space. This chapter provides a unifying framework and descriptive language for understanding series elastic actuators.

3.1 General Model

As discussed in the previous chapter there are many methods of actuation, each with its own set of desirable and detrimental characteristics. Typically, actuators with high force and high power density also have high output impedance. They are better at control of position or velocity output rather than force control.

The main idea behind series elasticity is to take a standard actuation method with high output impedance, add compliance at the end point and use feedback control to modulate the force acting through the spring. This is done by directly measuring spring deflection or strain in the spring.

Figure 3-1 shows the main components of a series elastic actuator with the shaded line indicating the division between power domain and signal domain. The main elements are:

- Elasticity
- Control System
- Motor
- System Inputs

It is important to point out that topologically, this minimal model is no different from any actuator with closed-loop force control. Any actuator of this sort will have a motor, a sensor with compliance and a control system. The major difference between series elasticity and other actuators with closed-loop force control lies in stiffness of the sensor. This subtle yet very important difference is the key to series elastic actuators.

In section 3.1.4 through section 3.1.2, I define and describe the four main elements of the general model for series elastic actuators. The definitions lead to the derivation of the open-loop model and subsequently the closed-loop general model for series elastic actuators in section 3.2.

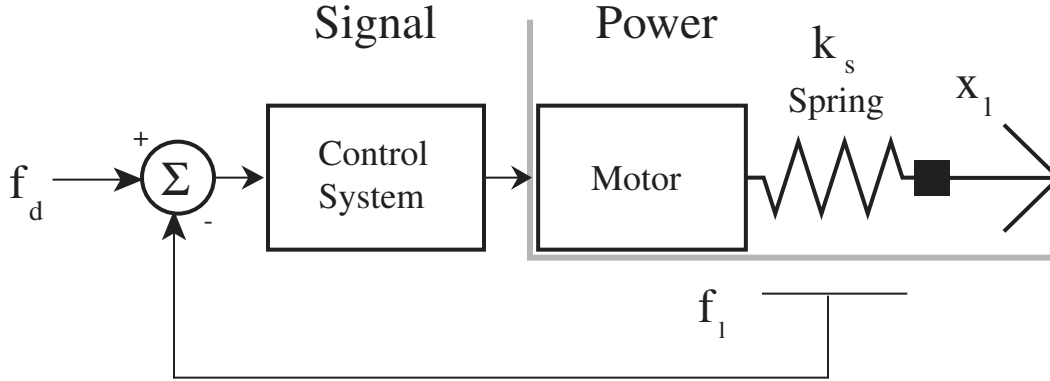


Figure 3-1: Minimal model for a series elastic actuators. There are four parts to a series elastic actuator: elasticity, control system, motor, and system inputs. The compliance is a simple linear spring with a stiffness of k_s . The force in the spring, f_l , is equal to the spring deflection times the stiffness. The control system consists of a simple proportional controller with gain K . The motor is modeled as a high impedance velocity source. The position output of the motor, x_m , is the time integral of the motor velocity. The system inputs or boundary conditions are the desired force, f_d and the load position, x_l .

3.1.1 Elasticity

The elasticity in the actuator is a transducer and thus has two parts. One part, the spring, is in the power domain and the other part, the strain or deflection sensor, is in the signal domain.

The elasticity is a simple linear spring with a spring constant of k_s . It is load bearing but passive and is placed at the output of the motor. Depending on the spring stiffness, the deflection can be significant in order to cover the full force output range of the actuator.

The sensor measures the deflection or strain in the spring which is a representation of the force, f_l , acting through the spring. I assume that there is no hysteresis in the spring and therefore the relationship between force and spring deflection is defined by Hooke's Law [18]:

$$f_l = k_s x_s \quad (3.1)$$

where x_s is the spring deflection.

In an ideal world x_s is defined by the difference between the actuator position x_a and the load position x_l .

$$x_s = x_a - x_l. \quad (3.2)$$

While it is possible to measure both x_a and x_l and take the difference for the measurement, it is not recommended. There may be uncorrelated noise between these two measurements due to transmission dynamics and other non-linearities. In order to reduce noise from the compliant sensor, it is much better to make a single direct measurement of the spring strain x_s . Regardless, I assume that the measurement of the spring strain is a very good representation of the force output of the actuator.

3.1.2 Control System

The spring strain measurement x_s implies the load force f_l (equation 3.1) or force in the spring and is used for feedback in a control system. Given that there is some desired force f_d for the actuator, the error between these two signals will define the input to the controller f_e :

$$f_e = f_d - f_l. \quad (3.3)$$

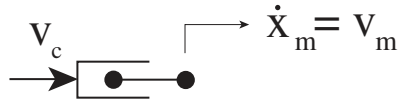


Figure 3-2: Graphical representation of the minimal motor model. The minimal motor model is a high impedance velocity source. It neglects inertia and has an instantaneous limit of force and velocity. It represents idealized models of both a hydraulic piston as well as an EM motor with a transmission.

Throughout this thesis, emphasis is placed on controller simplicity in order to understand the basic characteristics of the complete actuator. For the purpose of this discussion, the control system is represented by the controller gain K . Therefore, the control law for the general series elastic model is:

$$v_c = K f_e \quad (3.4)$$

K has the proper units to convert force error to desired actuator velocity.

With further controller development, improvements in overall system performance can be realized. However, a proportional control law K clearly demonstrates the closed-loop effects of the compliant load sensor. Premature introduction of complex control systems would cloud understanding of the underlying issues. There are ample methods for controller design once the basic concepts of the plant characteristics are clarified [42, 65].

3.1.3 Motor

The motor converts energy into mechanical force and motion. For the electro-mechanical domain, the actuator system consists of a motor, transmission and motor amplifier. Force on the motor mass creates a high impedance velocity output through the transmission. Similarly, for the hydraulic domain, the motor consists of a piston and servo valve connected to supply and return pressure. The servo valve modulates fluid flow and thus velocity of the piston output. The piston too can be considered a high impedance velocity source. Therefore, the motor in the minimal model is also assumed to be a high impedance velocity source and has a simple relationship between controller output, v_c , and motor output, v_m .

$$v_m = K_m v_c \quad (3.5)$$

where K_m is the gain of the actuator. In this representation, motor inertia is neglected and it is assumed that the actuator can perfectly generate the output velocity given the commanded velocity v_c . This is analogous to flow rate control in the hydraulic domain and velocity control in the electro-magnetic. The minimal motor model is graphically depicted in figure 3-2.

Since the force in the spring is a function of motor position, I relate the motor position as the time integral of the velocity

$$x_m = \int v_m(t).$$

In the Laplace domain it can be written as

$$X_m = \frac{V_m}{s}. \quad (3.6)$$

Substituting equation 3.6 into equation 3.5 and solving for the actuator position output X_m , creates a transfer function relating controller velocity to motor position

$$X_m = \frac{K_m}{s} V_c. \quad (3.7)$$

Since the actuator has such high impedance, it is assumed that the force in the spring, f_l , is

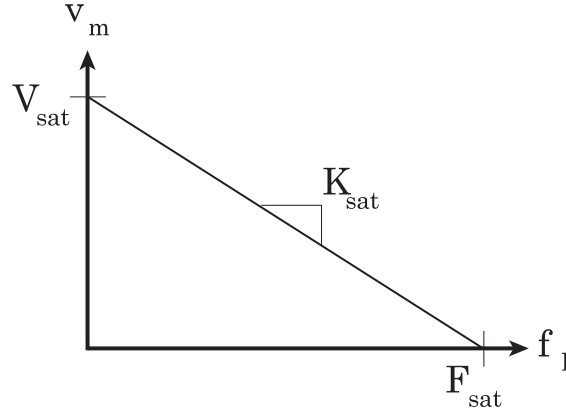


Figure 3-3: General motor saturation model. All motors have limits to the instantaneous force and velocity output capabilities. The line connecting the maximum load force, F_{sat} , and the maximum actuator velocity, v_{sat} , defines the envelope in which the motor can operate. The slope of the saturation line is $K_{sat} = \frac{v_{sat}}{F_{sat}}$.

equal to the force generated in the motor, f_m . Real motors typically have instantaneous limits on force and velocity output capabilities. Therefore, I include a simple saturation limit for this motor model. This is graphically shown in figure 3-3.

F_{sat} represents the maximum steady state force output of the actuator. V_{sat} is the maximum motor velocity under zero load. Therefore, the motor velocity, v_m , is limited by

$$v_m \leq V_{sat} \left(1 - \frac{f_l}{F_{sat}} \right). \quad (3.8)$$

It is important to point out that typically motor systems should be designed to be low impedance devices when used in force control situations. However, in this case it is actually advantageous to have a high impedance motor modulating the position of the spring for two reasons. First, the causality of the spring dictates that it should have a position input to give a force output. The better that the motor can modulate the spring position, the cleaner the force output of the spring. The second reason is that it is easier to control the velocity and thus the position output of real motors than it is the force. This is due to the fact that real motors and transmissions have non-linearities such as backlash and stiction that create force noise in the system.

Such a simple motor model is hardly representative of real motor and assumptions to justify this model are extreme. Nevertheless, a first order actuator model captures the essence of series elasticity. More complex actuator models will be applied when discussing the case studies of two real actuators in the following chapters.

3.1.4 System Inputs

The final part of the minimal model to discuss is the system input or the boundary conditions. There are two boundary conditions:

- f_d – desired output force.
- x_l – motion from the load or robot link.

The desired force is in the signal domain. The value of f_d is generated by a higher level controller. Ideally, the output force of the actuator equals f_d with one-to-one correspondence in magnitude and phase over the frequency spectrum.

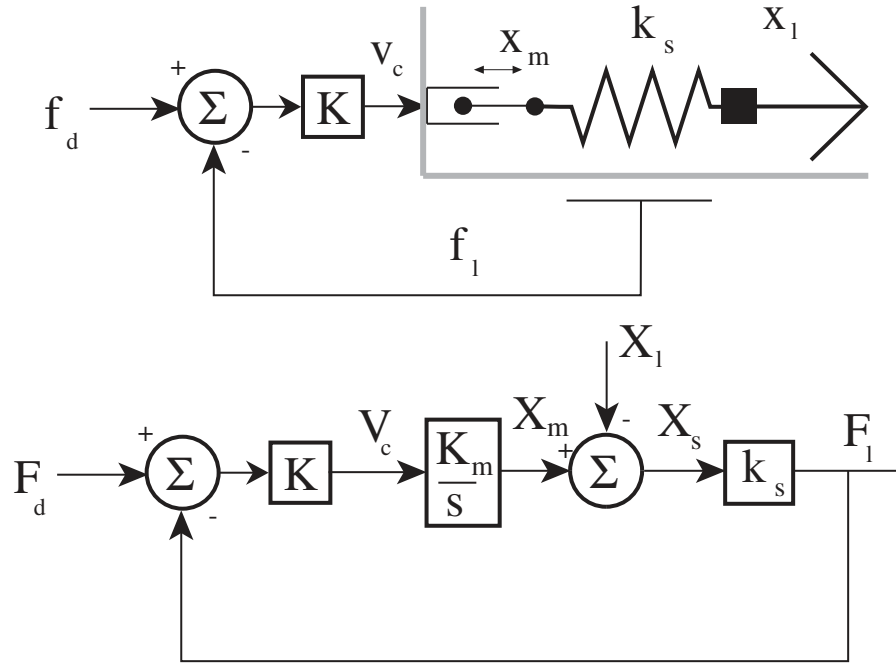


Figure 3-4: Minimal model and block diagram for a series elastic actuator. The figure on top is a time domain graphical representation of the the minimal series elastic actuator. The bottom figure shows a block diagram representation of the actuator.

The motion of the load, x_l , is in the power domain. Since the actuator is used in force control situations, it may be either directly in contact with the environment or it may be connected to a freely moving inertial load. When in contact with the environment, the load position can be considered a position source either fixed or moving. However, an inertial load moving in free space defines the load position as a function of the force in the spring and the load mass. There is energy interaction between the spring and the load that must be taken into account.

It is instructive to first look at the case when the load is in contact with the environment. In a subsequent section (section 3.4), I consider the case of the inertial load mass.

3.2 Minimal Linear Model Derivation

With each of the main elements of a series elastic actuator defined, the minimal model can now be derived. Figure 3-4 shows the model in both time and frequency domain representations.

The goal of the actuator is to control the force in the spring, F_l . I use the model in figure 3-4 to derive the linear dynamic equation for F_l as a function of the two inputs F_d (desired input force) and X_l (position of the load).

3.2.1 General Power Domain Open-Loop Model

The force in the spring F_l is directly proportional to the spring's displacement X_s (equation 3.1). X_s is a function of the motor output X_m and the boundary condition for position of the load X_l (equation 3.2). Substituting equation 3.2 into equation 3.1 for X_s

$$F_l = k_s X_s$$

$$= k_s (X_a - X_l)$$

and subsequently putting equation 3.7 into the result for X_a yields the open-loop dynamics for the force in the spring of a general series elastic actuator:

$$\boxed{F_l = k_s \left(\frac{K_a}{s} V_c - X_l \right)}. \quad (3.9)$$

Equation 3.9 shows that the open-loop power domain model for the force in the spring, F_l , is a function of the input from the controller and the position of the load.

3.2.2 General Closed-Loop Model

The closed-loop dynamic equation can be derived by including feedback and a control law. From equation 3.4, the input force to the actuator V_c is proportional to the error difference between the desired and load force.

$$V_c = K (F_d - F_l) \quad (3.10)$$

Combining the open-loop power domain model (equation 3.9) with the control law (equation 3.10) gives

$$\begin{aligned} F_l &= k_s \left(\frac{K_a}{s} V_c - X_l \right) \\ &= k_s \left(\frac{K_a}{s} K (F_d - F_l) - X_l \right). \end{aligned}$$

Solving the equation for F_l , we get the closed-loop dynamic equation of a general series elastic actuator

$$\boxed{F_l(s) = \frac{k_s K K_a F_d(s) - k_s s X_l(s)}{s + k_s K K_a}}. \quad (3.11)$$

The inputs for equation 3.11 are as described in the previous section 3.1.4, the desired force F_d and the motion of the load X_l .

3.3 Minimal Model Analysis

The open-loop model (equation 3.9) and the closed-loop model (equation 3.11) are symbolic and do not represent a physical actuator system. This generic model does, however, help us look at the key characteristics of series elastic actuators. In particular, the open-loop power domain model of equation 3.9 and the closed-loop model of equation 3.11 help us discuss:

- Bandwidth
 - Small force closed-loop bandwidth
 - Large force bandwidth
- Output Impedance
- Impact Tolerance

There are two inputs to the series elastic actuator, desired force, F_d , and load motion, x_l . By looking at the effects of each of these two inputs independently, the closed-loop bandwidth and output impedance can be understood as two separate cases. These two cases completely define the linear characteristics of the actuator.

The first case has fixed load motion where x_l is constant. Rewriting equation 3.11 with this constraint defines the *closed-loop bandwidth*. The relative values of the control gain, K , and the

spring stiffness of the sensor, k_s , play an important role in defining the actuator bandwidth. In the control of a series elastic actuator, a decrease in spring stiffness is compensated for an increase in control gain in order to maintain a high closed-loop bandwidth.

Under the same conditions of fixed load motion, it is also helpful to investigate the *large force bandwidth* capabilities of the actuator. Large force bandwidth is defined as the ability of the actuator to oscillate at a full steady-state output force level. Force and velocity saturation limits of the actuator and the low stiffness of the spring, reduce the ability of the actuator to output large forces at increased frequency. Low forces can be generated to the full closed-loop bandwidth. However, the large force bandwidth is typically smaller and is limited by the open loop dynamics of the system.

In the second input case, the load end is forced to follow a specific trajectory and the desired force is held constant. Rewriting equation 3.11 under this constraint defines the *output impedance* which is a measure of how well the system responds to external disturbances. In other words, the output impedance defines how well the internal dynamics of the actuator are decoupled from load motion. I explain the important role that the the spring stiffness, k_s , plays in minimizing output impedance.

Impact tolerance has to do with the ability of the actuator to handle impact loading. This is a function of the external motion constraint in the general model and the output impedance described in section 3.3.3. A soft spring stiffness in the sensor and an increased controller gain help the actuator lengthen the time of impact that in turn minimizes peak impact forces.

3.3.1 Case 1: Fixed Load – Closed-loop Bandwidth

By assuming a fixed load, $X_l = X_o$ where X_o is a constant (figure 3-5), we can write the closed-loop forward transfer function relating the load force F_l to desired force F_d .

$$G_{cl}(s) = \frac{F_l}{F_d} = \frac{k_s K K_m}{s + k_s K K_m}. \quad (3.12)$$

For low frequencies, the transfer function is unity. There is a one-to-one correspondence between the desired force and measured output force. As frequency increases, the actuator response begins to drop off (bandwidth). Since this is a first order model, the controlled bandwidth, ω_c , can be defined as:

$$\omega_c = k_s K K_m \quad (3.13)$$

It is a function of the spring constant, k_s , controller gain, K , and motor gain, K_m . In this simple case with an ideal actuator, there seems to be no limit to controlled actuator bandwidth. Increasing the gain K will give any desired bandwidth. However, practical intuition says that actuators cannot have infinite bandwidth.

Bandwidth limits

Research into the fundamental limits to force control bandwidth has been done previously [15, 16]. This previous work considers the problem of robot endpoint force control. In order to maintain clarity, the analysis in that research is simplified to focus on a one degree-of-freedom robot. The results of that research directly apply to this thesis which focuses on a one degree-of-freedom actuator. Topologically, the model used in the previous research and the general series elastic actuator are equivalent.

Since this work has been done previously, I do not perform an analysis of force controlled actuator bandwidth limitations. For the sake of completion, I list the findings of the previous work which gives several potential bandwidth limits. The fundamental factors that limit the force bandwidth applicable to series elastic actuators are five fold:

- Non-colocated dynamics – Dynamics between the the power modulator (i.e. motor amplifier or servo valve and the sensor).
- Plant nonlinearities (i.e. transmission backlash and friction, actuator saturation, intermittent contacts such as impacts)

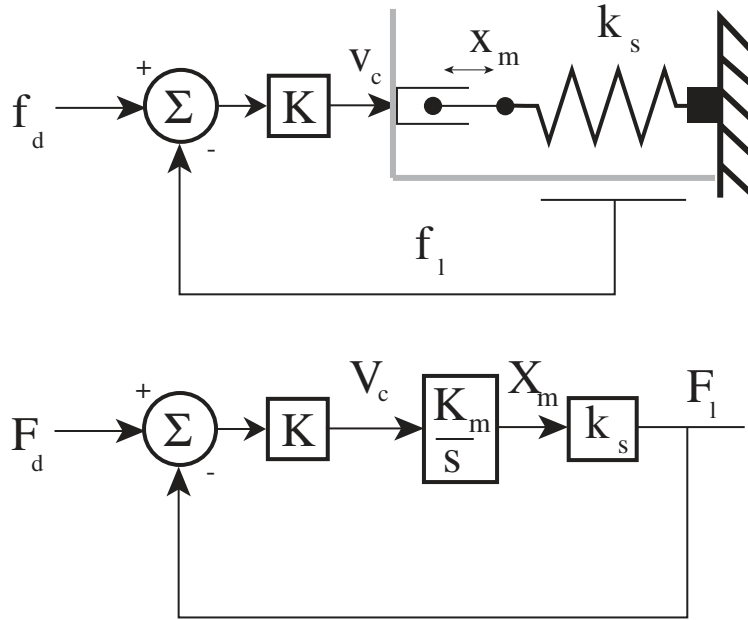


Figure 3-5: Fixed load model and block diagram – case 1. (Top) A fixed load constraint defines the closed-loop bandwidth of the system by isolating the relationship between desired force and load force. (Bottom) A block diagram of case 1 shows that the model is a simple first order system.

- Bandwidth limitations of the power modulator.
- Finite sensor resolution
- Controller Dynamics

Depending on the design of the actuator system, any of these five can be the limiting factor. I use the analysis in the previous work and discuss how each limitation applies to series elastic actuators.

Physical examples of non-colocated dynamics include compliance in the transmission of electro-mechanical actuators and compressibility of the fluid in hydraulic actuators. Non-colocated dynamics represent higher-order dynamics that may be excited as the closed-loop bandwidth of the actuator is increased. These, typically unmodelled dynamics, can drive the system to instability with very high controller gain.

For most actuator systems, the plant non-linearities, such as stiction or backlash in the transmission or intermittent contacts, hinder the ability to effectively modulate closed-loop force control. Control systems often cause these actuators to hunt around the desired force and cause chatter. To eliminate hunting and chatter, control gains are reduced which in turn reduces the controlled bandwidth. It is interesting to note that when using a stiff load sensor, the magnitude of backlash in a transmission can represent a significant portion of the sensor deflection. Using a compliant sensor reduces the effect of backlash and other non-linearities. This is discussed later in further detail.

Even though the power modulator in an actuator system is often assumed to have infinite bandwidth, it too has bandwidth limitations. A motor amplifier for the electro-mechanical domain and a servo valve for the hydraulic are physical examples of the power modulator. The motor amplifier operates in the kHz range. This is far above the frequency range of interest in series elastic actuators and probably does not significantly affect the overall bandwidth performance. Hydraulic servo valves, however, have low frequency first order dynamics that strongly affect actuator bandwidth performance.

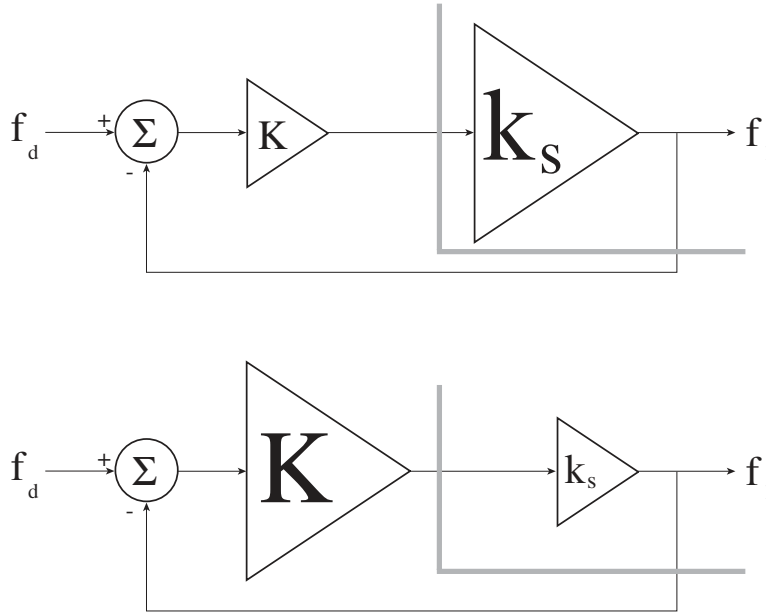


Figure 3-6: Zero order model for moving the gain from the power domain to the signal domain. A series elastic actuator removes gain from the stiffness of the spring. The control system can then increase control gain while maintaining actuator stability. The stiffness of the spring is *not* a limiting factor in the closed-loop stability of the actuator.

Sensor resolution can take on many forms: encoder ticks, noise floor of a potentiometer, hysteresis in strain sensors and discrete motor poles. Each of these reduces information passed in either the forward or feedback loops. The sensitivity and bandwidth of an actuator cannot be raised above the limitation set by the sensors. Noise in the sensors is amplified with increased controller gain, which can lead to instability.

Finally, the controller dynamics can affect the closed-loop bandwidth. Low-pass filtering a noisy sensor adds poles to the controller dynamics. A similar effect comes from using an integral term in a controller which adds phase lag. However, it may be necessary to filter signals or have PI control to get zero steady state error. Therefore, it is important to remember that the controller itself can be the limit in bandwidth.

Moving system gain

There are various factors that limit the actuator bandwidth. Depending on the design and configuration one of the limitations will be dominant. Increasing closed-loop bandwidth is an optimization problem between all of the potential limitations. It is interesting to point out, however, that the spring stiffness, k_s , in the sensor is *not* one of the limits. k_s may represent high or low stiffness, but the fundamental bandwidth limit is independent of k_s .

As an aid to understanding how the bandwidth is independent of k_s , notice that the spring constant k_s and the control gain K are always together in the loop gain. The key point of series elastic actuators is that the spring is very compliant in comparison to the stiffness of a load cell. Therefore, by decreasing k_s it is possible to increase the control gain a proportional amount and maintain the same bandwidth of the actuator. *Series elastic actuators take the gain out of the sensor and put it into the control system.* (figure 3-6)

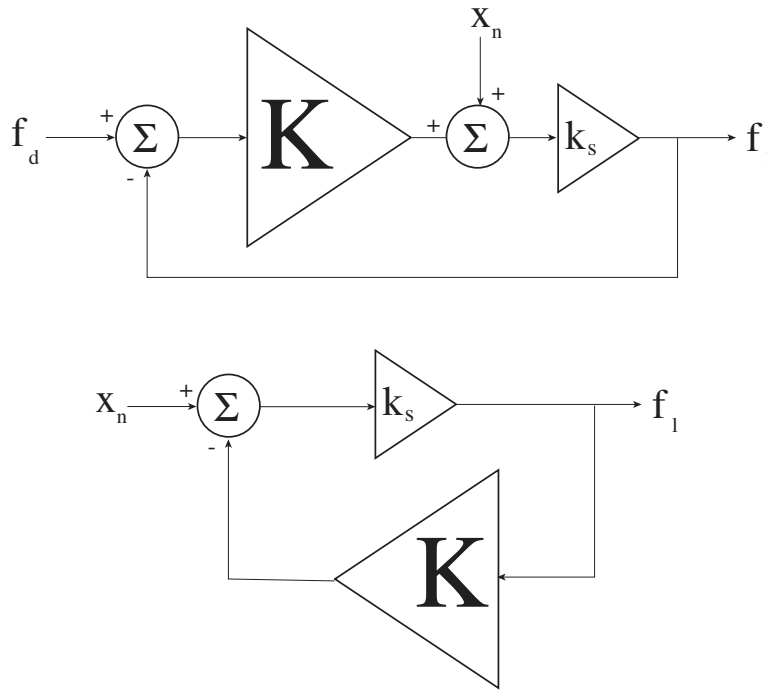


Figure 3-7: Zero order model for reducing sensitivity to internal position noise. With sensor stiffness gain and increased control system gain, internal position noise due to the transmission are greatly reduced. The provides for a very clean force output from the actuator.

Internal motion error rejection

Mathematically it is unimportant how gain is distributed in a perfectly linear system. However, in real systems it is important. A real motor does not have perfect velocity output and always has some position or motion error. A motion error in the motor means that for a given desired position or velocity output from the motor, there is some variation from that output as expected in a linear model. An example of this is backlash in a gear train or ballscrew.

I represent a motion error as a noise function x_n adding to the system just before the elasticity. Figure 3-7 shows a zero order model of the internal position noise in the motor. If the desired force is held constant, then we can see the reduction in sensitivity of the internal position noise on the output force of the actuator and written as:

$$\frac{f_l}{x_n} = \frac{k_s}{1 + k_s K}. \quad (3.14)$$

Essentially, the sensitivity to position noise is reduced by $1/K$. As discussed above, decreasing k_s means that K can be increased. Using a compliant sensor and increasing the control gain dramatically reduces the effect of motion errors such as backlash in a series elastic actuator. The high control gain helps the actuator to create a very clean force output.

3.3.2 Case 1: Fixed Load – Large force bandwidth

Decreasing spring stiffness and increasing control gain does come with one tradeoff. Keeping the same boundary conditions with the load position constant, let us look at the tradeoff. In order to generate large forces, there must be a large elastic deformation (Figure 3-8). At steady state, the actuator can produce the maximum force output as defined previously, F_{sat} .

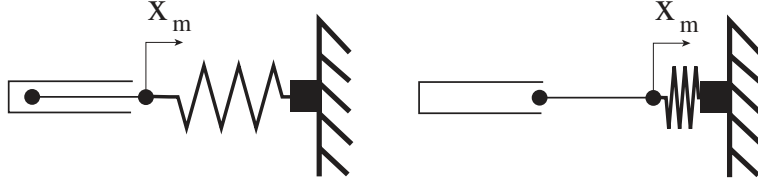


Figure 3-8: Large force equals large elastic deformation. In order to create a large force, there must be a large elastic deformation. This requires the motor must move. In order to oscillate at high force amplitude, the motor must move very quickly.

Remember that the motor has limits in its instantaneous force and velocity capabilities. As long as the motor operates within those limits, the overall linear bandwidth of the actuator is not affected by the compliance in the spring. However, the large force bandwidth is significantly altered. Large force bandwidth is defined as the frequency range over which the actuator can oscillate at a force amplitude equivalent to the maximum force, F_{sat} .

Because of the compliance, the actuator can only modulate the maximum force over a certain frequency range. This large force bandwidth, hereafter referred to as ω_o , is less than the bandwidth of the complete closed-loop system when using a very compliant sensor. The actuator can still produce force above ω_o but maximum force capability decreases with increased frequency.

This can be understood intuitively by remembering that the power producing element in the actuator must move a significant amount in order to compress the compliant springs and generate the maximum force. If the actuator has velocity and force saturation then there is a limit to the frequency at which the actuator can oscillate at maximum force. Decreasing the stiffness of the spring means that the distance the actuator must move to achieve maximum force is increased, thereby decreasing the large force bandwidth. The opposite is true for increasing the stiffness.

I introduce a function $F_{l_{max}}$ that is the maximum amplitude the actuator can oscillate at any given frequency.

$$f_l(t) = F_{l_{max}}(\omega) \sin(\omega t) = k_s x_m(t) \quad (3.15)$$

I also relate $F_{l_{max}}$ to the velocity of the motor.

$$\dot{f}_l(t) = F_{l_{max}}(\omega) \omega \cos(\omega t) = k_s v_m(t) \quad (3.16)$$

Take the force relationship in equation 3.15 and the motor velocity relationship in equation 3.16 and substitute them into the motor saturation constraint of equation 3.8 for v_m and f_l .

$$\begin{aligned} v_m &\leq V_{sat} \left(1 - \frac{f_l}{F_{sat}} \right) \\ \frac{F_{l_{max}} \omega \cos(\omega t)}{k_s} &\leq V_{sat} \left(1 - \frac{F_{l_{max}} \sin(\omega t)}{F_{sat}} \right) \end{aligned} \quad (3.17)$$

Solving the inequality for $F_{l_{sat}}$ gives

$$\frac{F_{l_{max}}(\omega)}{F_{sat}} \leq \frac{k_s \frac{V_{sat}}{F_{sat}}}{\omega \cos(\omega t) + k_s \frac{V_{sat}}{F_{sat}} \sin(\omega t)} \quad (3.18)$$

In order to better understand the function $F_{l_{sat}}$, let us look only at the magnitude of the function in equation 3.18.

$$\frac{F_{l_{max}}(\omega)}{F_{sat}} \leq \frac{k_s \frac{V_{sat}}{F_{sat}}}{\sqrt{\omega^2 + \left(k_s \frac{V_{sat}}{F_{sat}}\right)^2}} \quad (3.19)$$

Equation 3.19 has been normalized to the maximum force F_{sat} . In this minimal model case, the large force bandwidth or saturation bandwidth follows a first order profile. It can be thought of as

$$\frac{F_{l_{max}}(\omega)}{F_{sat}} \leq \frac{k_s \frac{V_{sat}}{F_{sat}}}{s + k_s \frac{V_{sat}}{F_{sat}}} \quad (3.20)$$

At low frequency $F_{l_{max}}$ equals F_{sat} . As frequency increases, the magnitude of $F_{l_{max}}$ begins to decrease. The break point is at the saturation frequency. Here the saturation frequency or large force bandwidth is defined explicitly

$$\omega_o = k_s K_{sat} \quad (3.21)$$

where K_{sat} is equal to $\frac{V_{sat}}{F_{sat}}$ or the slope of the instantaneous force and velocity limit of the motor.

ω_o is a function of two elements in the open-loop dynamics of the power domain, K_{sat} and k_s . K_{sat} represents the saturation characteristics of the actuator. It defines how much power can be put into the spring of the force sensor. k_s is the spring constant of the sensor. Since, k_s is very compliant in a series elastic actuator, the large force bandwidth is significantly lower than it would be if a stiff load cell were used in the feedback loop.

Figure 3-9 graphically demonstrates an example of large force bandwidth. The closed-loop bandwidth of the actuator is four times higher than the saturation bandwidth, $\omega_c = 4\omega_o$. The maximum output force for the actuator is 500 pounds. The plot has been normalized in frequency to ω_o . The actuator can oscillate up to the full closed-loop controlled bandwidth as long as it does not exceed the saturation limits of the motor. However, as the magnitude of oscillation increases, the motor saturation dominates the large force output capabilities of the actuator.

For many robotic applications, especially force control situations, having a large saturation bandwidth is unnecessary. The maximum output force of the actuators are only required at low frequencies. Having a reduced saturation bandwidth is the key engineering trade off of series elastic actuators. It is important to match the stiffness of the sensor to the requirements of a task. Therefore, choosing a proper ω_o for the actuator is critical for making closed-loop actuator force control work properly.

Equivalent saturation frequencies can be defined for the large force bandwidth as a function of the open loop dynamics of the power domain for both electro-mechanical and hydraulic systems. This will be discussed in the case studies of the following chapters.

A reduced large force bandwidth is the main reason for performance gains in the improved output impedance and impact tolerance discussed next.

3.3.3 Case 2: Forced Load Motion – Output Impedance

The second case of interest is when the load is free to move and the desired force is fixed $F_d = F_o$ (figure 3-10). With F_d fixed, the dynamics due to the desired force are eliminated. Therefore, the transfer function relating the change in load force F_l due to the load position x_l can be written as

$$Z(s) = \frac{F_l}{x_l} = \frac{-k_s s}{s + k_s K K_m}. \quad (3.22)$$

This equation is referred to as the output impedance. F_l has been adjusted to be centered on F_o . Therefore, this is the impedance around the constant desired force F_o . However, often it is important to know the impedance of the actuator when $F_o = 0$.

As described in the thesis introduction, mechanical impedance is adapted from the idea of impedance in electrical circuits [26]. Output impedance is a measure of the stiffness of a system for a given load motion. For example, the impedance of a spring is its spring constant because the spring constant relates an input position to output force. For robot actuators, low impedance is desirable.

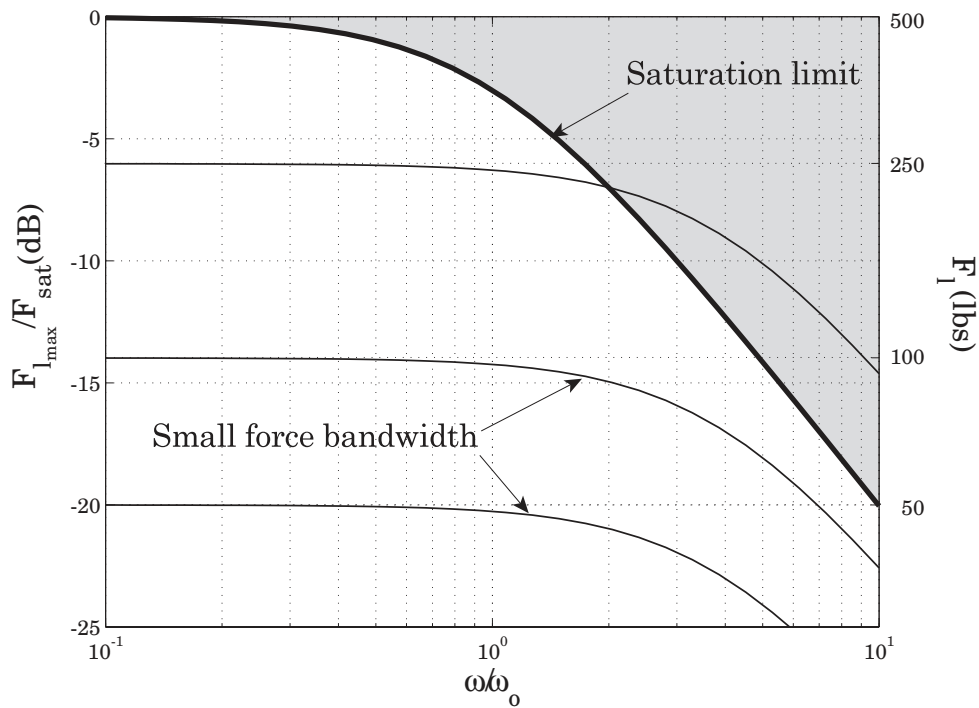


Figure 3-9: SIM Small force and large force bandwidth. The small force closed-loop bandwidth is unaffected by the large force saturation constraints. However, as the magnitude of oscillation increases, the motor saturation dominates the large force output capabilities of the actuator. The more compliant the spring, the smaller the large force bandwidth. This is the key engineering tradeoff for series elastic actuators.

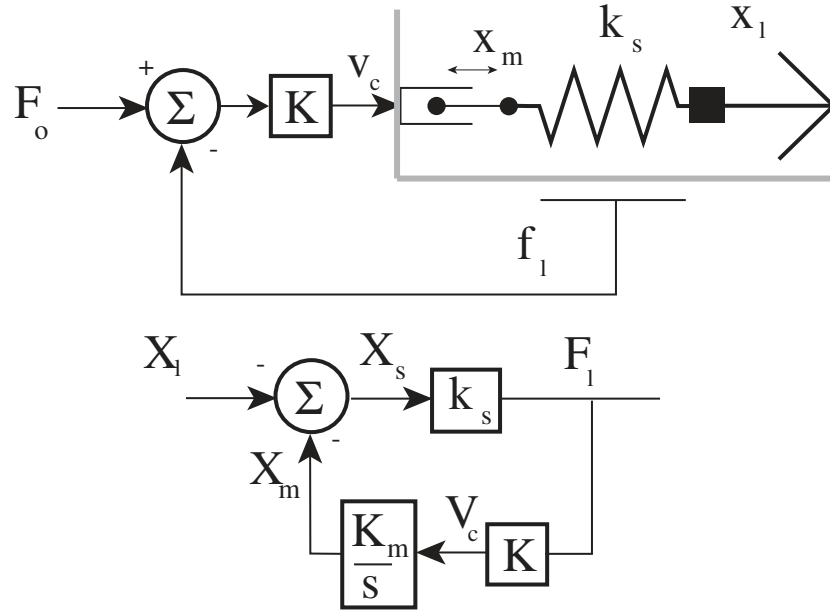


Figure 3-10: Forced load motion model and equivalent block diagram. (Top) The desired force is fixed constant, $F_d = F_o$, and the load motion is defined externally. The relationship between load motion and output force is defined as the output impedance. (Bottom) The block diagram shows that the feedback system and actuator dynamics are in the feedback loop.

Sensor	Stiffness (lbs/in)
Transducer Techniques LBO-500	500,000
Century Die Spring D-1222-A	$4 \times 450 = 1,800$

Table 3.1: Comparison of sensor stiffness. The top load cell is a standard off the shelf component. The bottom entry is the stiffness of the springs actually used in the prototype actuators of this thesis. The value shown is the one listed in the catalog. Experimentally, the springs were 12% more compliant.

The output impedance in equation 3.22 is minimal at low frequency. At high frequencies, the impedance is equal to the spring stiffness of the physical spring in the sensor. Very low impedance at low frequencies is equivalent to having a zero rate spring connected to the load. Any load mass will move around and react to the actuator force commands almost entirely decoupled from the dynamics of the actuator itself.

There are two factors that reduce the impedance of the series elastic actuator, one passive and one active. The first is the fact that the spring stiffness k_s is greatly reduced from that of a stiff load cell. This is a passive effect and the lower spring stiffness may reduce the impedance by several orders of magnitude by itself. Table 3.3.3 shows the difference in stiffness from an off-the-shelf load cell versus the springs used in the series elastic actuator prototypes. The difference is greater than two orders of magnitude.

The second effect in reducing output impedance is due to the active control system. Note that the characteristic equation for both closed-loop forward transfer function (equation 3.12) and closed-loop

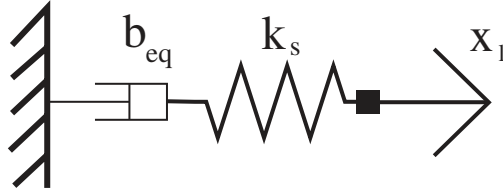


Figure 3-11: Equivalent impedance for the general series elastic actuator. The active impedance of the actuator can be thought of as an equivalent damper in series with the physical spring. At low driving frequencies, the actuator appears to be a damper. At high frequencies, the impedance is the stiffness of the spring.

output impedance (equation 3.22) is the same.

$$s + k_s K K_m = 0 \quad (3.23)$$

The argument previously given in case 1 for increasing the control gain K proportional to the reduction of spring stiffness k_s holds for the impedance as well. Therefore, not only is there a passive impedance reduction with the compliant spring, but the control system has an increased gain which further extends the low impedance range.

The output impedance has an active physical equivalent at low frequencies. Given that the load motion is slow enough or has low frequency content then the impedance looks like a physical damper.

$$F_l = b_{eq} s x_l \quad (3.24)$$

Where the equivalent damping coefficient is:

$$b_{eq} = \frac{1}{K K_m}. \quad (3.25)$$

The impedance of the actuator is graphically depicted in figure 3-11. It shows the equivalent damper in series with the physical spring. The damping effect is strongest at low frequencies and the passive impedance of the spring dominates at higher frequencies.

Depending on the actuator dynamics and the control system, the impedance can take on other physical equivalents at low frequencies such as an equivalent mass, m_{eq} . Although, the impedance is always equal to the spring stiffness at high frequencies.

The closed-loop bandwidth of the system, ω_c , is the frequency at which the damping effect and the passive impedance of the spring are the same. Regardless of the impedance bode profile, the increased compliance in the sensor dramatically reduces the overall output impedance of the actuator.

3.3.4 Impact Tolerance

Whenever a robot works in unknown surroundings it makes and breaks contact with that environment. The interaction power at the system interface is subsequently transferred through the robot structure and can be significant. To minimize interaction power, most force controlled robots move very slowly in anticipation of contact. If the impact power is too high, there is the potential for damage to the robot structure, actuators and to the environment. Series elastic actuators maximize impact tolerance by the use of the load bearing compliant sensor and can operate at high speeds even in the presence of potential impacts.

While the energy transferred to the actuator is independent of spring stiffness, the spring and control system reduce the peak impact power to a range within the actuators output power capabilities. This power matching insures that the impact energy does not exceed the load capability

of the actuator. The compliance allows the actuator to move out of the way of the impact while maintaining the proper desired force.

As an example of the impact power in the actuator from an unexpected load, I assume that the environment defines a sudden load motion v_l . The impact power, P_l , from the load is defined by the load force and velocity at the spring output.

$$P_l = F_l v_l \quad (3.26)$$

The spring compression defines F_l .

Assuming that the desired force in the actuator is $F_d = 0$, the general model for impedance (equation 3.22) can be redefined in terms of velocity rather than position.

$$\frac{F_l}{v_l} = \frac{k_s}{s + k_s K K_m} \quad (3.27)$$

Combining equations 3.26 and 3.27 gives the controlled impact power.

$$P_l = v_l^2 \frac{k_s}{s + k_s K K_m} \quad (3.28)$$

There are two parts to equation 3.28. The first is v_l which is defined by the environment. There is no control over this constraint. Therefore, in order to minimize interaction power, I focus on the second part of the equation which is due to the actuator.

The second part contains information about the actuator characteristics namely spring stiffness, control gain and bandwidth. Remember that this is the load interaction power regardless of the spring stiffness. The power contribution due to the actuator is at worst $1/KK_m$. As mentioned above, because of the sensor's compliance decreasing loop gain, the control gain K can be increased. Clearly from equation 3.28, as control gain increases, the impact power decreases. The impact power spectrum rolls off at higher frequency with the break point at the controlled bandwidth of the actuator but this effect is secondary.

3.4 Mass Load

The two inputs to the system model are desired force, F_d , and load motion, x_l . The use of load motion as an input irrespective of potential load dynamics has to do with the fact that the actuator load condition is typically unknown. The robot can be in contact with the environment but it could also be moving in free space. When the robot is in contact with the environment, the situation is analogous to case one with the load motion fixed. When the robot is not in contact with the environment, there is an inertial load on the actuator that can move in free space.

Let us look at the specific case for a mass load moving in free space under force control from a series elastic actuator in one dimension. Since the robot may be operating like this often, it is helpful in understanding how the load responds to the series elasticity in the actuator as a function of the input force F_d (figure 3-12).

I show that there are important differences when an actuator is connected to a finite inertial load from when it is rigidly connected to ground. Understanding these differences helps quantify actuator limitations.

3.4.1 Forces on the load

Since the load mass is moving in free space, its motion, x_l , is defined by the force through the spring, F_l , and by its own mass, m_l .

$$x_l = \frac{F_l}{m_l s^2} \quad (3.29)$$

This is equivalent to Newton's classic equation $F = ma$ written with Laplace variables.

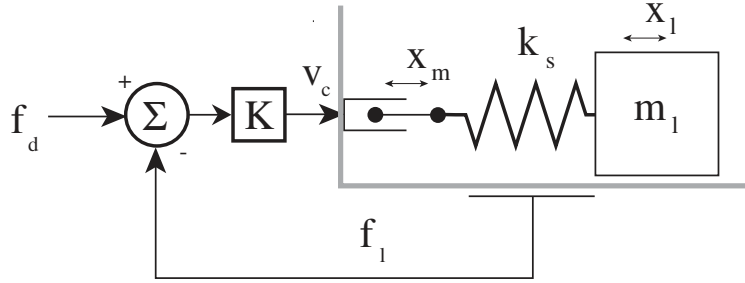


Figure 3-12: General series elastic actuator with load mass moving in free space. In this particular case, the load motion, x_l , is explicitly defined as a function of the loads mass, m_l , and the force in the spring, F_l .

We know from equations 3.1 and 3.2 that the force in the spring is

$$F_l = k_s(x_m - x_l) \quad (3.30)$$

where x_m is the actuator motion defined previously. I rewrite the expression for x_m using equations 3.7 and 3.10

$$\begin{aligned} x_m &= \frac{K_m}{s} F_c \\ &= \frac{K_m}{s} K(F_d - F_l) \end{aligned}$$

By putting the actuator motion, x_m (equation 3.31), and the load motion, x_l (equation 3.29), into the equation for the force in the spring (equation 3.30) gives

$$\begin{aligned} F_l &= k_s(x_m - x_l) \\ &= k_s \left(\frac{K_m}{s} K(F_d - F_l) - \frac{F_l}{m_l s^2} \right). \end{aligned}$$

Solving this equation for F_l , we get the force in the spring as a function of the desired force. Remember that in this case the load mass is free to move.

$$\frac{F_l}{F_d} = \frac{k_s K K_m s}{s^2 + k_s K K_m s + \frac{k_s}{m_l}} \quad (3.31)$$

Notice that the characteristic equation of the transfer function in equation 3.31 is now second order due to the load mass and spring resonance. Our previously derived transfer function (equation 3.12) relating desired force to load force was only first order.

Let us focus on the last term in the denominator of equation 3.31. I define this term as the load frequency, which is the resonant frequency of oscillation for the load mass and spring.

$$\omega_l^2 = \frac{k_s}{m_l} \quad (3.32)$$

Ideally, ω_l should be as small as possible meaning that m_l should be large. As $\omega_l \rightarrow 0$, equation 3.31 reduces to

$$\frac{F_l}{F_d} = \frac{k_s K K_m}{s + k_s K K_m}.$$

This is identical to closed-loop bandwidth in equation 3.12 discussed previously with the load position

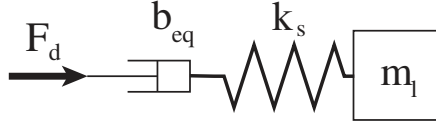


Figure 3-13: Equivalent model of the general series elastic actuator with load mass. The desired force is seen through a damper before the spring. A simple proportional controller does not make the actuator a force device.

held constant.

There are two terms in the definition of ω_l : m_l and k_s . Both of these terms can reduce the effect of the resonance on closed-loop force performance.

As m_l increases, ω_l gets smaller. In the limit, as $m_l \rightarrow \infty \implies \omega_l \rightarrow 0$, and shows that infinite load mass is equivalent to a fixed end condition. However, load mass of a robot is always finite when moving in free space. If the the link inertia is large enough, it may be negligible. In the other extrem, when load inertia is zero, the actuator has nothing to push on and therefore generates no output force. Regardless, it is important to understand the robot link inertia to determine whether or not its effects are important.

In series elastic actuators, the k_s of the elasticity is small in comparison to standard load cell stiffness. This is good since a small k_s lowers ω_l just like an large m_l . This shows one more reason for the benefit of intentional elasticity in series with the load.

Load mass motion

Now that we know the force in the spring, we can look at the load motion as a function of the input force. Substituting equation 3.31 into equation for load motion as a function of force (equation 3.29), yields

$$\frac{x_l}{F_d} = \frac{1}{m_l s^2} \frac{k_s K K_m s}{s^2 + k_s K K_m s + \frac{k_s}{m_l}}. \quad (3.33)$$

Remember that $b_{eq} = \frac{1}{K K_m}$ and the equation further simplifies to

$$\frac{x_l}{F_d} = \frac{1}{m_l s^2} \frac{\frac{k_s}{b_{eq}} s}{s^2 + \frac{k_s}{b_{eq}} s + \frac{k_s}{m_l}}. \quad (3.34)$$

A careful examination of equation 3.34 shows that it is equivalent to a force pushing on a damper, spring and the load mass all in series. This is graphically represented in figure 3-13. The transfer function for the load motion consists of two parts. The first part is

$$\frac{1}{m_l s^2}. \quad (3.35)$$

This is the equivalent of a force pushing on a mass to produce motion. Ideally, the second part of the transfer function would be the equation for the closed-loop bandwidth of the actuator.

$$\frac{F_l}{F_d} = \frac{k_s K K_m}{s + k_s K K_m}$$

While equation 3.34 shows this, because of the free zero in the numerator, the force pushing on the mass changes a little bit at low frequencies. In order help clarify the meaning of all the term in the

load motion transfer function (equation 3.34), the parameters can be rearranged to give

$$\frac{x_l}{F_d} = \frac{1}{b_{eq}s} \frac{1}{\frac{m_l}{k_s}s^2 + \frac{m_l}{b_{eq}}s + 1}. \quad (3.36)$$

The motion of the load is a function of the desired force and appears to be a damper rather than a mass at low frequency. It has significantly decreased magnitude and increase phase lead. This effect is true up to the load mass spring resonant frequency ω_l . After that point in the frequency spectrum, the actuator behaves as expected with performance beginning to drop off above the controlled bandwidth.

The impedance of the actuator at low frequencies is a damper. This is perhaps a mismatched impedance with the load mass. A more appropriate impedance for the actuator could be an equivalent mass. Since the actuator model is first order, in order to have equivalent mass impedance, it requires an additional pole. Using an integrator in the control system, changes the dynamics of the actuator to second order. A second order actuator can match the impedance of the mass load and produce much better forces within the actuator closed-loop bandwidth.¹

Regardless of the impedance of the actuator (equivalent damper or inertia), the load inertia does have effect on the closed-loop force generation properties of the actuator. Creating a controlled system that at low frequencies looks like an equivalent mass is an important lesson used in the construction and control of the physical actuators. The case studies show that by understanding the actuator plant and developing an appropriate controller, it is possible to create an actuator that can be more reliably considered a virtual force source throughout the frequency spectrum of its controlled bandwidth.

3.5 Dimensional Analysis

Dimensional analysis often helps in understanding the basic relationships of the different variables in an equation. The equations in this chapter are simple enough to understand without going through the formality of dimensionless group reformulation. However, rewriting the equations for closed-loop bandwidth, large force bandwidth, output impedance and inertial load force from this chapter is a good exercise and will be helpful when applying dimensional analysis to the models in the case studies.

For the general model there are three dimensionless groups. The large force bandwidth, ω_o , defined in section 3.3.2 is used to normalize frequency. The other groups are a generalized system gain, κ , and a normalized mass-spring resonant frequency of the inertial load, L .

$$\begin{aligned} S &= \frac{s}{k_s K_{sat}} = \frac{s}{\omega_o} \\ \kappa &= \frac{k_s K K_m}{\omega_o} = \frac{k_s}{b_{eq}} \frac{1}{\omega_o} \\ L &= \sqrt{\frac{k_s}{m_l}} \frac{1}{\omega_o} = \frac{\omega_l}{\omega_o} \end{aligned} \quad (3.37)$$

- S is a scaled Laplace variable which normalizes s to ω_o .
- κ is the normalized gain in the system. In this case it represents the increase in frequency of the controlled system above the saturation bandwidth.
- L is the normalized load resonance of the actuator attached to a load mass. It represents the inertial load resonance in comparison to the saturation bandwidth.

¹Derivation of the closed-loop properties of general series elastic actuator with PI control is not done here. This derivation is similar enough to the hydro-elastic actuator contained in chapter 4 that the reader is encouraged to refer to that case study. Closed-loop dynamic equations that both include and do not include the load mass are explained there.

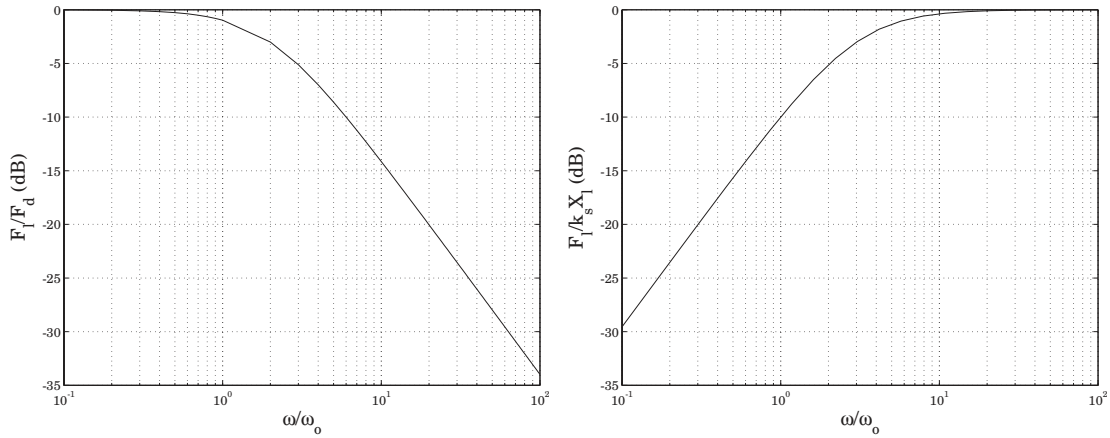


Figure 3-14: SIM General closed-loop forward transfer function (left) and output impedance (right). These figures are normalized to the saturation frequency ω_o and have $\kappa = 3$.

Closed-loop Bandwidth

The closed-loop forward transfer function relating the output force as a function of the desired force is written in equation 3.12. It is rewritten here for convenience.

$$G(s) = \frac{F_l}{F_d} = \frac{k_s K K_m}{s + k_s K K_m}.$$

Applying the dimensionless groups from equation 3.38 gives

$$G(S) = \frac{F_l(S)}{F_d(S)} = \frac{\kappa}{S + \kappa}. \quad (3.38)$$

This equation shows that the DC gain of the closed-loop system is still unity. κ indicates the breakoff frequency above the saturation frequency where the controlled system rolls off.

Closed-loop Output Impedance

The closed-loop output impedance is taken from equation 3.22. It is rewritten here.

$$G(s) = \frac{F_l}{x_l} = \frac{k_s s}{s + k_s K K_m}.$$

Applying the dimensionless groups from equation 3.38 gives

$$G(S) = \frac{F_l(S)}{k_s X_l(S)} = \frac{S}{S + \kappa}. \quad (3.39)$$

This equation is normalized to k_s and shows that the impedance is very low and increases at 20dB/dec up to the controlled bandwidth of the actuator. Remember that this is an equivalent damper with a low damping coefficient. At the point of transition, the impedance is equal the spring constant of the physical spring.

Both the normalized closed-loop forward dynamics and the output impedance are shown graphically in figure 3-14.

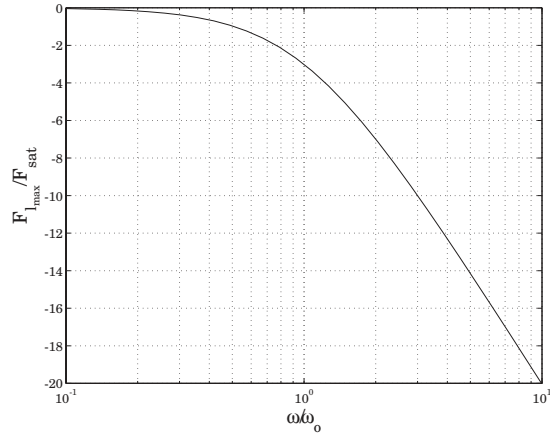


Figure 3-15: SIM General large force saturation bandwidth. The ability of an actuator to output its full steady state force level is compromised by the introduction of a very compliant spring. ω_o is the break frequency and is defined by the open loop dynamics of the actuator. The large force bandwidth is typically less than the controlled bandwidth of the actuator. Even though the actuator cannot achieve full force output at high frequency, it can and does operate above ω_o .

Large force bandwidth

Similarly, I normalize the large force bandwidth from equation 3.20.

$$\frac{F_{l_{max}}(S)}{F_{sat}} = 1S + 1 \quad (3.40)$$

This equation is pictured in figure 3-15. The saturation frequency is independent of the control system and is defined completely by the open-loop actuator dynamics and the spring constant k_s . Reduced saturation bandwidth is the tradeoff that must be made in the design of series elastic actuators.

Load Forces

Finally, I normalize the force in the spring as a function of the desired force when a load mass is attached to the actuator and is free to move. I rewrite equation 3.31

$$\frac{F_l}{F_d} = \frac{k_s K K_m s}{s^2 + k_s K K_m s + \frac{k_s}{m_l}}$$

Using the dimensionless groups gives

$$\frac{F_l(S)}{F_d(S)} = \frac{\kappa S}{S^2 + \kappa S + L^2} \quad (3.41)$$

This equation is graphically depicted in figure 3-16. In this case, $\kappa = 2$ and $L = 0.2$. The figure shows that up to the load natural frequency, the forces are equivalent to a damper. However, after that frequency, the actuator follows the expected bandwidth profile similarly depicted in figure 3-14.

3.6 General Model Summary

The minimal model helps to demonstrate some of the key ideas of using a significantly compliant force sensor for closed-loop actuator force control. In summary, the simple linear actuator model

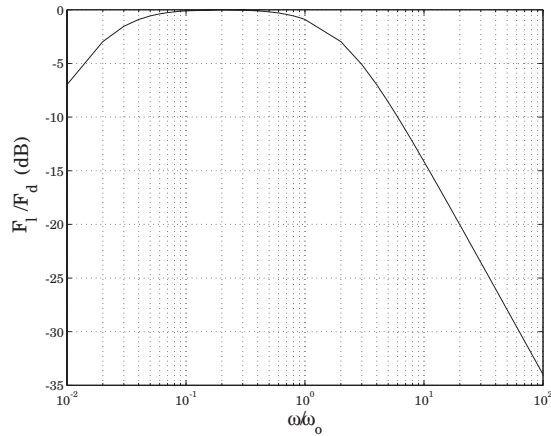


Figure 3-16: SIM General force bandwidth profile with load inertia moving in free space. The variables in the figure are $\kappa = 2$ and $L = 0.2$. Any finite load inertia causes the system to have damper like qualities at low frequency as well as the bandwidth reduction at higher frequencies. As $L \rightarrow 0$, the system behaves as if it has a fixed load end.

demonstrates and quantifies closed-loop bandwidth, large force bandwidth, output impedance, impact tolerance and the effects of an inertial load.

- **Closed-loop bandwidth** is *independent* of the spring constant. The reduction in sensor gain can be compensated for an increase in controller gain. The bandwidth is limited by other factors such as non-colocated dynamics and valve and amplifier limitations. The increased control gain gives a very clean force output.
- **Large force bandwidth** (saturation bandwidth) is reduced with the compliant sensor. The actuator can still operate above the saturation bandwidth even though the maximum force output capability is limited. Large force bandwidth is independent of control system. Understanding the difference between large force bandwidth and closed-loop bandwidth is key to the success of series elastic actuators.
- **Low output impedance** in the actuator is achieved by decreased spring stiffness and increased controller gain. Even stiff flow source actuator systems can be made to be actively backdriveable and have an impedance no greater than the spring stiffness k_s of the sensor.
- **Impact tolerance** comes from the spring absorbing energy from the environment which allows the actuator control system to minimize peak impact power. This protects actuator components from overload damage.
- The effects of an **inertial load** moving in free space are also demonstrated. In order to have the actuator be able to apply load forces to a mass, it must have the proper dynamics. It will be shown in the case studies that making the actuator appear as an equivalent mass at low frequencies is important for proper actuator operation.

The above ideas are discussed in further detail in specific case studies of applying series elasticity to the hydraulic domain and electro-mechanical domain.

Chapter 4

Hydro-Elastic Case Study

The minimal model for a series elastic actuator in the previous chapter is helpful for quantifying the important characteristics and tradeoffs when using series elasticity. The deficiency of the minimal model is the oversimplification of the motor. There are key differences between the minimal model and specific actuator implementations that deserve discussion.

This first case study looks at series elasticity applied to a hydraulic piston. The case is presented in a manner similar to the general model. The open and closed-loop models are derived and reformulated in terms of dimensional analysis. These models are used to discuss closed-loop bandwidth, saturation and impedance. The effects of load mass attached to the actuator moving in free space is also explained. A physical prototype has also been developed (figure 4-1). Where appropriate, experimental results are compared to the mathematical models.

4.1 Model Derivation

The hydro-elastic actuator is similar to the minimal model, with a few key differences in the control system and motor model. After clarifying these differences in the model definition, I derive two relationships from the closed-loop dynamic equations which quantify closed-loop bandwidth and output impedance. These equations are at the heart of understanding the hydro-elastic actuator.

4.1.1 Model Definition

There are four main components to the hydro-elastic actuator as seen in figure 4-2.

- System Inputs
- Motor
- Compliant Sensor
- Control System

The system inputs and the compliant sensor are the same as the general model. Specifically there are two system inputs. F_d is the desired output force and x_l is the motion of the load. The compliance of the sensor is defined by its spring constant, k_s . The spring is assumed to be linear in both tension and compression.

While the system inputs and elasticity are the same as the previous model, figure 4-2 shows that motor and the control system are different. Therefore, I focus on these differences.

Motor model

The power domain model for the hydro-elastic actuator consists of a servo valve connected to a hydraulic cylinder and piston. The piston is directly connected to the elastic element (figure 4-3).



Figure 4-1: Prototype Actuator CAD model. A 20MPa pressure source is connected to a MOOG series 30 flow control servo valve (not shown) that directs flow to the two chambers of the hydraulic cylinder. The piston is coupled to the output through four die compression springs. The spring compression is measured with a linear potentiometer which implies force. A closed-loop controller actively moves the piston to maintain a desired spring deflection.

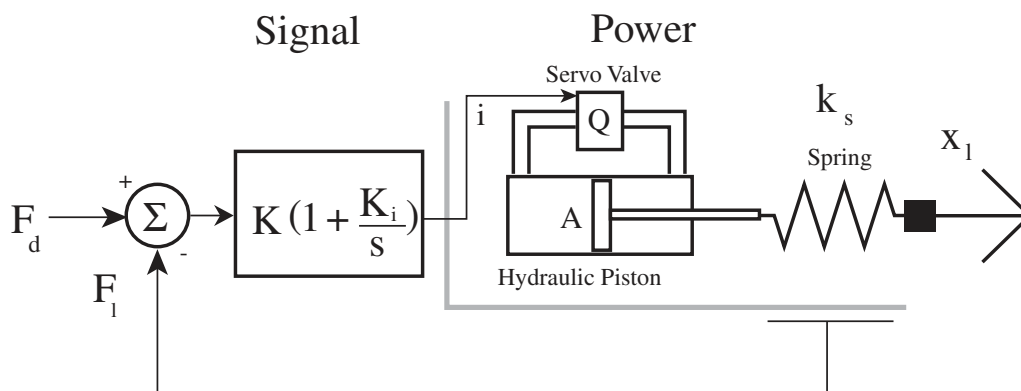


Figure 4-2: Hydro-elastic actuator model. The servo valve directs fluid flow into the hydraulic cylinder which moves the piston and thus compresses the elastic element. The strain in the spring is measured and used in a proportional-integral feedback control system.

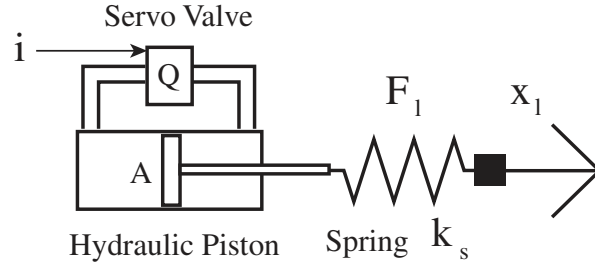


Figure 4-3: Power domain model for the hydro-elastic actuator. The force output of the actuator is determined by the compression of the spring. There are two inputs to the power domain. Q is the fluid flow from the servo valve and is a function of the input current i . x_l is a motion input from the environment.

The servo valve directs high pressure fluid flow, Q , into one of the two chambers in the hydraulic cylinder. The literature for the servo valve defines it as a third order system consisting of a low first order pole and a higher second order pole pair. Higher order dynamics in the valve are more than an order of magnitude above the frequency range of interest for the actuator. Therefore, in the mathematical analysis, the servo valve is assumed to be first order. Also, assuming no power saturation in the actuator for now, flow is a direct function of input current as seen in equation 4.1.

$$Q(s) = \frac{K_v}{\tau_v s + 1} i. \quad (4.1)$$

K_v is valve gain relating electrical current to fluid flow rate. τ_v is the first order time constant for the valve. Flow and pressure limits of the actuator are discussed later in the chapter.

The hydraulic cylinder houses the piston. Potentially, the piston could be double acting and the piston areas would be the same on both sides. Having different piston area essentially changes the *transmission ratio* from the fluid to the mechanical domain depending on which side of the piston is pressurized. This in turn alters the loop gain of the closed-loop system as well. Even though the physical actuator prototype is not double acting, in the model I assume that the piston areas are equivalent and defined by the area A . I do this for three reasons. First, in the real actuator the two areas are not significantly different from each other. Second, the gain margin of the actuator is very high. Therefore, there is a built in stability margin for change in loop gain. Finally, it simplifies analysis and aids in understanding the basic principles of the actuator.

A servo valve and hydraulic piston are very much like the ideal velocity controlled actuator system described in the previous chapter. The velocity of the piston output, v_p , is directly proportional to the flow rate, Q .

$$v_p = \frac{Q}{A} \quad (4.2)$$

The position of the piston can be written in laplace terms directly from equation 4.2

$$X_p = \frac{Q}{As}$$

Substituting equation 4.1 in for Q yields the piston position as a function of valve current.

$$X_p = \frac{K_v}{As(\tau_v s + 1)} i \quad (4.3)$$

Comparing the piston position (equation 4.3) to the actuator position output of the general

model in the previous chapter (equation 3.7 rewritten here for convenience)

$$X_m = \frac{K_m}{s} V_c$$

shows that they are essentially the same with two exceptions. The first is differences from simple parameter name variation. $\frac{K_v}{A}$ compared to K_a and i to F_c . The second difference comes from the bandwidth limitation of the servo valve, $\tau_v s + 1$. Up until the frequency $1/\tau_v$ the two systems are essentially the same. Therefore, much of the analysis applied to the general model also applies to the hydro-elastic actuator.

Control System

Feedback control of the actuator is closed by measuring the deflection of the spring which implies the force output, F_l , of the actuator and comparing that to a desired output force, F_d .

I use a PI controller on the error with controller gain K and integral gain K_i . As can be seen in equation 4.3, there is already one free integrator in the system. This is due to the fact that the valve controls fluid flow and the force in the spring is defined by position. The additional integrator is important for two reasons. The first is to help automatically compensate for non-linearities in the servo valve not accounted for in linear analysis. The second reason is that it is beneficial to make the actuator second order. This is especially important for the impedance at low frequencies as the actuator can be made to appear as an equivalent mass m_{eq} . The calculation for m_{eq} is defined later.

Returning to the control definition, I assume that the control gain K and K_i have the proper units to take voltage signals F_d (desired force) and F_l (load force) in the spring to control current, i , sent to the servo valve. This relationship is determined by:

$$i = K\left(1 + \frac{K_i}{s}\right)(F_d - F_l). \quad (4.4)$$

This controller puts a pole at the origin and a zero at $-\omega_i$ on the negative real axis where $\omega_i = K_i$.

4.1.2 Power Domain Model

The spring deflection determines the load force, F_l . This is a function of the piston position, X_p , and load motion, X_l . The hydraulic piston deflects the spring. Assuming that there is some counter force from the load, the force in the spring, F_l , is defined as a function of two variables: the flow from the servo valve, Q , and the relative position of the load, X_l . This relationship is derived to be:

$$\begin{aligned} F_l(s) &= k_s(X_p - X_l) \\ &= k_s\left(\frac{Q}{As} - X_l\right) \\ &= k_s\left(\frac{K_v}{As(\tau_v s + 1)}i - X_l\right) \end{aligned} \quad (4.5)$$

where k_s is the spring stiffness of the series elasticity.

4.1.3 Closed-loop Model

I derive the closed-loop model by substituting the controller equation (equation 4.4) into the power domain model (equation 4.5) for the valve current i . Rearranging and solving for F_l yields the closed-loop equation for the force through the spring as a function of the desired force, F_d , and the load position, X_l

$$F_l(s) = \frac{\left(\frac{s}{K_i} + 1\right)F_d(s) - \frac{A}{KK_iK_v}s^2(\tau_v s + 1)X_l(s)}{\frac{A}{k_sKK_iK_v}s^2(\tau_v s + 1) + \frac{s}{K_i} + 1}. \quad (4.6)$$

With the addition of the integral term in the controller, the closed loop system characteristic equation is third order.

4.1.4 Two input cases

As in the general model, it is helpful to write equation 4.6 as a function of the isolated input variables. For the first case, I assume that the load position is constant ($X_l = 0$). This eliminates the load motion. The second case is with the load end free to move and the desired force fixed. This is the output impedance and eliminates the dynamics due to desired force modulation. The transfer functions for these two cases completely specify the linear characteristics of the actuator.

Case 1: Fixed Load

By imposing a fixed end condition on the output and using equation 4.6, I write the closed-loop forward transfer function for case one which relates the desired force to the output force:

$$\frac{F_l(s)}{F_d(s)} = \frac{\left(\frac{s}{K_i} + 1\right)}{\frac{A}{k_s K K_i K_v} s^2 (\tau_v s + 1) + \frac{s}{K_i} + 1}. \quad (4.7)$$

At low frequency, this transfer function is equal to unity regardless of the controller values. In the limit as frequency goes to infinity the transfer function goes to zero. The servo valve may or may not have a significant effect on the closed-loop dynamics depending on the bandwidth of the actuator. As the controller gain increases, increasing bandwidth, the servo valve plays a more dominant role. Therefore, the true bandwidth limit of the system will depend on the servo valve characteristics.

Case 2: Free end with zero force

The other case is to assume that the desired force is zero and the output is free to move. This will be the zero load impedance. For case two, we write:

$$\frac{F_l(s)}{x_l(s)} = \frac{-\frac{A}{K K_i K_v} s^2 (\tau_v s + 1)}{\frac{A}{k_s K K_i K_v} s^2 (\tau_v s + 1) + \frac{s}{K_i} + 1}. \quad (4.8)$$

Opposite of the closed loop forward transfer function, the impedance at low frequency is small. This is the property we desire in order to make the actuator very insensitive to position inputs. A low output impedance implies that the actuator dynamics are decoupled from that of the load motion. With active control, the actuator is backdrivable. At high frequency, the transfer function is equal to the value of k_s , the spring constant of the physical spring. Essentially at higher frequency the piston cannot move and therefore the load only sees the spring.

4.2 Model Analysis

I discuss the hydro-elastic actuator with respect to the following characteristics:

- Saturation
- Closed-loop bandwidth
- Output impedance
- Proportional Control

Regardless of the control system, when using series elasticity, saturation plays an important roll in defining the large force output capabilities of the actuator. Taking some simplifying assumptions about the load/flow characteristics of the servo valve, I define a frequency at which the performance

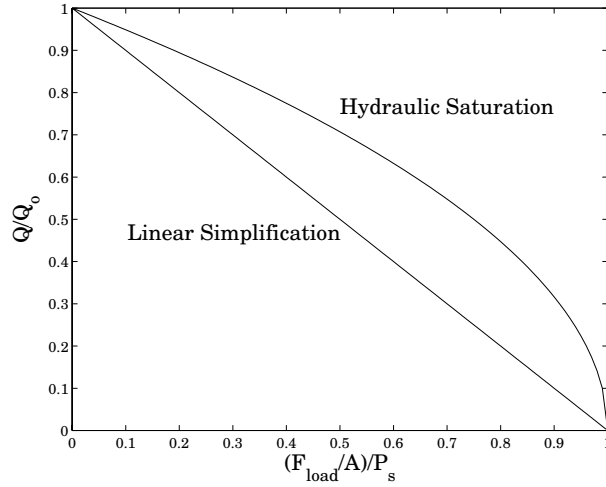


Figure 4-4: SIM The power saturation profile for a hydraulic servo valve is a square root relationship between flow and pressure. In order to understand the effects of saturation on the actuator through linear analysis, a linear saturation relationship is assumed. The linear profile is a worse case than the square root saturation.

of the actuator begins to diminish due to saturation. This frequency is then used to normalize the dynamic equations.

I next investigate equation 4.7 to understand the closed-loop bandwidth limitations of the actuator. Since the actuator is third order, I look at limitations of the control gains.

The output impedance of the hydro-elastic actuator is small at low frequencies. I look at the output impedance of equation 4.8 and quantify how well the actuator dynamics are decoupled from that of the load.

In an exercise of comparing the hydro-elastic model with the general model in the previous chapter, I eliminate the integral term of the controller and look at the effects on the closed-loop dynamic equations.

4.2.1 Saturation and Large Force Bandwidth

Regardless of the control system, the open loop characteristics of the actuator dominate the response when operating at the force and velocity limits of the servo valve. The maximum flow rate assuming a fully open valve is

$$Q = C \sqrt{P_s - \frac{F_l}{A}} \quad (4.9)$$

where P_s is the supply pressure, C is a servo valve sizing factor and F_l and A given previously. Equation 4.9 assumes a negligible return pressure in comparison to the supply.

Square root saturation is difficult to use in linear analysis. By assuming a linear saturation profile that is close to but a worse case than the square root saturation (equation 4.9), it is possible to understand the effect that the spring has on the large force bandwidth of the actuator (figure 4-4).

The linear saturation profile is defined as

$$Q = K_{sat} \left(P_s - \frac{F_l}{A} \right). \quad (4.10)$$

In this case $K_{sat} = \frac{Q_o}{P_s}$, where Q_o is the maximum flow rate for the rated current of the valve given no load. C in equation 4.9 and K_{sat} in equation 4.10 perform the same function relating pressure

to flow but they are not equivalent.

As a baseline for understanding the large force or saturation bandwidth, I assume that the load is fixed as in case 1. The load motion does effect the large force bandwidth but I take this one data point as a fixed reference. I also assume that the controller knows just what to do in order for the actuator to generate maximum force over the entire frequency spectrum. Since the actuator is good at low frequencies the large force bandwidth is independent of controller and is solely a function saturation characteristics of the hydraulic power domain.

As in the minimal model analysis, I define a function $F_{l_{max}}$ that is the maximum force amplitude of oscilation for the actuator at any given frequency. I insert the linear flow rate saturation into the open-loop power domain dynamic equation for the maximum force in the spring (equation 4.5).

$$\begin{aligned} F_{l_{max}} &= k_s \frac{Q_{max}}{A_s} \\ &= k_s \frac{K_{sat} \left(P_s - \frac{F_{l_{max}}}{A} \right)}{A_s} \end{aligned} \quad (4.11)$$

Simplifying this equation to solve for $F_{l_{max}}$ and normalizing by the maximum steady state output force, $P_s A$, shows that the actuator oscillating at its saturation force level has a first order bandwidth profile.

$$\frac{F_{l_{max}}}{P_s A} = \frac{1}{\frac{A^2}{k_s K_{sat}} s + 1} \quad (4.12)$$

Oscillating at low frequency, the system can achieve the maximum force output of the supply pressure times the piston area. However, the capability of the actuator begins to decline after the break frequency

$$\omega_o = \frac{k_s K_{sat}}{A^2}. \quad (4.13)$$

The careful selection of this frequency is critical to the performance of the actuator for its specified tasks. Even though, the actuator can still operate above ω_o , its maximum force capabilities are reduced. The large force bandwidth requirement of the task should be well defined. Note that this relationship was made independent of the control system.

Dimensionless formulation

In order to generalize and see the effects of the various parameters, both the closed-loop transfer function, equation 4.7, and the output impedance, equation 4.8, can be written in dimensionless form.

I normalize frequency about ω_o (equation 4.13) and generate the following dimensionless groups.

$$\begin{aligned} S &= \frac{s}{\omega_o} \\ I &= \frac{K_i}{\omega_o} \\ V &= \frac{1}{\tau_v \omega_o} \\ \kappa &= \frac{k_s K K_v}{\omega_o A} \end{aligned} \quad (4.14)$$

- S is a scaled Laplace variable which normalizes s to ω_o .
- I can also be written as ω_i/ω_o . It is the scaled placement of the zero on the negative real axis due to the integral term in the controller.
- V is the scaled time constant from the servo valve first order model. It is a measure of how much faster the servo valve is in comparison to the saturation bandwidth.

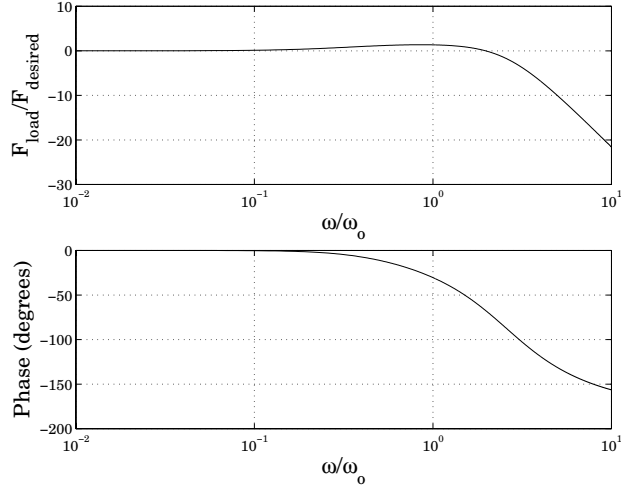


Figure 4-5: SIM This is a bode plot of the dimensionless closed loop system scaled to ω_o . Values for the plot were calculated from real parameters on the device: $\omega_o = 152$ rad/sec (25 Hz), $\kappa = 2$, $I = 0.3$ and $V = 4.4$.

- κ represents the scaled loop gain determined by the spring, size of the cylinder, valve gain and controller gain.

Using the dimensionless groups and the scaled Laplace variable, the dimensionless forward closed-loop and output impedance transfer functions can be written as:

$$\frac{F_l(S)}{F_d(S)} = \frac{\kappa V(S + I)}{(S + V)S^2 + \kappa V S + \kappa I V} \quad (4.15)$$

$$\frac{F_l(S)}{k_s x_l(S)} = \frac{-(S + V)S^2}{(S + V)S^2 + \kappa V S + \kappa I V} \quad (4.16)$$

In order to make the impedance, equation 4.16, truly dimensionless, it has been normalized to the spring constant k_s .

4.2.2 Case 1: Closed-loop Bandwidth

Figure 4-5 shows a bode plot for equation 4.15. The plot is normalized to ω_o . For reference, in the real actuator $\omega_o = 150$ rad/sec (≈ 25 Hz). The other values used in the plot are $\kappa = 2$, $I = 0.3$ and $V = 4.4$. These values are taken from the physical actuator discussed later. At low frequency, the system tracks very well. The system response dies quickly at a frequency above ω_o . The apparent resonance in figure 4-5 is a strong function of the zero introduced by the control system.

There are two major closed-loop bandwidth and stability limitations for the hydro-elastic actuator. The first is due to the dynamics of the servo valve. The second is due to the introduction of an integral term in the controller. The second limitation is not completely independent of the first but it is helpful to look at each separately.

Valve dynamics

The servo valve used in this thesis is specified as third order. However, given that the frequency range of interest for the actuator is low enough, a first order model is deemed sufficient for the basic analysis of understanding the fundamental characteristics of the actuator.

For the moment assume that the servo valve is linear and does not require integral control. Eliminating I from equation 4.15 and simplifying yields:

$$\frac{F_l(S)}{F_d(S)} = \frac{1}{\frac{S^2}{\kappa V} + \frac{1}{\kappa}S + 1}. \quad (4.17)$$

The natural frequency and the damping of the system are coupled. Nevertheless, increasing gain does not limit system bandwidth. The actuator may have very low damping at high gain but it still stable. This is true until the point at which the servo valve higher order dynamics come into play. The addition of just a small amount of phase from the unmodelled dynamics push the dominant poles of the controlled system into the right half plane. I realize that a simple lead controller could effectively extend the usable bandwidth of the actuator further. The important point though is that the actuator has fundamental limits in its bandwidth and stability due to the limitations of the valve.

Integral limitations

Unfortunately, the servo valve is not linear. At steady state there is a wandering null offset that must be accounted for using an integral term in the controller.

When using integral control, there is a controller pole placed at the origin that eliminates steady state error and a controller zero placed at a frequency equal to the integral gain K_i . The dimensionless group I represents the controller zero frequency with respect to the saturation frequency.

In order to understand the effect and limit of the integral term, it is helpful to apply Routh's stability criterion to equation 4.15. The expanded characteristic equation is:

$$S^3 + VS^2 + \kappa VS + \kappa IV = 0.$$

All of the coefficients are positive numbers. The array of coefficients becomes

$$\begin{array}{l|ll} S^3 & 1 & \kappa V \\ S^2 & V & \kappa IV \\ S^1 & \frac{\kappa V^2 - \kappa IV}{V} & 0 \\ S^0 & \kappa IV & 0 \end{array} \quad (4.18)$$

The condition that all roots have negative real parts is given by the term in the S^1 row.

$$\frac{\kappa V^2 - \kappa IV}{V} \geq 0$$

Reducing this equation to its simplest form, shows an important relationship between the servo valve time constant and the placement of the controller zero due to the integral term.

$$\begin{array}{l} V \geq I \\ \frac{1}{\tau_v} \geq K_i \end{array} \quad (4.19)$$

The controller zero must be placed at a frequency less than the first order bandwidth of the servo valve. It is interesting that this relationship is independent of the loop gain of the system.

Since our frequency range of interest is so low relative to the higher order dynamics in the servo valve they are typically neglected. However, similar to the proportional control case, the higher order dynamics also limit the overall loop gain of the actuator.

In summary, the stability and thus the bandwidth of the actuator is primarily limited by the relative slow dynamics of the servo valve. Regardless, the control system is capable of increasing gain high enough that the bandwidth of the actuator is sufficient for operation.

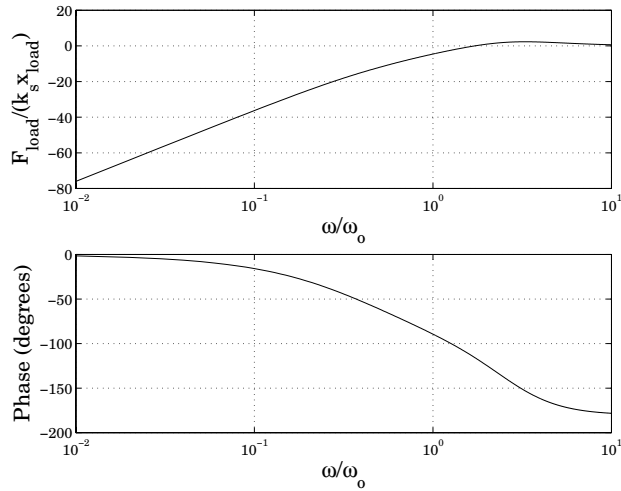


Figure 4-6: SIM The impedance of the actuator at low frequency is zero and is k_s at high frequency. The plot represents equation 5.14. It uses values $\omega_o = 152$ rad/sec (25 Hz), $\kappa = 2$, $I = 0.3$ and $V = 4.4$ which were calculated from the prototype actuator.

4.2.3 Impedance: Case 2

Equation 4.16 shows the dimensionless form of output impedance. I rewrite it here for convenience.

$$Z_{cl}(S) = \frac{F_l(S)}{k_s x_l(S)} = \frac{-(S + V)S^2}{(S + V)S^2 + \kappa V S + \kappa I V}$$

At low frequencies the impedance is small but in the limit as frequency increases, the impedance is equal to the stiffness of the physical spring, k_s . Equation 4.16 normalizes to k_s and figure 4-6 shows an example of the impedance. The figure uses the same values as in the closed loop forward transfer function in figure 4-5 and equation 4.15. In this example, the impedance up to and including the saturation frequency, ω_o , is significantly reduced.

Remember that the reduction in impedance comes from two characteristics of the series elastic actuator.

- Decreased the spring constant.
- Increased the control gain.

Increasing the control gain is desirable for increasing the bandwidth of the actuator. Here we see that a larger control gain will also decrease impedance. At high frequency the impedance will be equal to the stiffness of the spring in the load sensor, k_s . The unique part of series elastic actuators is that k_s is relatively low. Increasing the spring constant will actually hurt the impedance. For example, if $k_s \rightarrow \infty$ we will have the equivalent of a stiff load cell in series with the output. On the contrary, $k_s \rightarrow 0$ will be an actuator with almost zero impedance. Including a compliant spring dramatically reduces the impedance. Nevertheless, there must be an engineering decision which balances the desire for large force bandwidth and low impedance. Later, we discuss this tradeoff in more detail.

Notice that the impedance is rising at low frequencies at 40dB/dec. This means that there are two free zeros at low frequency. This can also represent an equivalent mass m_{eq} where

$$F_l = m_{eq} s^2 x_l. \tag{4.20}$$

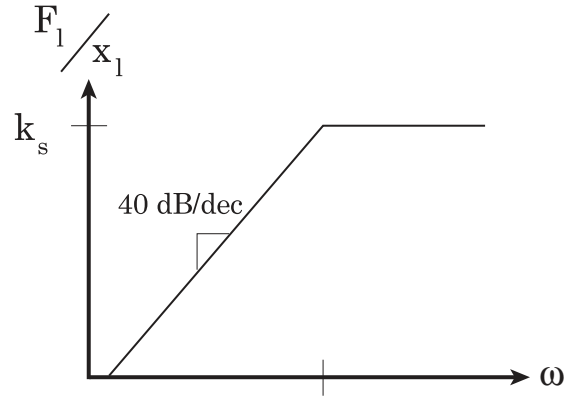


Figure 4-7: Rough characterization of hydro-elastic impedance. As shown in the simulation, the impedance at low frequencies is equivalent to a mass and is equal to the spring constant of the sensor at high frequencies.

m_{eq} does not represent a physical mass but rather an apparent one as defined by the impedance equation when frequency is very small.

$$m_{eq} = \frac{A}{KK_iK_v} \quad (4.21)$$

The higher the gain, the lower the equivalent mass.

Using a simple figure, let me summarize impedance. Figure 4-7 shows the impedance. At low frequencies, up to the controlled bandwidth of the actuator, the impedance can be considered equivalent to a mass. The load is essentially decoupled from the actuator dynamics except for this equivalent mass. At high frequencies, the load only sees the physical spring. Shock loads and other high frequency disturbances are filtered through this spring. Overall the impedance of the actuator is very low.

4.2.4 Proportional Control

It is interesting to look at the effects of the closed-loop system when the integral term of the controller is turned off. This leaves the controller as a simple proportional controller.

I rewrite equations 4.7 and 4.8 with $K_i = 0$.

$$\begin{aligned} \frac{F_l(s)}{F_d(s)} &= \frac{1}{\frac{A}{k_s K K_v} s(\tau_v s + 1) + 1} \\ \frac{F_l(s)}{x_l(s)} &= \frac{-\frac{A}{K K_v} s(\tau_v s + 1)}{\frac{A}{k_s K K_v} s(\tau_v s + 1) + 1} \end{aligned} \quad (4.22)$$

Eliminating the valve dynamics makes the equations identical to those of 3.12 and 3.22 except that the parameter names are different.

$$\frac{F_l(s)}{F_d(s)} = \frac{1}{\frac{A}{k_s K K_v} s + 1}$$

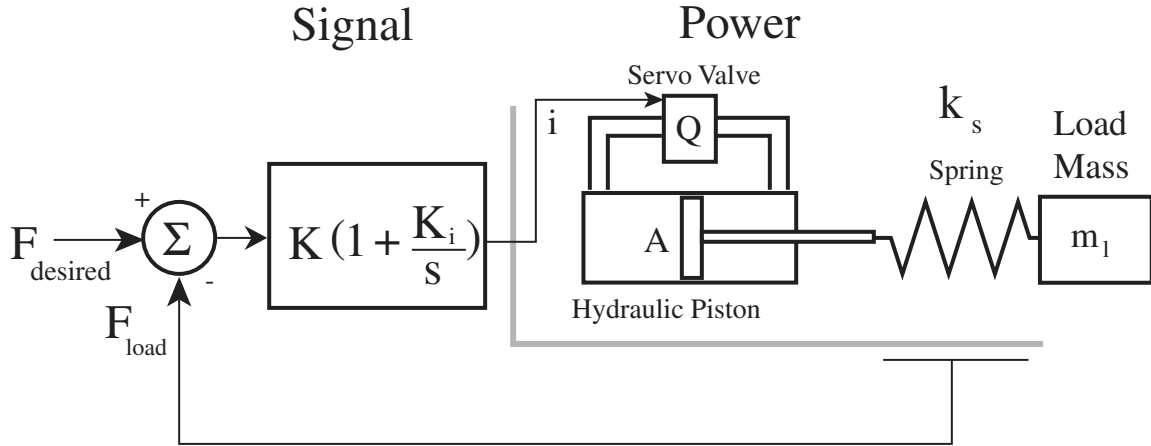


Figure 4-8: Hydro-elastic actuator model with load inertia moving in free space. Unlike the previous model where x_l is a system input defined by the environment, in this model the load inertia defines the motion of x_l as a function of the force in the spring. The load mass is part of the power domain and stores and releases kinetic energy as it moves.

$$\frac{F_l(s)}{x_l(s)} = \frac{-\frac{A}{KK_v}s}{\frac{A}{k_s KK_v}s + 1} \quad (4.23)$$

Notice that both equations are now first order. This is particularly important for the impedance. Since now it has only one free zero. The low frequency impedance now looks like a damper. In fact it is possible to even define an equivalent damping term for the hydro-elastic actuator just like was done for the general model.

$$b_{eq} = \frac{A}{KK_v}$$

From an impedance perspective, this exercise shows how important it is for the hydro-elastic actuator to have integral control. The extra zero in the impedance helps to further decouple the actuator dynamics from that of the load. This is further explained in the next section.

4.3 Effect of Load Mass

To this point in the case study, the load motion has been considered a system input. The reason for this is that the load has intermittent dynamics as it contacts the environment and then releases from it. Those types of interactions are difficult to model comprehensively. When in contact, the dynamics equations derived and discussed so far can be considered accurate. However, the actuator is most likely attached to an inertial load. When the load inertia is moving in free space, it becomes part of the power domain (figure 4-8). This situation is very important to understand. Ideally the low impedance of the actuator decouples the actuator dynamics from that of the load inertia. I show that if the load is above a minimum mass then the actuator can still be thought of as a pure force source within its closed-loop bandwidth capabilities.

4.3.1 Load Forces

Let us first derive the transfer function for the force in the spring, F_l , as a function of the desired force, F_d , with the inertia load free to move. The force in the spring is

$$F_l = k_s(X_p - X_l)$$

where X_p is the piston position and X_l is the load position. X_p is defined previously (equation 4.3)

$$X_p = \frac{K_v}{As(\tau_v s + 1)} i.$$

The motion of the load moving in free space comes from the force in the spring. I can write the force/position relationship as

$$X_l = \frac{F_l}{m_l s^2}. \quad (4.24)$$

Finally, recall that the current to the servo valve is defined by the controller as (equation 4.4)

$$i = K \left(1 + \frac{K_i}{s} \right) (F_d - F_l).$$

Substitute the controller into the equation for X_p . Use that result and the definition of the load motion to solve for the force in the spring, F_l as a function of the desired force F_d .

$$\frac{F_l(s)}{F_d(s)} = \frac{\frac{s}{K_i} + 1}{\frac{A}{k_s K K_i K_v} s^2 (\tau_v s + 1) + \frac{s}{K_i} + 1 + \frac{A}{m_l K K_i K_v} (\tau_v s + 1)} \quad (4.25)$$

Assume that the servo valve dynamics are negligible and the equation simplifies to

$$\frac{F_l(s)}{F_d(s)} = \frac{\frac{s}{K_i} + 1}{\frac{A}{k_s K K_i K_v} s^2 + \frac{s}{K_i} + \left(1 + \frac{A}{m_l K K_i K_v} \right)} \quad (4.26)$$

With one exception, equation 4.26 is identical to that of equation 4.7 derived earlier assuming that the load was fixed. The one exception is the s^0 term of the characteristic equation. This is the only term that contains the load inertia. In the case the $m_l \rightarrow \infty$, equation 4.26 becomes equal to that of the fixed load case.

Assuming that there is a finite load mass, let us analyze equation 4.26. Remember that the equivalent impedance mass of the actuator defined in equation 4.21 is

$$m_{eq} = \frac{A}{K K_i K_v}$$

The transfer function in equation 4.26 can be rewritten as

$$\frac{F_l(s)}{F_d(s)} = \frac{\frac{s}{K_i} + 1}{\frac{m_{eq}}{k_s} s^2 + \frac{s}{K_i} + \left(1 + \frac{m_{eq}}{m_l} \right)} \quad (4.27)$$

This equation clarifies that it is important to understand the relative magnitude of the ratio $\frac{m_{eq}}{m_l}$. The smaller the magnitude or the greater the load mass the less power interaction the load mass has with the spring.

Proportional control and load motion

Referring back to the transfer function in equation 4.26, I rewrite this equation eliminating the integral control gain, $K_i = 0$.

$$\frac{F_l(s)}{F_d(s)} = \frac{s}{\frac{A}{k_s K K_v} s^2 + s + \frac{A}{m_l K K_v}} \quad (4.28)$$

Again, as in the PI control case, if m_l is very big, equation 4.28 reduces to closed-loop dynamic equation for a fixed load. However, given a finite load, equation 4.28 ends up exactly as described in the general model case. Instead of being an equivalent mass and spring in series with the load, it

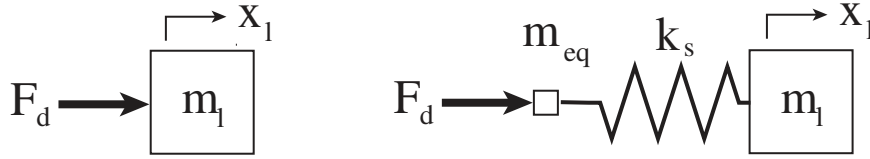


Figure 4-9: Control abstraction for the hydro-elastic actuator pushing on an inertial load. Ideally, the actuator produces the desired force directly on the load. However, the dynamics of the actuator turn out to be an equivalent mass and spring. The equivalent mass is defined by the control system and power domain characteristics. The spring is the actual physical spring in the actuator.

is an equivalent damper and spring. The equivalent damper for the hydro-elastic actuator is defined as

$$b_{eq} = \frac{A}{K K_v}. \quad (4.29)$$

An equivalent damper forcing the spring and load inertia has two problems having to do with the free zero in the numerator. The free zero causes the system to have phase lead at low frequencies. It also high pass filters all low frequency forces. If these limitations are not important or if these effects are unnoticeable, then the using a simple proportional controller is fine. However, caution should be used when looking at this problem. The effects of using a proportional controller with the hydro-elastic actuator is demonstrated experimentally as well.

4.3.2 Load Motion

Let us now look at the effect of the load motion with this dynamic equation. This relationship can be written as

$$\frac{X_l}{F_d} = \frac{1}{m_l s^2} \frac{\frac{s}{K_i} + 1}{\frac{m_{eq}}{k_s} s^2 + \frac{s}{K_i} + \left(1 + \frac{m_{eq}}{m_l}\right)} \quad (4.30)$$

There are two parts to equation 4.30. The first part is the dynamics of the load mass as a function of a simple force $F_d = m_l s^2 X_l$. The second part of the transfer function comes from equation 4.27 and represents the closed-loop dynamics of the actuator assuming a load inertia.

As long as the load mass is significant relative to the equivalent inertia of the actuator at low frequencies, the actuator performs quite well as a force source.

An abstraction of the actuator operation can be seen in figure 4-9. Ideally, the actuator pushes on a load with the exact desired force. The actuator, however, is limited. In its simplest model, the desired force pushes on and equivalent mass and spring in series with the load. The equivalent mass has been defined before and the spring is the physical spring in the actuator. Therefore, at low frequencies, the actuator works very well assuming that $m_l \gg m_{eq}$. Then the performance begins to taper off as the actuator reaches its bandwidth limit.

4.4 Physical Actuator

The following discussion elaborates on decisions made during the design and construction of a prototype hydro-elastic actuator (figure 4-10). This section also includes experimental results taken from the actuator.

4.4.1 Component Selection

The design space for hydro-elastic actuators is very large. Along with geometry and topology there are five major components in addition to the supply pressure source: servo valve, piston, spring,

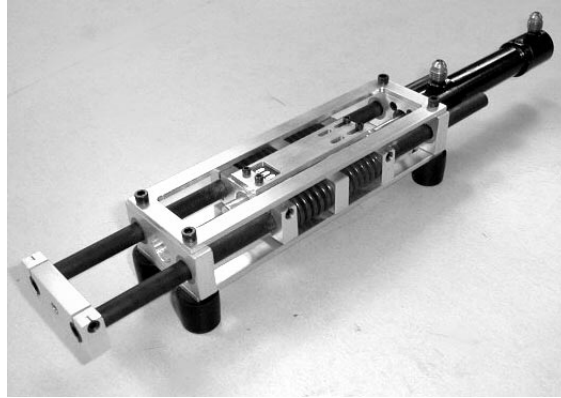


Figure 4-10: Prototype hydro-elastic actuator. The actuator has a piston with $0.2in^2$ area in one direction and $0.15in^2$ in the other. The piston pushes on precompressed die compression springs. Spring deflection is measured with a linear potentiometer. Although not shown, fluid is directed into the piston via a servo valve with a 3000psi pressure source.

sensor, and controller. Of all five components, choosing the spring is the only part of the actuator which requires unique perspective and is discussed in the next section.

The specifications for the servo valve, piston, and supply pressure need to be done based on the force, speed, and power requirements for a given task. These design requirements are not unique to hydro-elastic actuators and would be done for any hydraulic actuator. It is just important to remember that the bandwidth of the actuator will typically be some fraction of the servo-valve bandwidth. Therefore, when choosing the servo valve, it must have sufficient bandwidth to allow for that reduction.

Previous work done on force controllable hydraulics sacrificed seal tolerances on the piston and cylinder to help reduce stiction and coulomb friction during sliding [52, 73]. In the hydro-elastic actuator, since there is such a large motion to signal ratio, the effects of stiction and friction are virtually eliminated. Therefore, seals can be very tight with little to no degradation in performance.

The other limiting component to achieve high feedback gain is the sensor. The sensor needs to directly measure the spring deflection. This insures that the feedback measurement is a representation of true force regardless of any hysteresis or other losses in the spring. In the prototype, we use a linear potentiometer to measure spring deflection.

4.4.2 Choosing the Spring Constant

Selecting the spring constant is a balance between large bandwidth needing a high k_s and impedance needing a low one. We present some guidelines for choosing a spring constant.

1. Select a servo valve, piston, and supply pressure based on the force, speed, and power requirements for the given task. The characteristics of the servo valve will then define the maximum bandwidth of the actuator.
2. Define a minimum acceptable break point ω_o for large force bandwidth. Since the characteristics of servo valve, piston area and spring constant define this value, ω_o defines a lower bound on the stiffness of k_s .
3. Define a minimum tolerable impedance level which must also come from the task description. This places an upper bound on k_s .
4. Choose a spring within the two set bounds. It may be necessary to iterate. The non-dimensional equations will help in guiding to know whether to increase or decrease k_s and

Parameter	A1	A2	Units
Area	1.29	0.97	cm^2
Max. Force	2500	2000	Newton
Cont. Force	2500	2000	Newton
Min. Force	0.5	0.5	Newton
Max Speed	1.25	1.5	m/s
Spring Constant	286	286	kN/m
Max. Power	1500		Watts
ω_o	25		Hz

Table 4.1: Physical properties of Hydro-elastic prototype actuator. These properties are taken from component literature and from experimental tests.

how much effect it will have.

4.4.3 Physical Actuator Characteristics

A prototype actuator is used to demonstrate and test series elasticity in the hydraulic domain. Figure 4-10 shows the prototype actuator used in the experiments and table 4.4.3 gives the physical properties of the actuator. The experimental actuator is used to verify and demonstrate the following.

- Open-loop dynamics
- Controlled bandwidth
- Saturation (Large force bandwidth)
- Dynamic range
- Inertial load forces
- Shock tolerance

Where appropriate the experimental data is compared with theoretical models.

Open-loop dynamics

The prototype was built as an experimental test bed and did not necessarily have specific task requirements. Nevertheless, as a guideline, I attempted to design both the hydro-elastic actuator and the EM series elastic actuator to have similar characteristics. Table 4.4.3 shows the actual physical characteristics of the actuator.

I use a MOOG series 30 servo valve with a supply pressure of 20MPa (3000 psi). The 12.5 mm diameter cylinder is from Custom Actuator Products. The springs are Century die compression springs. The actuator output is connected in series with these springs. Regardless of whether the piston is pushing or pulling, the actuator maintains a linear measurable stiffness and deflection. The spring deflection is measured by a Novotechnik linear potentiometer. This measurement is then used in a feedback PI controller which has a desired force input. The output of the controller then defines a control input current to the servo valve.

The actuator is tested to verify its open-loop dynamic model. Frequency response for the open loop system of the servo valve, piston, spring and sensor system is shown in figure 4-11 for the both mathematical model and experimental setup. The figure is in units of Hertz and is not scaled to the saturation frequency as is done with the dimensionless model. For comparison sake only, the simulation includes a full third order servo valve. Model and experimental data match well in both magnitude and phase. The model even predicts the frequency of the higher order resonance but

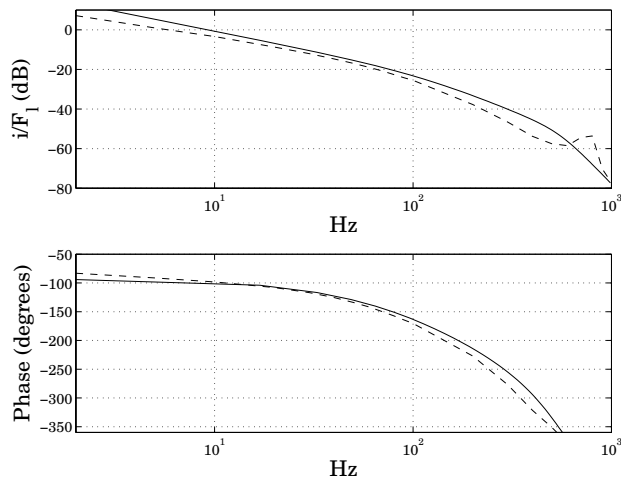


Figure 4-11: **REAL** Open-loop response for the servo, piston, spring and sensor. The solid line represents the mathematical model and the dashed line is experimental data. The simulation model uses a full third order servo valve. The model captures all important features except the light damping on 800 Hz resonance of the real servo valve.

does a poor job of matching the damping of that pole pair. Nevertheless, since the frequency range of interest is more than an order of magnitude below this frequency and the magnitude of this pole pair is virtually nil. Thus, the first order servo valve assumption is justified.

Closed-loop bandwidth

The open-loop model is closed with a PI controller. Remember that closed-loop bandwidth is measured with the load end fixed (case 1). For figure 4-12, $K = 3$ and $K_i = 50$. $K_i = 50$ indicates that the zero in the controller is placed at approximately 8Hz.

The closed loop actuator experimental frequency response is close to the mathematical model. Figure 4-12 shows there is good low frequency response. Somewhere in the 35-40 Hz range the response begins to drop off. Again, the 800 Hz pole pair is visible but has no effect on the overall system performance since its magnitude is so low in the closed loop system.

With the load end fixed, it is interesting to show a step response for the actuator (figure 4-13). The rise time is ≈ 10 msec and the system is settled in 50 msec. The actuator step response not only shows the speed of the actuator but it also demonstrates controller interaction non-linear stick-slip present in the open-loop system and how dither on the servo-valve helps to overcome it.

Figure 4-13 shows that the integrator in the controller keeps working on the errors in the system. Given that there is a small amount of stiction on the piston-cylinder interface or perhaps in the servo spool valve itself, the integrator slowly winds up the current to the servo valve. At some point, the stiction gives and then stops again. The integrator causes the actuator to hunt around the desired force in steady state.

To overcome this problem, I add a small amount of dither on the to the servo valve and the hunting behavior disappears. For this particular servo valve, I put the dither at 1% of its rated current oscillating at 100 Hz. Dither increases fluid leakage through the valve decreasing efficiency. However, the tradeoffs for closed-loop steady state performs are probably worth it.

Large force saturation

In section 4.2.1 we explain that with the introduction of significant elasticity, the actuator may often be operating at saturation levels because it must physically move a large distance to compress

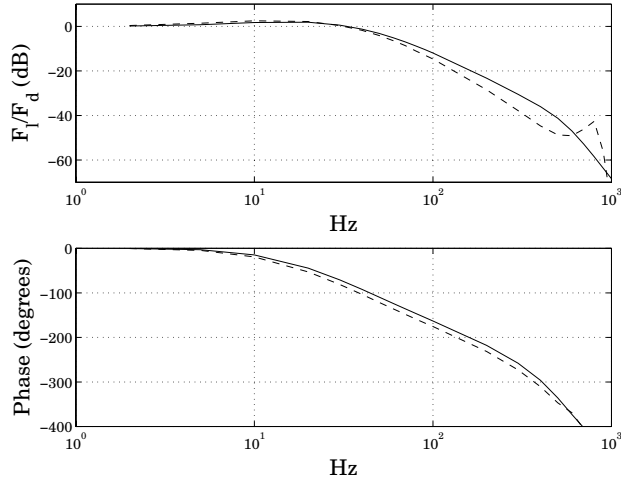


Figure 4-12: REALClosed loop response for the hydro-elastic actuator under PI control. The solid line represents the mathematical model and the dashed line is experimental data. As in figure 4-11, the simulation model uses a full third order servo valve. The two models match very well in both magnitude and phase for the useful frequency range.

Parameter	A2	Units
Spring Constant (k_s)	1600	$\frac{lbs}{in}$
Max. Flow Rate (Q_o)	12	$\frac{in^3}{s}$
Supply Pressure (P_s)	3000	$\frac{lbs}{in^2} (psi)$
Area (A)	0.2	in^2

Table 4.2: Important physical properties for force saturation. The point at which the actuator begins to show signs of large force saturation is dependent upon these physical parameters.

the spring to full force levels. The point at which the actuator performance begins to drop off at maximum force levels is defined as the saturation frequency and is solely a function of the open-loop characteristics of the actuator. For the hydro-elastic case, this saturation frequency is written in equation 4.13 and is rewritten here as

$$\omega_o = \frac{k_s K_{sat}}{A^2} = 160 \frac{rad}{s} = 25 Hz$$

and

$$K_{sat} = \frac{Q_o}{P_s}$$

where Q_o is the maximum valve flow rate given no load and P_s is the supply pressure. The values for the equation are taken from the literatur and are shown in table 4.2. It is important to point out that the value of K_{sat} is a constant for a given servo valve. If the actual operating supply pressure is less than the rated value, the maximum flow rate compensates such that the K_{sat} stays constant.

As a demonstration of the effects of force saturation on the hydro-elastic actuator, I command the actuator to oscillate at its maximum force level at different frequencies from 2 to 100 Hz. Figure 4-14 shows the results of the experiment.

The figure shows both the experimental data as well as a simulated large force profile. Both real and simulated data break around 25 Hz. However, the real data falls off at -40 dB/dec rather and

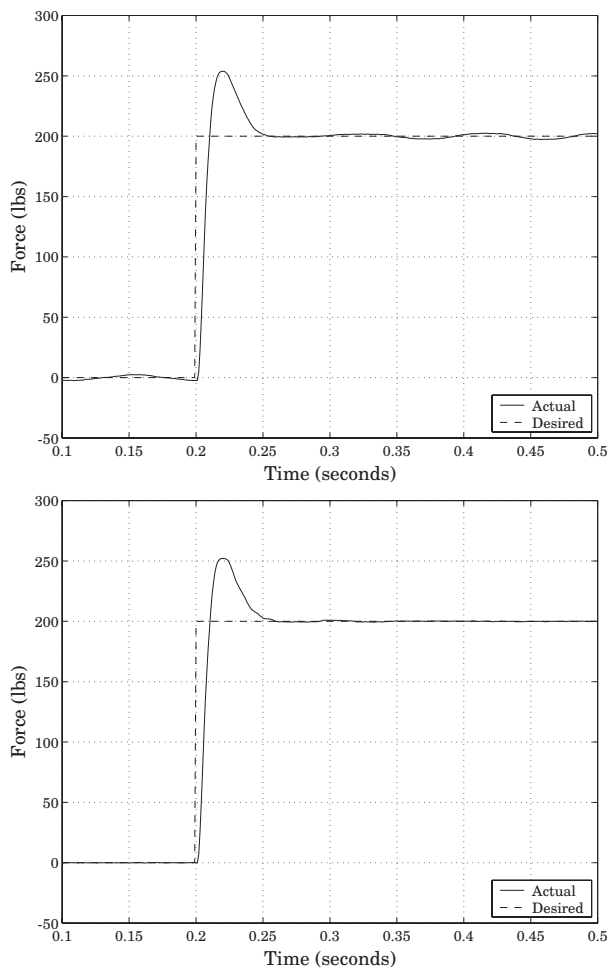


Figure 4-13: **REAL** PI control step response without and with servo valve dither. The integrator in the controller keeps working on the errors in the system. Given that there is a small amount of stiction on the piston-cylinder interface, the integrator keeps hunting around the desired force. I add a small amount of dither on the to the servo valve and the hunting behavior disappears. Regardless of the dither, notice the fast response time of the actuator. The rise time is ≈ 10 msec and the system is settled in 50 msec.

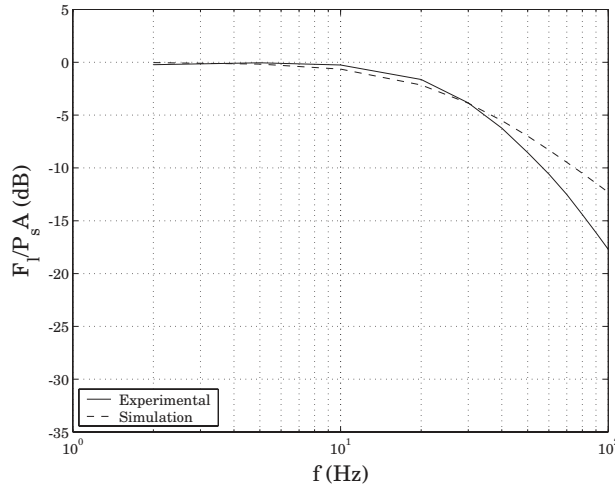


Figure 4-14: REAL Large force saturation for the hydro-elastic actuator. This is the response of the actuator when it is oscillating at its maximum force for different frequencies. The large force performance begins to drop off near the predicted saturation point of 25 Hz. After the response starts to die off, the first order bandwidth limitations of the servo valve begin to come into effect. This effect is not accounted for in the simulation. Therefore, there is a difference in the experimental and simulated responses at frequencies above the saturation point.

-20 as in a first order system. This is because at higher frequencies, the effect of the first order valve dynamics begin to play a role in the large force bandwidth.

Dynamic range

Formal impedance spectrum measurements have not been performed on the actuator. However, informally one can observe (experience) that it is easy to *backdrive* the actuator with finger force. The actuator *feels* massive with zero little friction it is commanded to output zero force. The minimum resolvable DC force was measured to be 1lb. This corresponds to a spring deflection equivalent to the noise floor of the sensor.

In an attempt to verify high force impedance and force sensitivity, we put the actuator in a configuration referred to as the *risky tester*. (figure 4-15). We suspend the actuator from the ceiling and then suspend me under the actuator in a swing. When the actuator is given a commanded force just above my weight, the actuator rises to the top of its stroke. If I pick up a 2 lb weight, then the actuator drops to the bottom. Releasing the weight causes it to rise again.

Depending on which side of the piston is pressurized, the maximum force level is 450lbs to 600lbs. With the minimum resolvable force equal to 1 lb then the dynamic range is $\sim 500:1$.

Inertial load forces

Earlier in the chapter, I discussed the effects of inertial loads moving in free space. Those results showed that an inertial load, m_l , has greatest effect on the actuator when the load mass is small in comparison the equivalent mass, m_{eq} , of the actuator. The closed-loop transfer function of equation 4.27 is rewritten here.

$$\frac{F_l(s)}{F_d(s)} = \frac{\frac{s}{K_i} + 1}{\frac{m_{eq}}{k_s} s^2 + \frac{s}{K_i} + \left(1 + \frac{m_{eq}}{m_l}\right)}$$

The most important thing to notice about the above equation is that if $m_{eq} \sim m_l$ then at low frequency, the steady state force on the load is reduced.



Figure 4-15: Risky testing the hydro-elastic actuator. The author is suspended under the hydro-elastic actuator. The actuator is supporting the load by a commanded force 1 lb above the downward force of gravity ($\sim 250lbs$). The author is holding a 2lb weight which drops the actuator. Releasing the weight causes the actuator to rise. The minimum resolvable force is 1 lb and is due to the noise floor of the sensor.

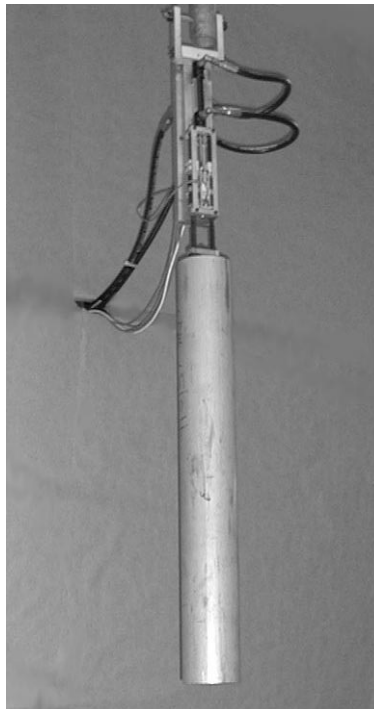


Figure 4-16: The hydro-elastic actuator rigidly connected to a hanging mass. The mass is 18kg. By commanding desired force on the mass oscillating and different frequencies, the effect of the load mass can be verified.

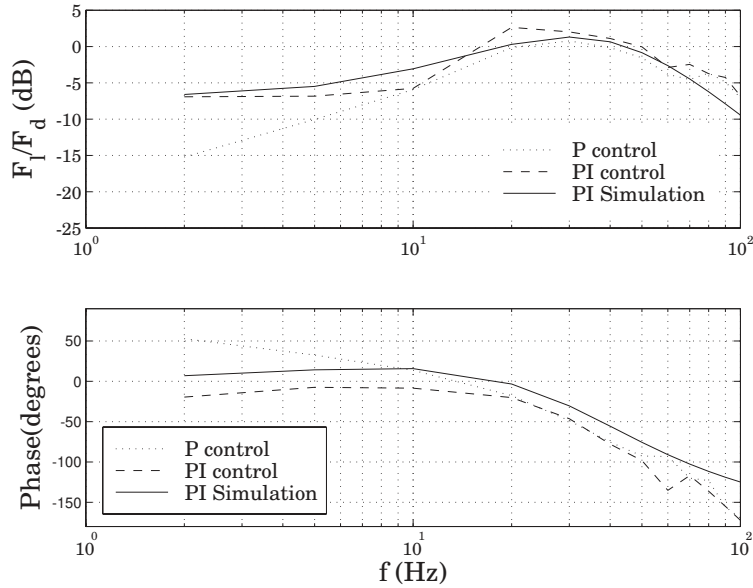


Figure 4-17: **REAL** Actuator force output with an inertial load. The inertial load mass and the actuator equivalent mass are 18 kg and 20 kg respectively. Since the two are so close, at low frequency the actuator displays a significant non unity magnitude under PI control as expected. The response magnitude rises as frequency increases and then drops at the closed-loop bandwidth of the actuator. Proportional control shows that the damper characteristics are significant for this actuator and inertial load combination. Using a proportional controller dramatically decreases low frequency force magnitude far beyond that of the PI controller.

In order to experimentally verify the effect of an inertial load, I rigidly attach an 18 kg mass to the output of the actuator suspended from the ceiling as seen in figure 4-16. I then command an oscillating force signal from 2 to 100 Hz that causes the mass to go up and down. The results of the experiment are shown in figure 4-17.

The equivalent mass of the actuator in the experiment is calculated to be

$$m_{eq} = \frac{A}{K K_i K_v} = 20kg.$$

Since the inertia load, $m_l = 18$, and m_{eq} are so close, the mass load cannot be neglected. The load mass was explicitly chosen to demonstrate this fact.

The low frequency response of the actuator matches with theory in that the magnitude function is reduced (figure 4-17). This is because the load mass begins to accelerate when it feels the force through the spring. The spring needs something to push on in order to compress. Therefore, the bigger the load mass in comparison to the equivalent actuator mass, the less effect the load mass has on actuator performance.

Remember also, that the hydro-elastic actuator under P control exhibits damper like characteristics at low frequency. As a damper at low frequency there is a free zero in the forward closed-loop transfer function. The experimental data in figure 4-17 verifies this by showing the 20dB/dec rise in the magnitude and phase lead at low frequencies under P control. For this particular actuator, simple proportional control is not recommended.

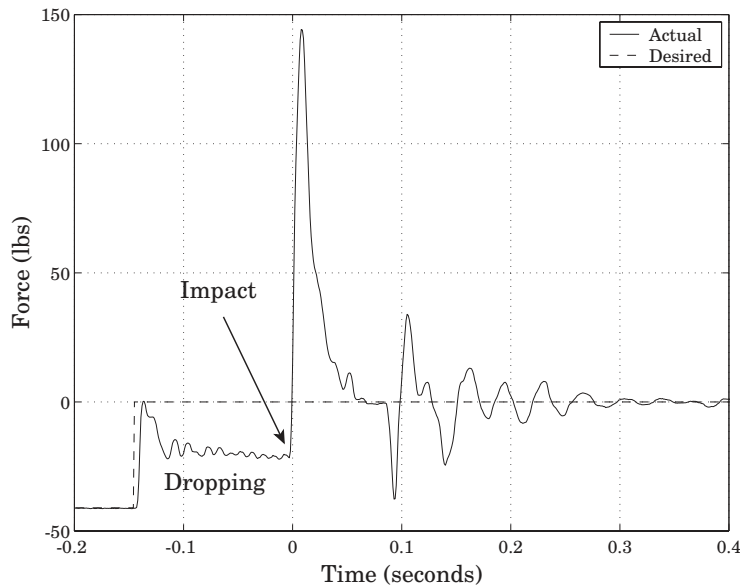


Figure 4-18: **REAL** Results of drop testing an 18kg (40lb) mass attached to the actuator. At time $t = -0.2$, the actuator is pulling the mass with an upwards force (force up is defined negative). At about $t \approx -0.15$, the mass is released to drop. Even though the desired force of the actuator is set to zero, the impedance is not perfect and keeps pulling upwards with a 20lb force. At $t = 0$, the mass hits the end stop and the force spikes. The mass actually bounces a few times but the peak impact power is just after $t = 0$.

Shock tolerance

The physical elasticity in the actuator allow it to have tolerance to shock loads. The spring in the actuator maintains stability with an impact and spreads the impulse out over time. In so doing it minimized the peak impact power.

In order to test the shock tolerance of the actuator, a load mass is again connected to the actuator. This is the same as in figure 4-16. The load inertia is suspended at the top of the actuator stroke with a force equal to the gravity pull on the mass, $F = m_l g$. The desired force is then set to zero and the actuator drops to the bottom of the actuator stroke exerting a sharp impulse load to the actuator. Figure 4-18 shows the forces in the spring during the drop test.

At time $t = -0.2$, the actuator is pulling the mass with an upwards force (force up is defined negative) of 40 lbs. At about $t \approx -0.15$, the desired force is set to zero and mass begins to drop. As the mass is dropping, there is still an upwards force of roughly 20 lbs. This is due to the impedance of the actuator. Ideally the actuator would have zero impedance and the load would only feel the pull of gravity. However, recall that the impedance is an equivalent mass and spring in series with the load as shown in figure 4-19. Only the inertial load feels the pull of gravity. Nevertheless, in order to move, the gravity force is distributed between the two masses and the load and actuator drop.

At $t = 0$, the mass hits the end stop and the force spikes. The mass actually bounces a few times but the peak impact power is at about 8-10 msec after impact and spreads out over 40 msec (figure 4-20). The impulse, J , is equal to the area under the curve of the force profile. Doing a rough numerical integration shows that the impulse is

$$J = 12kg \cdot \frac{m}{s}.$$

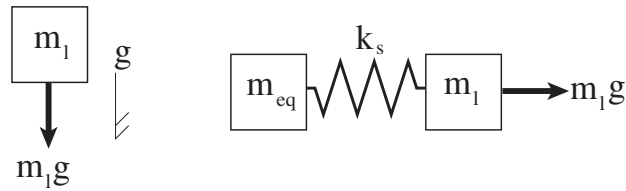


Figure 4-19: Model of the load mass during the drop test. Ideally, the load mass only feels the force of gravity, $F = m_l g$, since the actuator is set to output zero force (left). However the actuator still has impedance. The gravity pull only affects the load mass. The equivalent mass of the actuator does not feel the gravity. Therefore, in order for the load to drop, the gravity force on the load must be distributed between the two masses, one real, one apparent (right). In the drop test case, the $m_{eq} \approx m_l = 20\text{kg}$ and the gravity force is distributed equally between the two inertias.

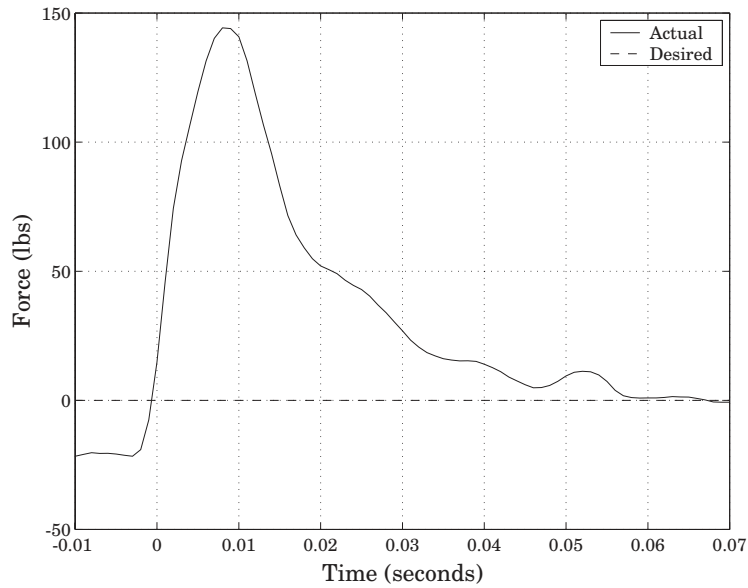


Figure 4-20: **REAL** Close-up of drop test impact forces. This shows the first impact of the load mass. The impulse or change in momentum of the mass, J , is the area under the force curve. A numerical integration shows that $J = 12\text{kg} \cdot \frac{\text{m}}{\text{s}}$.

The impulse can also be verified by looking at the expected impact velocity of the mass load, v_l . v_l can be calculated by applying work and energy balances. The potential energy of the load mass, m_l , is equal to its kinetic energy just before impact plus work done on the mass over the travel of the actuator, h .

$$m_lgh = \frac{1}{2}m_lv_l^2 + Fh \quad (4.31)$$

Rearranging yields the velocity just before impact.

$$v_l = \sqrt{2h \left(g - \frac{F}{m_l} \right)} = 0.7 \frac{m}{s}$$

Therefore, the momentum just before impact is

$$p_l = m_lv_l = 13kg \cdot \frac{m}{s}.$$

The calculations are close enough for verification.

The springs and the control system passively and actively spread out the impulse transfer so that impact power is minimized. Because of the springs, the time of impact is longer. With a slower impact, the control system can respond to it. By doing so the components are protected and the system maintains stability. Figure 4-21 shows three plots regarding the drop test. The top is the force in the spring again. The middle plot shows the energy stored in the spring. The actual energy is not that high. The bottom plot shows the time derivative of the energy which is instantaneous mechanical power. Notice that the maximum power levels are well within the power capabilities of the actuator.

It is interesting to imagine what sort of forces are present in a comparable actuator with a stiff spring. The required impulse is the same as the analysis just presented. However, the major difference is the time of impact. Conservative estimates for time of impact are in the range of a few milliseconds [20]. Assume that the impact takes 2 msec. The average force of the impact is

$$F_{ave} = \frac{J}{\Delta t} = 4000N!$$

This force is an order of magnitude greater than without elasticity! This is also just the average force not to mention the peak force.

In summary, series elasticity helps with shock tolerance.

4.5 Hydro-Elastic Summary

We use a third order model of a Hydro-Elastic Actuator to investigate the closed loop forward transfer function and the impedance of the system. These two cases completely describe the linear characteristics of the actuator. The model is generalized by using dimensional analysis. We examine force bandwidth and minimizing impedance as a function of controller gain and spring constant.

The model has helped to create a basic design guideline for hydro-elastic actuators with particular emphasis placed on choosing the spring constant for the elastic element. Large force bandwidth requires a higher spring constant. Minimizing impedance requires a low spring constant. The choice of spring constant has been shown to be a compromise between these competing requirements.

In both the analysis and physical actuator, we use a linear spring. Future work will investigate nonlinear stiffening springs which may ease the design tradeoffs currently required. Further testing will also be done to experimentally verify impedance and saturation.

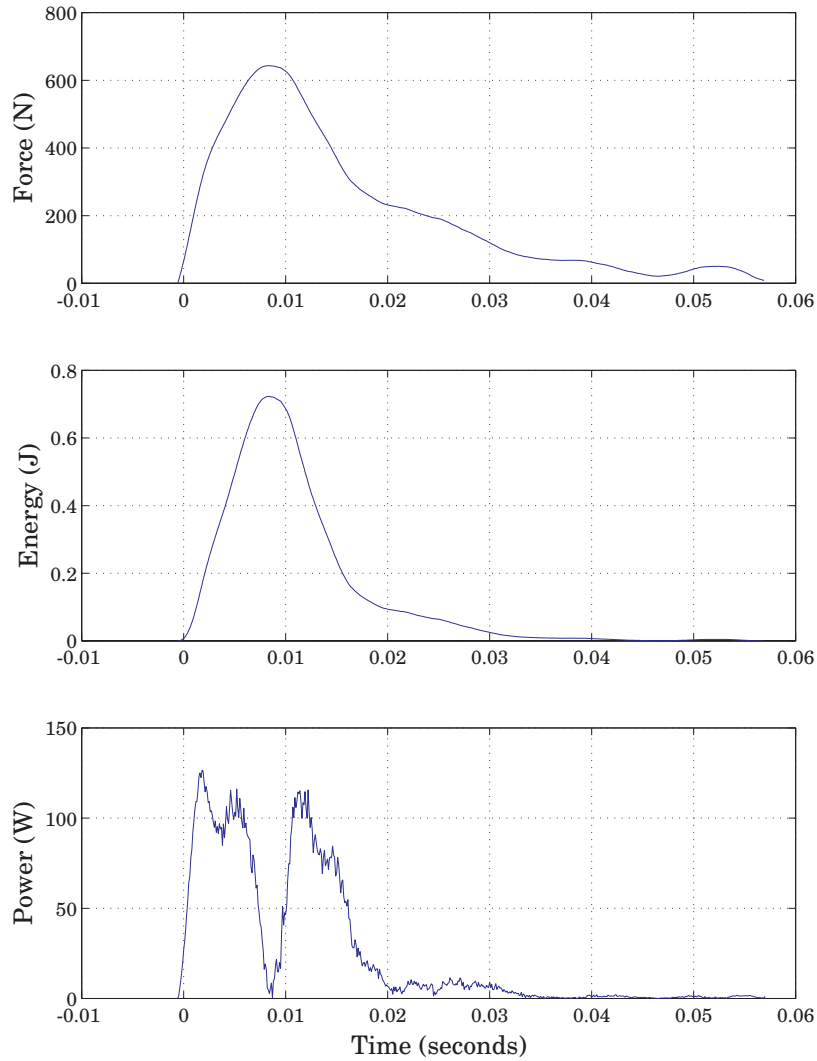


Figure 4-21: **REAL** Impact power. The top figure shows the force in the spring on the first impact. By taking the area under the force curve, we can calculate the impulse, J , of the impact. $J \approx 12 \text{ kgm/s}$. The middle figure shows the energy stored in the spring. It is $E = \frac{1}{2} \frac{F_1^2}{k_s}$. Finally, the impact power is estimated in the bottom figure by looking at the rate of energy change $P = \frac{\Delta E}{\Delta t}$. The series elasticity spreads the impact time out so that the required power is well within the actuator's output power capabilities.

Chapter 5

Electro-Magnetic Series Elastic Case Study

This chapter presents the second case study for series elasticity applied to an electro-magnetic motor in series with a linear transmission. The case is presented in a similar manner as the general model. Unlike the hydraulic case, the power domain of the EM actuator is significantly different from that of the general model. Despite these differences in the actuator model, the actuator displays all of the same characteristics of series elasticity.

The open and closed-loop models for the actuator are derived and reformulated in terms of dimensional analysis. These models are used to discuss bandwidth, impedance, error rejection, impact tolerance and saturation. The effects of load mass moving in free space are also discussed. A physical prototype has been developed (figure 5-1). Where appropriate experimental results are compared to the mathematical models.

5.1 Model Derivation

There are some key differences between the EM series elastic actuator and the general model. After defining and explaining the parameters of the actuator, I derive three relationships. The first is the open-loop power domain model. The second two come from the closed-loop dynamic equation and describe the closed-loop bandwidth and the actuator output impedance. These equations are at the heart of understanding EM series elastic actuators.

5.1.1 Model Definition

As in the general model, there are four main components to the EM series elastic actuator as seen in figure 5-2 .

- System Inputs
- Motor and Transmission
- Compliant Sensor
- Control System

The system inputs and the compliant sensor are the same as the general model. Specifically there are two system inputs. F_d is the desired output force and X_l is the motion of the load. Also, identical to the general model, the compliance of the sensor is defined by the linear spring constant k_s .

While the system inputs and sensor are the same as in the general model, figure 5-2 shows that motor model and the control system are different. Therefore, I focus on the discussion on these differences.

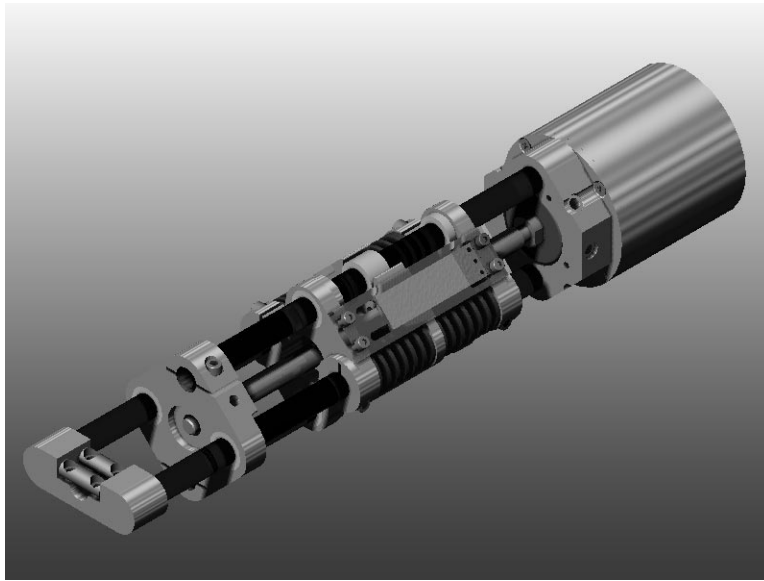


Figure 5-1: The prototype actuator has a brushless DC motor rigidly connected to a ballscrew which drives the linear motion. The ballscrew nut is coupled to the output through four die compression springs. The spring compression is measured with a linear potentiometer. The actuator can output over 1350 N and move at 25 cm/second.

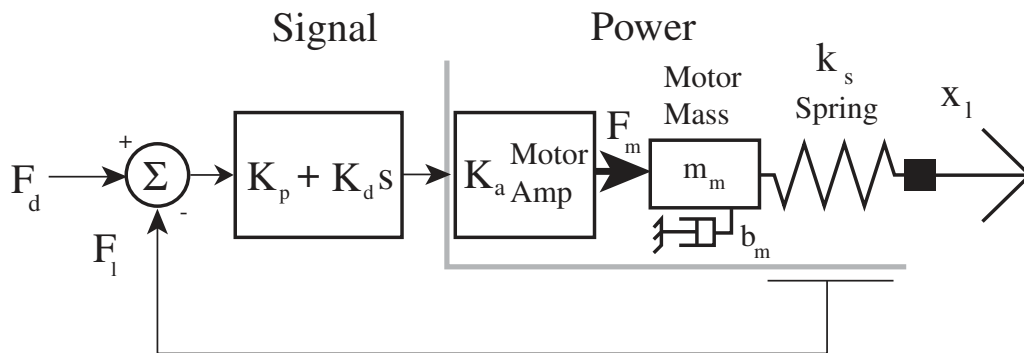


Figure 5-2: Electro-magnetic series elastic actuator model. The motor mass has a driving force and viscous friction. The controller drives the motor mass to compress the spring which gives the desired force output.

Motor model

The motor model in the power domain consists of a motor amplifier, motor mass and a viscous friction element.

The motor amplifier creates a force on the motor mass given a signal from the controller. For the initial linear analysis of the actuator, I make two assumptions about the motor amplifier. I assume that the actuator can produce any desired output force up to the force saturation limit, F_{sat} , and that the amplifier dynamics are fast enough that they are assumed to be negligible. In the physical prototype actuator, the amplifier gain K_a , that relates the desired force (input voltage) to torque on the motor mass (output current), is unity. K_a is therefore lumped into the controller gain and eliminated throughout the chapter to reduce equation complexity.

The lumped mass m_m includes the dynamic motor mass and the mass of the transmission elements as seen through the transmission. Remember that this reflected inertia is N^2 the actual mass value where N is the transmission reduction.

The motor friction b_m is also seen through the transmission. It too is N^2 of its actual value. Even so, depending on motor and transmission construction, the viscous friction can be very low.

There are two modes of operations for an EM motor, torque control and velocity control. In this model, I choose to use torque control. This is a deviation from the previous two models. Velocity control, to some degree, masks the effect of motor mass which happens to be very important in defining the large force bandwidth for the EM series elastic actuator. Therefore, while torque control is perhaps the more difficult method of controlling a series elastic actuator, I do so in order to highlight effects of the motor mass that makes the actuator inherently second order.

Control System

Feedback control of the actuator is closed by measuring the deflection of the spring which implies the force output, F_l , of the actuator. I use a PD controller on the error of the signal with gains K_p and K_d for the proportional and derivative terms respectively. Since the system is already second order, I do not include an integral term. By remembering that I assume the motor amplifier to be ideal, the force on the motor mass, F_m is determined by

$$F_m = (F_d - F_l)(K_p + K_d s). \quad (5.1)$$

The actuator can be controlled with proportional control alone. However, it is helpful to have a damping term as well to help reduce the natural resonance on the mass and spring in the sensor.

It would be very easy to also use a feed-forward term in the controller and attempt to keep the set point of the system equal always centered on the desired force. This would allow the control system to focus on controlling the error in the spring rather than requiring a large error signal just to compress the spring at high forces. However, in order to keep the control system complexity to a minimum, feed-forward is *not* included.

5.1.2 Power Domain Model

Figure 5-3 shows the model for the power domain for a series elastic actuator. The two constitutive equations for the power domain are defined by the force in the spring and the motion of the motor mass.

$$\begin{aligned} F_l &= k_s(x_m - x_l) \\ m_m \ddot{x}_m + b_m \dot{x}_m &= F_m - F_l \end{aligned} \quad (5.2)$$

These equations can also be written with laplace variables.

$$\begin{aligned} F_l &= k_s(X_m - X_l) \\ X_m &= \frac{F_m - F_l}{m_m s^2 + b_m s} \end{aligned} \quad (5.3)$$

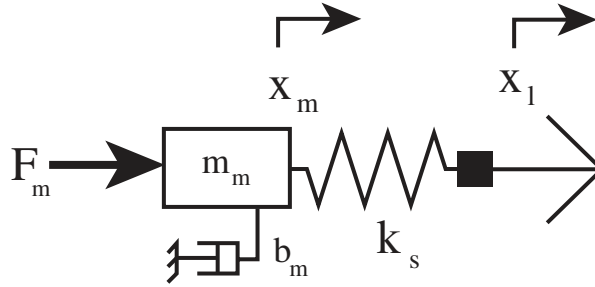


Figure 5-3: EM series elastic actuator power domain model. The motor mass has a driving force and viscous friction. The F_l is the force output through the spring.

By combining the two equations in 5.3, the force in the spring, F_l , can be written as a function of two variables: the force input from the motor, F_m , and the relative position of the load, X_l . This relationship is derived to be:

$$F_l(s) = \frac{F_m(s) - (m_m s^2 + b_m s)X_l(s)}{\frac{m_m}{k_s} s^2 + \frac{b_m}{k_s} s + 1}. \quad (5.4)$$

This is the open-loop dynamic equation for the force F_l in the spring as a function of the motor force and the load motion.

5.1.3 Closed-loop Model

As shown in figure 5-2 the open-loop power domain model is modulated by a force feedback loop. Combining power domain model (equation 5.4) and the feedback signal commands from the controller (equation 5.1) yields the closed-loop dynamic equation for the force through the spring:

$$F_l(s) = \frac{(K_d s + K_p)F_d(s) - (m_m s^2 + b_m s)X_l(s)}{\frac{m_m}{k_s} s^2 + \frac{b_m + k_s K_d}{k_s} s + (K_p + 1)}. \quad (5.5)$$

The closed-loop dynamic equation for the force F_l in the spring is a function of the desired force, F_d , and load motion, X_l .

5.1.4 Two input cases

As in the previous chapters, it is helpful to write the force in the spring, F_l , in the power domain model and the closed-loop model as a function of isolated input variables. For the first case, the load end is fixed eliminating the load motion. The second case is with load end free to move and the desired force fixed. The second case eliminates the dynamics due to desired force modulation.

Case 1: Fixed Load

By eliminating the load motion, the transfer function between motor force input and actuator output can be taken from equation 5.4 and written explicitly as:

$$\boxed{\frac{F_l(s)}{F_m(s)} = \frac{1}{\frac{m_m}{k_s} s^2 + \frac{b_m}{k_s} s + 1}}. \quad (5.6)$$

Equation 5.6 will be referred to as is the open-loop transfer function.

By imposing the fixed end condition again and using the closed-loop dynamic equation (equation 5.5), we can write the closed-loop forward transfer function for case one which relates the desired force to the output force:

$$\frac{F_l(s)}{F_d(s)} = \frac{K_d s + K_p}{\frac{m_m}{k_s} s^2 + \frac{b_m + k_s K_d}{k_s} s + (K_p + 1)}. \quad (5.7)$$

Depending on the magnitude of K_p , at low frequency, this transfer function is close to unity. In the limit at high frequency it goes to zero. The zero in the numerator is an artifact of the taking the derivative of the desired force via the error signal.

For series elastic actuators, K_p is typically very high. It is at least an order of magnitude greater than 1 if not more. Therefore,

$$K_p + 1 \simeq K_p.$$

Case 2: Free end with zero force

With the desired force fixed constant, the force in the spring due to the load motion under closed-loop force control can be written from equation 5.5 as

$$\frac{F_l(s)}{X_l(s)} = \frac{-(m_m s^2 + b_m s)}{\frac{m_m}{k_s} s^2 + \frac{b_m + k_s K_d}{k_s} s + (K_p + 1)}. \quad (5.8)$$

This is the output impedance. The impedance at low frequency is ideally equal to zero. At high frequency, it is equal to k_s , the spring constant of the physical spring.

Whenever, either of the closed-loop equations are used in the rest of the chapter, it is assumed that $K_p + 1 \simeq K_p$. Even though this assumption is not technically and mathematically precise, it is accurate enough.

5.2 Model Analysis

As done in the previous chapters, I discuss the EM series elastic actuator with respect to the following characteristics:

- Saturation
- Closed-loop bandwidth
- Output impedance
- Error rejection

I deviate slightly from the pattern in the previous chapter and begin by discussing actuator saturation. I use the power domain model of equation 5.6 to help explain saturation. I define a saturation frequency for the EM series elastic actuator and rewrite the dynamic equations in terms of dimensionless groups. Power domain saturation is a function of natural viscous damping and back emf as well as the motor mass-sensor spring resonance. It is important to remember that saturation is independent of control system.

In order to understand the closed-loop bandwidth, I investigate equation 5.7. I discuss the selection of control gains to get proper actuator performance as well as the tradeoffs of reduced sensor gain and increased control gain.

The output impedance of the actuator is defined by equation 5.8. This equations demonstrates how well the actuator responds to external motion disturbances. The lower the impedance, the better the actuator dynamics are decoupled from the load.

As mentioned in Chapter 3, internal errors such as stiction are reduced when using a compliant sensor. This is explained specifically for the controller case of the EM series elastic actuator.

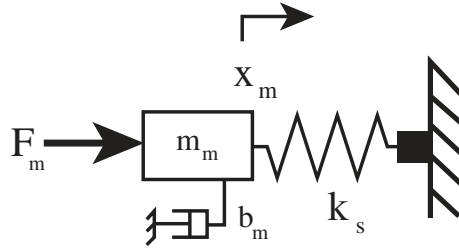


Figure 5-4: Electro-magnetic series elastic actuator model with a fixed load. This configuration helps to define the saturation limits of the actuator.

5.2.1 Saturation

I begin by discussing actuator saturation. This allows for a definition of the saturation bandwidth. With this definition in place, I can reformulate the dynamic equations into dimensionless terms using the saturation bandwidth as a normalization point.

In order to clarify saturation at the most basic level in the EM series elastic actuator, I fixed the load as in case 1 (figure 5-4). Obviously, saturation is affected by load motion. Depending on the frequency and phase of the load motion, it can either help or hinder the actuator. However, by fixing the load, I have a fixed point of reference for understanding saturation.

Assuming no velocity saturation for the moment, the amplifier can produce large motor forces over a wide frequency range. However, in order to create large forces in the spring, the force from the amplifier must move the motor mass. The force from the amplifier is independent of the force in the spring. For the EM motor with a transmission in series with an elastic element, the mass-spring resonance of the motor mass and series elasticity define the plant dynamics. Therefore, the ability of the actuator to produce large forces is limited in frequency by these dynamics independent of control system. The frequency at which the open-loop characteristics of the plant begin to fall off is defined as the saturation frequency ω_o .

$$\omega_o = \sqrt{\frac{k_s}{m_m}} \quad (5.9)$$

Since the sensor spring is very compliant, ω_o can be low. Typically, it may be a few hertz to tens of hertz depending on the reflected inertia as seen through the transmission.¹ The saturation bandwidth is well within the controlled bandwidth discussed later. The actuator still operates and can generate forces at frequencies above ω_o . The actuator is simply limited in the magnitude of large forces at high frequency.

Other saturation effects, such as back emf and viscous friction, also play a role in defining the large force bandwidth profile near the saturation frequency ω_o . These effects are explained after reformulating the open and closed-loop transfer functions in dimensionless terms.

Dimensionless formulation

Both the open and closed loop transfer functions, equation 5.6 and equation 5.7, and the output impedance, equation 5.8, can be written in dimensionless form.

First, notice that there are two natural frequencies in the dynamic equations. The first is the saturation frequency of the motor mass and spring just described ω_o . The second is the controlled

¹These number are taken from macro scale actuators built previously.

natural frequency ω_c .

$$\begin{aligned}\omega_n &= \sqrt{\frac{k_s}{m_m}} \\ \omega_c &= \sqrt{\frac{k_s K_p}{m_m}}\end{aligned}\quad (5.10)$$

Using these two frequencies and the following dimensionless groups we can non-dimensionalize both the open and closed loop equations equations of case one and the impedance of case two.

$$\begin{aligned}S &= \frac{s}{\omega_o} \\ \kappa &= \frac{\omega_c}{\omega_o} = \sqrt{K_p} \\ B &= \frac{b_m}{k_s} \omega_o \\ \Gamma &= K_d \omega_o\end{aligned}\quad (5.11)$$

- S normalizes the equation to the saturation frequency or the natural resonance of the motor mass-spring system of the actuator.
- κ represents the gain in the system and is a measure of the increase in controlled bandwidth above the saturation frequency. Remember that the definition of κ assumes that $K_p \gg 1$.
- B is a scaled natural damping term due to viscous friction physically present in the construction of the actuator.
- Γ represents the scaled controller damping gain.

The dimensionless open-loop, closed-loop, and output impedance transfer functions are:

$$G_{ol}(S) = \frac{F_l(S)}{F_m(S)} = \frac{1}{S^2 + BS + 1} \quad (5.12)$$

$$G_{cl}(S) = \frac{F_l(S)}{F_d(S)} = \frac{\Gamma S + \kappa^2}{S^2 + (\Gamma + B)S + \kappa^2} \quad (5.13)$$

$$Z_{cl}(S) = \frac{F_l(S)}{k_s x_l(S)} = \frac{-S(S + B)}{S^2 + (\Gamma + B)S + \kappa^2} \quad (5.14)$$

Back-emf, Friction and Large Force Bandwidth

Back-emf and friction play an important role in defining the frequency profile of large force bandwidth or as stated previously saturation bandwidth. In order to better understand these effects, I introduce a simple velocity motor saturation model:

$$|f_m| \leq \begin{cases} F_{sat} \left(1 - \frac{|v_m|}{V_{sat}}\right) & : |v_m| \leq V_{sat} \\ 0 & : |v_m| > V_{sat} \end{cases} \quad (5.15)$$

where F_{sat} and V_{sat} are the maximum force from the amplifier and maximum velocity of the motor respectively. v_m is the actual motor mass velocity. This is graphically depicted in figure 5-5.

When the motor is not pegged at saturation conditions, it still follows a linear back-emf model where:

$$F_{emf} = \frac{F_{sat}}{V_{sat}} v_m. \quad (5.16)$$

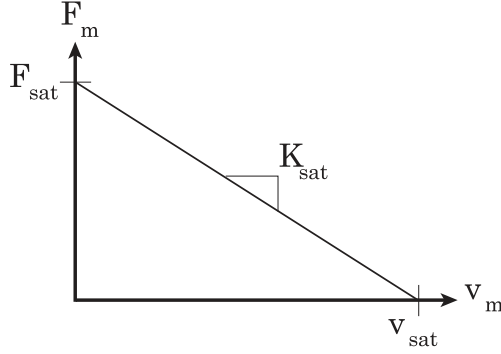


Figure 5-5: Velocity saturation model for the EM series elastic actuator. Simple velocity saturation limits the ability of the amplifier to produce high forces. This model is slightly different than the force saturation model described in the previous chapters but has very similar results. Here $K_{sat} = \frac{F_{sat}}{v_{sat}}$.

The back-emf can be thought of as an equivalent damping because it relates a loss in motor force due to motor velocity just like the term b_m . The equivalent damping coefficient for the back EMF is $K_{sat} = F_{sat}/V_{sat}$. I then modify the dimensionless B group to be

$$B = \frac{b_m + \frac{F_{sat}}{V_{sat}}\omega_o}{k_s} \quad (5.17)$$

The B group plays an important role in the large force bandwidth. Also, by incorporating the velocity saturation as an equivalent force we can investigate large force bandwidth in terms of the saturation force only.

Large force bandwidth is independent of the control system and is only a function of the open-loop dynamics of the power domain, equation 5.12. While the magnitude of equation 5.12 relates the load force F_l as a function of the motor force F_m in the linear range, it can also relate maximum load force output, $F_{l_{max}}$, as a function of the maximum motor output, F_{sat} .

$$\frac{F_{l_{max}}}{F_{sat}} = \frac{1}{S^2 + BS + 1} \quad (5.18)$$

There are three frequencies of interest in the large force bandwidth transfer function: above, below and near the saturation frequency ω_o . At low frequencies, those below ω_o , the transfer function is unity and the actuator can output the maximum force capable by the motor. At high frequencies above ω_o , the maximum force output capability of the actuator is limited. This is because the motor cannot accelerate the motor mass fast enough to deflect the spring to full compression. The dimensionless group B defines what the large force bandwidth profile looks like near ω_o .

Figure 5-6 shows different values for B with respect to the maximum available force output due to force saturation. B is an equivalent damping term for the saturation profile. The damping affects how well the system handles large forces near the natural frequency. With an overdamped system, the available force amplitude at resonance dramatically reduces the available force amplitude. Regardless of the damping in the system, high amplitude forces at high frequency are limited.

This analysis confirms previous work stating that elasticity in an actuator reduces large force bandwidth and increases control effort at high frequencies [29, 46]. The primary variable in defining ω_o is the stiffness of the elasticity, k_s . Increasing k_s will increase large force bandwidth. When choosing an appropriate k_s , an actuator designer must understand the large force requirements for the application. The frequency, ω_o , is used as a reference point and defines the lower bound for the spring constant, k_s .

The profile of the large force bandwidth near ω_o is solely a function of the dimensionless group

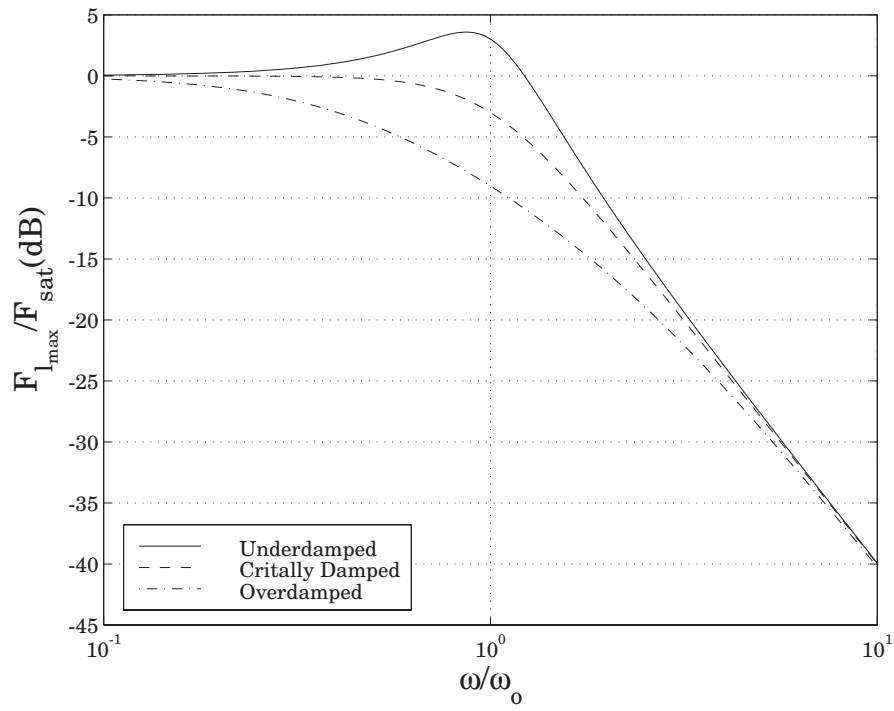


Figure 5-6: $\boxed{\text{SIM}}$ EM large force bandwidth due to force and velocity saturation. The motor mass spring resonance ω_o defines the large force bandwidth of the actuator. The B group (generalized damping) defines the shape of the profile around the saturation frequency. The three lines represent underdamped, critically damped, and overdamped frequency response. This plot only represents the large force capabilities of the actuator with the load fixed.

B . In standard control textbooks [42], the resonance for second order systems is defined by the magnitude of ζ , the damping ratio. Since the natural frequency has been normalized to one for the open loop transfer function, ζ is related to B by:

$$\zeta = \frac{B}{2}. \quad (5.19)$$

Therefore, we can talk about B in terms of under, critical, and over damping as the three curves in figure 5-6 show.

Let us now take a closer look at B .

$$\begin{aligned} B &= \frac{b_m + \frac{F_{sat}}{V_{sat}}}{k_s} \omega_o \\ &= \frac{b_m + \frac{F_{sat}}{V_{sat}}}{k_s} \sqrt{\frac{k_s}{m_m}} \\ &= \left(b_m + \frac{F_{sat}}{V_{sat}} \right) \sqrt{\frac{1}{k_s m_m}} \end{aligned} \quad (5.20)$$

Equation 5.20 helps us see the relationship of B to the physical model parameters. In general, we want B to be as small as possible to increase bandwidth. Equation 5.20 can help define design guidelines regarding friction.

- b_m — Make the actuator with as little drive friction as possible.
- $\frac{F_{sat}}{V_{sat}}$ — Minimize back EMF.
- m_m — Using a larger motor mass will decrease resonant frequency thus making the apparent damping smaller.
- k_s — A larger spring constant decreases spring deflection. Spring and motor velocity subsequently decrease and therefore damping decreases.

It is also important to remember that both b_m and m_m as represented in this model are seen through a transmission reduction and are scaled by N^2 , where N is the reduction. Therefore a decrease in reduction decreases the damping.

5.2.2 Bandwidth

Up to this point in the analysis I have only worked with the open-loop forward transfer function. From here, I will be dealing with the closed-loop behavior.

The controlled bandwidth is significantly higher than the saturation bandwidth for the EM series elastic actuator. In the previous chapter, I outlined several things that can potentially limit the bandwidth of the actuator. None of those limitations were a function of the compliance in the sensor. Therefore, the loop gain reduction from sensor compliance can be proportionally increased in the controller. This essentially takes the gain out of the spring and into the control system.

Controller Gains

Using the closed-loop characteristic equation (denominator of equation 5.13 and 5.14)

$$S^2 + (\Gamma + B)S + \kappa^2 = 0 \quad (5.21)$$

in conjunction with the dimensionless groups (equation 5.11), the controller gain values for a PD controller can be explicitly defined to get a desired closed loop natural frequency w_c and damping ratio ζ_c .

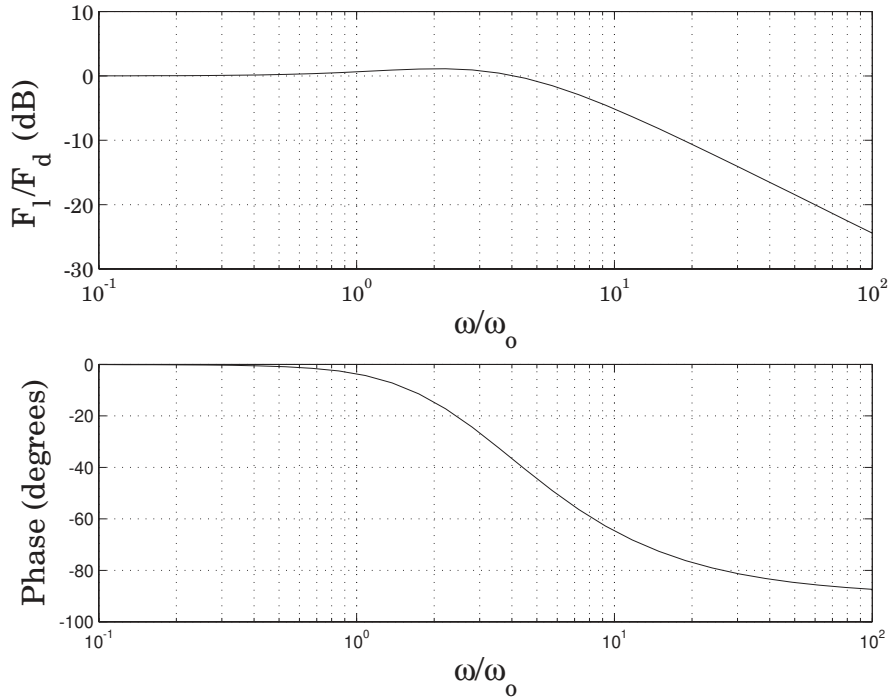


Figure 5-7: SIM Closed-loop bode plot of the EM series elastic actuator with PD control. This is a bode plot of the closed loop system with $\kappa = 3$ and $\zeta_c = 1$. The zero from the controller adds the apparent resonance near the controlled natural frequency.

The proportional gain is found from the definition of κ .

$$\begin{aligned} \kappa^2 &= K_p \\ \implies K_p &= \frac{w_c^2}{w_o^2} \end{aligned} \quad (5.22)$$

The derivative gain is found from the damping term of the characteristic equation.

$$\begin{aligned} 2\zeta_c\kappa &= B + \Gamma \\ \implies K_d &= \frac{2\zeta_c\omega_c m_m - b_m}{k_s} \end{aligned} \quad (5.23)$$

As an example figure 5-7, shows a bode plot of the closed loop forward transfer function: $\kappa = 3$ and $\zeta_c = 1$.

5.2.3 Impedance

Equation 5.14 shows the dimensionless form of output impedance. I rewrite it here for convenience

$$Z_{cl} = \frac{F_l(S)}{k_s x_l(S)} = \frac{-S(S+B)}{S^2 + (\Gamma+B)S + \kappa^2}$$

At low frequencies the impedance is small. As input frequency increases, so too does the impedance. In the limit, the output impedance levels off and is equal to the spring constant, k_s , of the force sensor. Equation 5.14 normalizes to k_s and figure 5-8 shows an example of the impedance

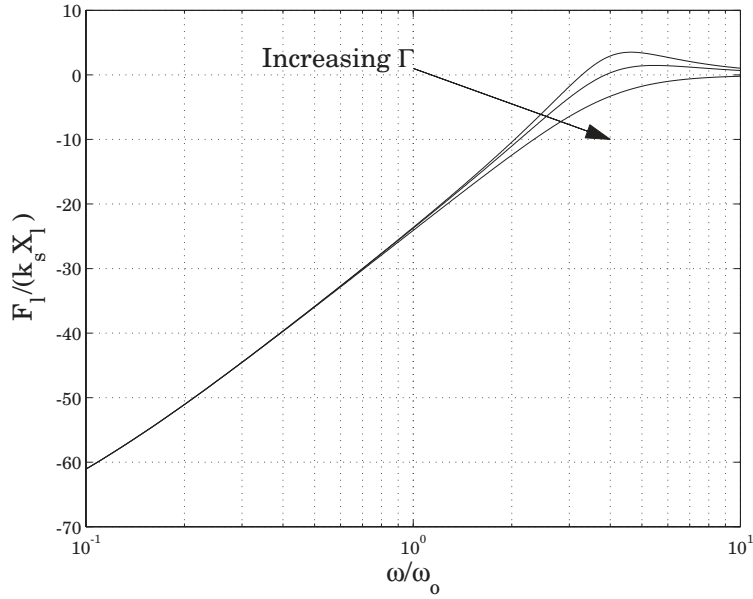


Figure 5-8: **SIM** EM output impedance. The impedance of the actuator at small frequencies is low and is equal to k_s at high frequency. In this example $\kappa = 4$ and $B = 0.1$. For low frequencies, the actuator has an equivalent mass characteristic. The equivalent mass is, $m_{eq} = \frac{m_m}{\kappa}$. The higher the controller gain the lower the impedance. As Γ increases there is an effective reduction in the impedance at the controlled natural frequency.

for different values of Γ which represents the derivative gain.

There are four regions of interest in figure 5-8. The first is at very low frequency: very low, mid-range near ω_o , near ω_c and high frequencies.

The natural damping of the system B is quite low but its effects are still just noticeable. For the most part however, the effects of B can be neglected.

For the rest of the low frequencies up to the controlled natural bandwidth the impedance has an equivalent mass characteristic because it is rising at 40dB/dec. This means that it has two free zeros in the numerator²

$$F_l = m_{eq} s^2 X_l \quad (5.24)$$

m_{eq} is some fraction of the reflected motor inertia m_m defined by the controller gain.

$$m_{eq} = \frac{m_m}{K_p} = \frac{m_m}{\kappa^2} \quad (5.25)$$

Therefore, the higher the gain, the lower the equivalent mass.

The break point or resonance is at κ . In figure 5-8, $\kappa = 4$.

As mentioned previously, at frequencies above the controlled natural frequency ω_c , the actuator's output impedance is the spring constant of the sensor. All high frequency disturbances and shock loads are filtered through the spring.

There are three ways to decrease the output impedance for the series elastic actuator.

- Increase the control gain. This drives the impedance resonance further away from the operational bandwidth.

²For all practical purposes, a zero with a very slow time constant can also be considered a free zero in the impedance equation when trying to calculate the equivalent mass.

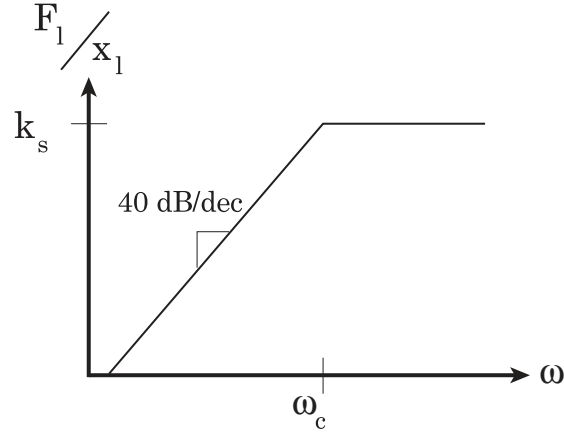


Figure 5-9: Rough characterization of EM impedance. As shown in the simulation, the impedance at low frequencies is equivalent to a mass and is equal to the spring constant of the sensor at high frequencies.

- Decrease the spring constant. This linearly lowers the impedance profile.
- Increase the derivative gain. As seen in figure 5-8, Γ 's major contribution is to reduce impedance resonance at the controlled natural frequency.

It is important to remember that the key benefit of series elastic actuators is low impedance. Controlled bandwidth can remain constant by increasing control gain proportionally to the reduction in spring stiffness. Impedance however, is dramatically reduced when the spring stiffness is lowered.

5.2.4 Force Error Rejection

As described in chapter 3, coulomb friction and stiction are dramatically affected by the introduction of the spring into the actuator. The compliant spring allows for an increase in controller gain. Stiction is one of the main reasons why the actuator cannot respond to low forces and thus reduces dynamic range.

Because of stiction, the lumped mass will not move until

$$F_m - F_l = F_m - F_d + F_e = F_s \quad (5.26)$$

where F_e is the feedback force error and F_f is the force due to stiction. Since, stiction is a low frequency phenomenon, we assume that the derivative term of the controller is negligible. The force to the motor due to the error then becomes

$$F_m \approx K_p F_e + F_d. \quad (5.27)$$

Using equations 5.26 and 5.27 we can solve for the force error F_e .

$$F_e \approx \frac{1}{K_p + 1} F_s \quad (5.28)$$

This shows that the force error due to stiction is related by the dimensionless group κ .

$$F_e \approx \frac{1}{\kappa^2} F_s \quad (5.29)$$

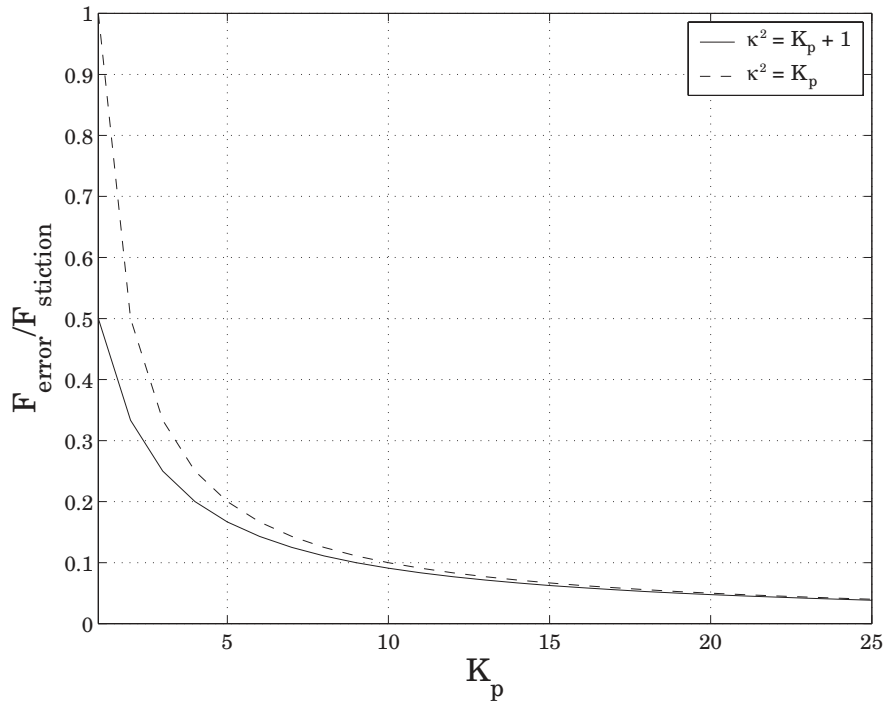


Figure 5-10: SIM Inverse parabolic relationship of the force error due to stiction force. As control gain, K_p , increases non-linear friction forces are dramatically decreased. The two curves represent the estimate of κ^2 . The solid line includes the +1 and the dashed line does not. In the physical actuator, $K_p = 25$. As can be seen, at that level of gain there is very little difference between the two curves.

Remember that κ is an approximate ratio between the resonant frequency of the mass-spring system, ω_o , and the controlled natural frequency, ω_c . Increasing κ reduces the effect of stiction. There are two ways to effectively reduce stiction: 1—increase ω_c by increasing the gain or 2—decrease ω_o by reducing the spring constant. The relationship is inverse parabolic and can be visualized in figure 5-10. Theoretically, to eliminate stiction we should have as soft a spring as possible. However, part of the design is to evaluate an acceptable level of stiction reduction.

As the gain is increased, there is a rapid decrease in the noticeable stiction force in the system. If we set our controlled natural frequency 5 times greater than the mass-spring resonance ($K_p = 25$) as is done in the physical actuator, the apparent stiction is reduced to 5% of its original value.

5.3 Effect of Load Mass

Even though series elastic actuators have variable load conditions due to intermittent contact with the environment, it is helpful to analyze the dynamics of a mass load moving in free space (figure 5-11). Ideally, the mass load is decoupled from the actuator dynamics such that the actuator looks like a pure force source. I show that given the load has some minimum mass, then the actuator can be considered a pure force source within its closed-loop bandwidth capabilities.

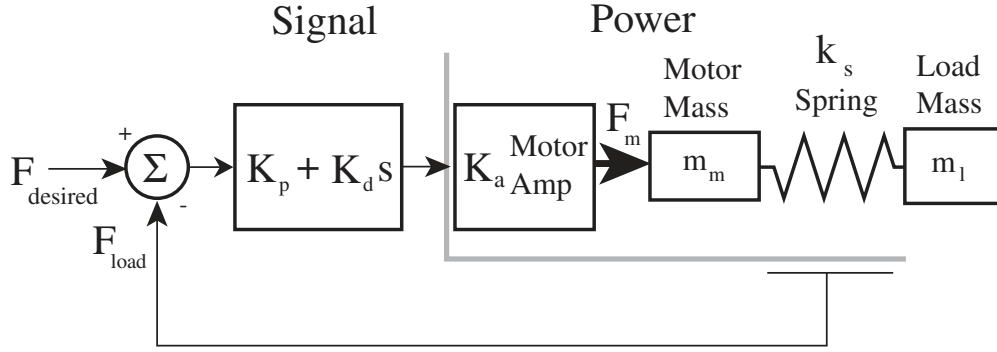


Figure 5-11: EM series elastic actuator model with load mass moving in free space. The load mass defines the load motion x_l .

5.3.1 Load Forces

Consider the force balance relationships for force in the spring, F_l , and motor mass motion, x_m derived previously for the laplace domain (equation 5.3).

$$\begin{aligned} F_l &= k_s(X_m - X_l) \\ X_m &= \frac{F_m - F_l}{m_m s^2} \end{aligned} \quad (5.30)$$

With the load mass moving in free space, I can also write the laplace domain equation for the load motion, X_l . It is solely a function of the force in the spring, F_l .

$$X_l = \frac{F_l}{m_l s^2}$$

For enhanced clarity and understanding, I eliminate the viscous damping on the motor mass. Remember that the motor force F_m is a function of the control system.

$$F_m = (K_p + K_d s)(F_d - F_l)$$

Substitute the controller into the equation for X_m . Then use this result and the equation for X_l to solve for the force in the spring, F_l as a function of desired force F_d .

$$\frac{F_l}{F_d} = \frac{K_d s + K_p}{\frac{m_m}{k_s} s^2 + K_d s + \left(K_p + 1 + \frac{m_m}{m_l}\right)} \quad (5.31)$$

With two exceptions, equation 5.31 is the same as the closed-loop dynamic transfer function for the fixed load case (equation 5.7). The first exception is the elimination of the viscous damping term. Only controller damping remains. The second difference is in the s^0 term of the characteristic equation in the denominator. Instead of just being $K_p + 1$, there is an additional term, $\frac{m_m}{m_l}$, that is the ratio of the motor mass to the load mass.

There are two important things to remember about the s^0 term. The first is that $K_p \gg 1$. The proportional gain is high due to the fact that k_s is low. As mentioned before, $K_p + 1 \simeq K_p$. This leads to the second important point. The additional term, $\frac{m_m}{m_l}$, is only significant for the case where there is very little load inertia in comparison to the motor mass. Fortunately, this is hardly ever true.

Typically these actuators are used in robots with articulated joints. Therefore, m_l is a linear

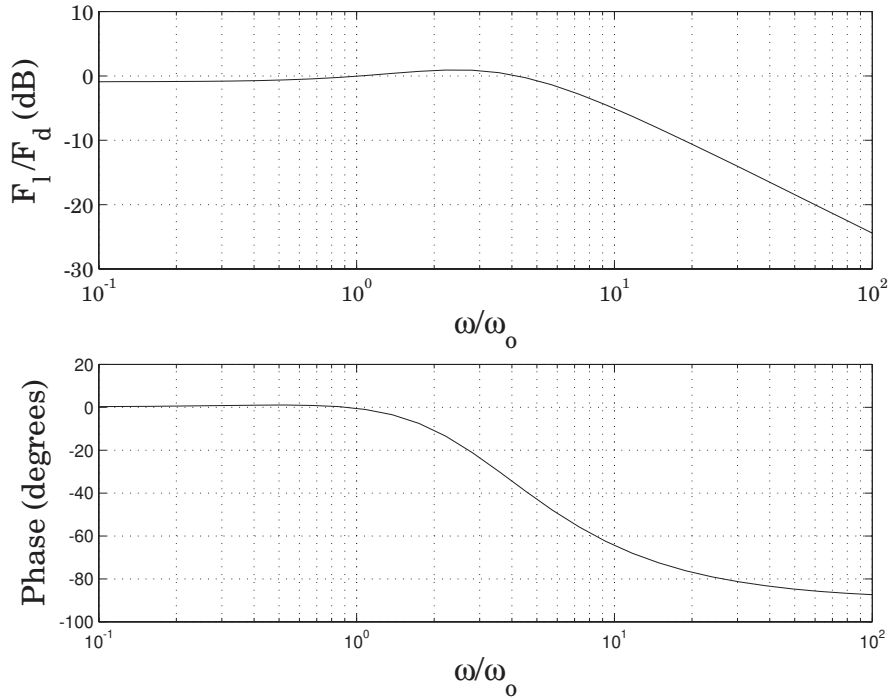


Figure 5-12: SIM Force on a load that is free to move. This plot shows that the actuator can output forces on a load mass even when it is free to move.

equivalent of a rotary inertia

$$m_l = \frac{I_{rot}}{r^2}$$

where I_{rot} is the robot link inertia about the joint and r is the radius through which the actuator force is converted into a torque. Practical experience with using the actuators on robots have shown that $m_l \approx m_m$. Therefore, again K_p dominates and $\frac{m_m}{m_l}$ can be assumed small in comparison. At low frequency, the actuator has good force response.

Remember that the load mass resonates with the spring at a frequency $\omega_l = \sqrt{\frac{k_s}{m_l}}$ and that ω_l is part of the non dimensionless group L where

$$L = \frac{\omega_l}{\omega_o}$$

I write the load force equation in non dimensional terms as

$$\frac{F_l(S)}{F_d(S)} = \frac{\Gamma S + \kappa^2}{S^2 + (\Gamma + B)S + \kappa^2 + L^2} \quad (5.32)$$

This equation is depicted in figure 5-12 with $\kappa = 3$, $\Gamma = 6$ and $L = 1$. At low frequency, there is a small reduction in the output magnitude due to the load force. However, the force is in phase and is close to the actual desired value.

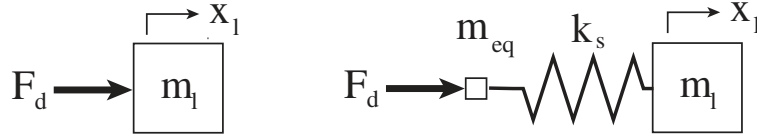


Figure 5-13: Control abstraction for the EM series elastic actuator. At frequencies below the controlled bandwidth, the actuator can be considered a pure force source. Above the controlled bandwidth, the dynamics of the equivalent mass m_{eq} (equation 5.25) and the spring come into play.

5.3.2 Load Motion

Assuming that the load mass is significant, we can refer back to the load motion in equation 5.30, we can write the load motion as a function of the desired input force.

$$\frac{x_l}{F_d} = \frac{1}{m_l s^2} \frac{K_d s + K_p}{\frac{m_m}{k_s} s^2 + K_d s + \left(K_p + 1 + \frac{m_m}{m_l}\right)} \quad (5.33)$$

There are two parts to equation 5.33. The first part is just the dynamics of the load mass as a function of a simple force $F_d = m_l s^2 X_l$. The second part of the transfer function come from equation 5.31 and represents the closed-loop characteristics of the actuator. Equation 5.33 verifies that the actuator performs well as pure force source over over its closed-loop bandwidth as long as load mass is significant.

In summary, a load mass feels a pure force at low frequency for the EM series elastic actuator. As drive frequency increases, the dynamics of the actuator begin contribute to the force on the load. In the very simplest model, it follows the diagram in figure 5-13. The actuator dynamics are a small equivalent mass, m_{eq} (equation 5.25) and the physical elasticity followed by the load mass.

5.4 Physical Actuator Prototype

The theoretical work just presented has a practical side too. The following discussion elaborates on design decisions made during the design and construction of the actuator prototype (figure 5-1). The discussion focuses on component selection, with particular emphasis on picking the correct series elasticity. Experimental results are also given which help to quantify actuator capabilities.

5.4.1 Component Selection

The design space for Series Elastic Actuators is very large. Besides geometry and topology there are six major components: motor, amplifier, transmission, elasticity, sensor, and controller. Of all five components, choosing the spring in the elasticity is the only part of the actuator which requires unique perspective and is discussed in the next section.

The specifications for the motor, amplifier and transmission need to be done based on the force, speed, and power requirements for a given task. These design requirements are not unique to Series Elastic Actuators and would be done for any actuator.

As a helpful aid to the final operation, the motor and transmission should be selected with the idea of keeping friction and motor saturation low. Motor friction b_m which is seen through the transmission with a multiplication of N^2 , is kept at a minimum in the prototype actuator by using a brushless DC motor. The actuator design also reduces drive friction by designing the center of mass, center of friction, and center of stiffness to be colinear along the ball screw axis [64].

Transmission dynamics should also be kept to a minimum as these can be a primary limiting factor in using high feedback gain [16]. We used a frameless motor configuration where the motor



Figure 5-14: EM series elastic actuator used in testing. The actuator uses a brushless DC motor with a direct connection to a 2mm lead ball screw. The ball nut drives the springs in series with the load. The springs are precompressed die compression springs. A linear potentiometer measures the deflection of the springs and uses that signal for feedback to the controller.

magnets are mounted directly onto an extended ballscrew journal instead of using a coupling, a belt drive, or gears.

The other limiting component to achieve high feedback gain is the sensor. The sensor needs to directly measure the spring deflection. This insures that the feedback measurement is a representation of true force. Noise in the sensor is also detrimental to operation.

5.4.2 Choosing Sensor Spring Constant

Selecting the spring constant for the sensor needs to be balanced when trading off the effects of large force bandwidth with low impedance and error rejection. I present some guidelines for choosing a spring constant.

1. Select a motor and transmission based on the force, speed, and power requirements for the given task. This will define the lumped motor mass, damping, and saturation characteristics seen through the reduction.
2. Define an operational bandwidth, ω_o , for which the actuator will need large forces. In other words, define a required large force bandwidth profile (section 5.2.1). This profile is independent of controller and depends solely on ω_n and B . This places a lower bound on k_s . Most likely, the operational bandwidth may be a little greater than but close to the selected natural frequency.
3. Minimizing impedance places an upper bound on k_s . This is a function of the controller values κ and Γ . Insure that the controller gains can be raised to acceptable levels of stiction and impedance reduction.
4. It may be necessary to iterate. The non-dimensional equations will help to guide to know whether to increase or decrease k_s and how much effect it will have.

5.4.3 Actuator Characteristics

A prototype actuator is used to demonstrate and test series elasticity in the electro-mechanical domain. Figure 5-14 shows the prototype actuator used in the experiments and table 5.4.3 shows the physical properties of the actuator. The experimental actuator is used to verify the following.

Parameter	Value	Units
Max Force	1350	N
Cont. Force	750	N
Min Force	4.0	N
Max Speed	0.25	m/s
Max Power	300	W
Cont. Power	150	W
Actuator Mass	1.13	kg
Dynamic Mass m_m	128	kg
Spring Constant k_s	286	kN/m
Damping b_m	2500	Ns/m
ω_o	7.5	Hz
ω_c	30	Hz
ζ	0.2	no units
κ	4	no units
B	0.1	no units

Table 5.1: Physical properties of EM prototype actuator. Some of the values are calculated from motor literature and others are measured.

- Open-loop dynamics
- Saturation
- Controlled bandwidth
- Power density
- Dynamic range

Where appropriate the experimental data is compared with theoretical models.

Open-loop Dynamics

As done previously, the actuator is tested for its open-loop properties. By fixing the load end of the actuator and forcing the mass with motor torque, the actuator exhibits its second order behavior. Figure 5-15 shows the loop gain of the actuator compared with simulated data.

There are three things that this plot demonstrates: natural frequency, damping and open-loop gain.

The natural frequency of the actuator is at 7.5 Hz as calculated from the dynamic mass and spring constant in table 5.4.3. This frequency is ω_o , or the frequency at which large force performance of the actuator begins to drop off. The system is second order as the gain plot drops off at 20 dB/decade and the phase goes to -180° . There are signal filters on the feedback from the sensor. However, they are set high enough that their effects are not noticeable.

The damping term, b_m , in table 5.4.3 was figured experimentally from figure 5-15. The mass-spring resonance is underdamped with $\zeta = 0.2$ [42].

The final item to notice is that the open loop gain is not unity. This deviation from unity is compensated for in the control system gain discussed later.

Saturation

Because of the mass-spring resonance, the actuator is limited in its ability to control large forces. The resonance defines the frequency at which the actuator begins to decrease in large force performance. This constraint is independent of control system.

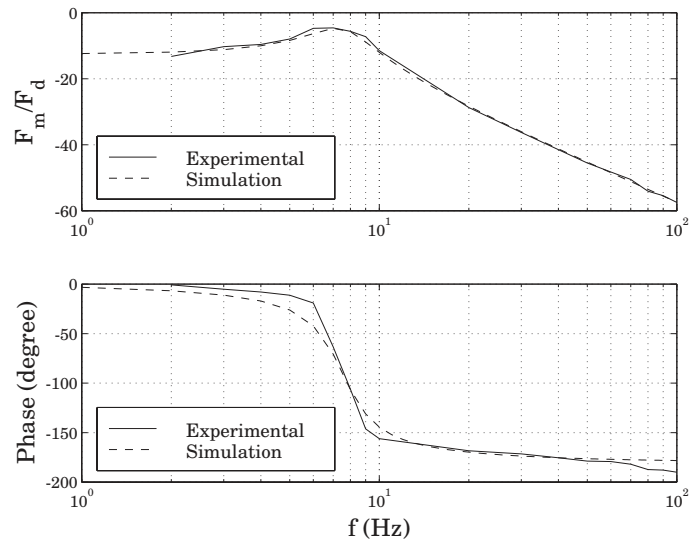


Figure 5-15: **REAL** Open loop bode plot for electro-magnetic series elastic actuator with fixed end condition. This is a simple second order lumped mass spring system with a natural frequency of 7.5 Hz. The dynamic mass is the motor mass as seen through the transmission and the spring is the physical elasticity.

The maximum output force capability of the experimental actuator is 1350 N (300 lbs). In order to test the theory of large force bandwidth, the actuator is commanded to oscillate through the frequency spectrum at an amplitude of 1350 N with the output end of the actuator fixed. Figure 5-16 shows the results of the experiment. As predicted, the large force capability of the actuator is limited. At 8 Hz the performance begins to drop off and follows a second order profile.

It is important to remember that the actuator can still produce some fraction of the maximum output force at high frequency. The controller can command high frequency forces but its peak to peak magnitude will be limited due to saturation.

Bandwidth

It is possible to find the closed-loop bandwidth of the actuator assuming small forces. Experimentally this is found by again fixing the load of the actuator and sweeping the frequency spectrum. Figure 5-17 shows both the experimental and mathematical closed-loop model.

Experimentally, the -3dB point is at 35 Hz. The calculated controlled natural frequency is $\omega_c = 30\text{Hz}$ and the damping was fixed at $\zeta = 0.707$. The derivative term of the controller introduces a zero into the system that represents the apparent resonance in the closed loop system.

Power Density

In order to test the mechanical output power of the actuator, and to prove that the actuator can operate as designed, I suspend myself hanging from the actuator in a chair with 60 lbs in my lap (figure 5-18). This is referred to as the *risky tester*. The total combined load on the actuator is 300 lbs (1350 N).

The desired force in the actuator is set to just balance the gravity pull on the mass load. By oscillating the desired force around the equilibrium point, the actuator moves up when it has greater force and drops when it has less. In this configuration, the actuator can move a load mass with a continuous mechanical power output of 150 W. The peak inertial load power is more than 300 W.

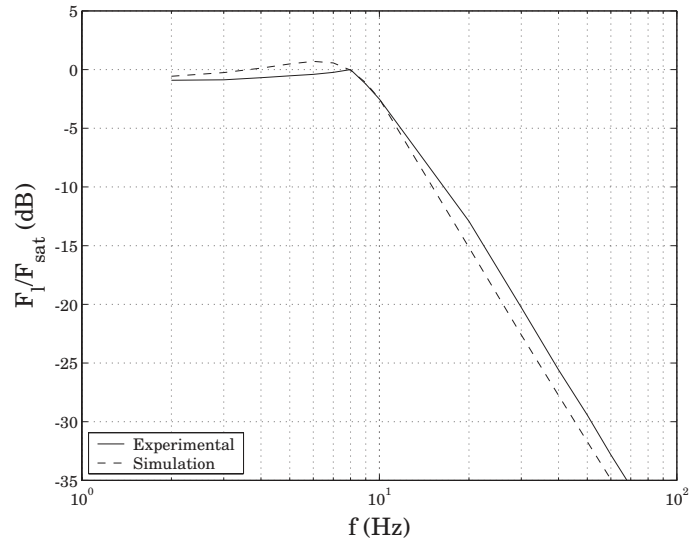


Figure 5-16: **REAL** Experimental maximum force saturation for the electro-magnetic series elastic actuator with fixed end condition. The actuator can only generate the maximum output force up to the ω_o , the mass-spring resonance frequency.

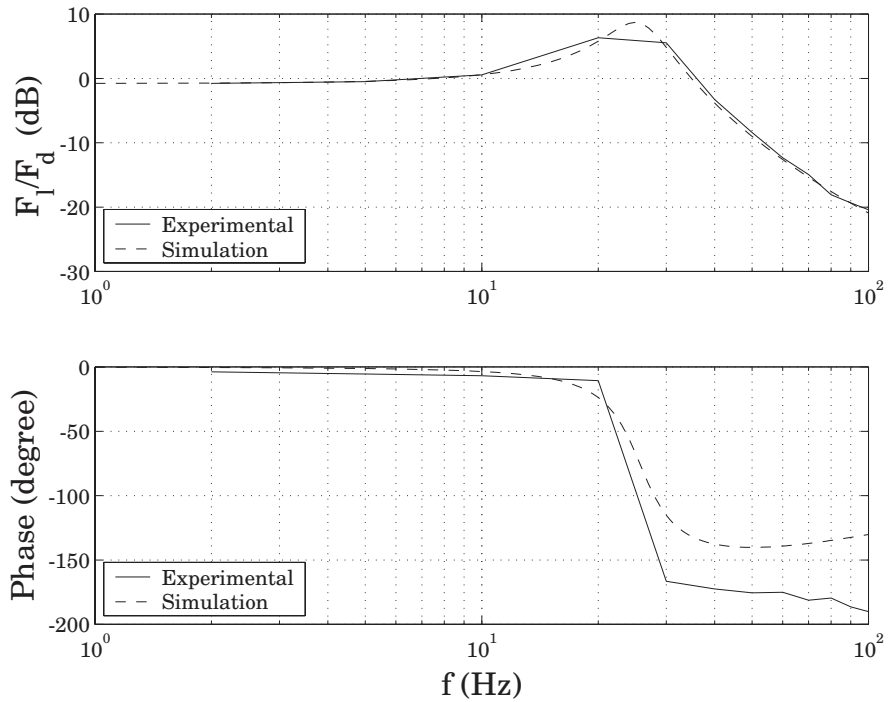


Figure 5-17: **REAL** Experimental closed-loop bandwidth for the electro-magnetic series elastic actuator with fixed end condition. The -3dB point is at 35Hz. The zero in the closed-loop equation causes the apparent resonance.



Figure 5-18: Risky testing. The EM prototype actuator is suspended from the ceiling and loaded with 300 lbs (me, seat and weights). The displacement of the spring is commanded so that it compensates for the gravity pull on the load mass. With small variations in the set point, the actuator moves the load up and down.

An itemized breakdown of the experimental actuator mass is given in table 5.4.3. The power density of this specific actuator is on the order of 300W/kg. This power density is about 3 times that of a direct drive actuator with equivalent force output [27] assuming no forced cooling of the motor coils.

Dynamic Range

The actuator has a large dynamic range despite having a high power density. The minimum resolvable force is 4.0 N and it can output over 1350 N which gives a dynamic range over 300. Considering the actuator has 2mm/rev reduction in the ball screw, the dynamic range is impressive [27]. The limitations on the bottom end of force sensitivity is the noise floor of the sensor and static friction.

The dynamic range of the actuator is demonstrated by fully loading the actuator and setting it in equilibrium with its load. The load is moved up and down with finger force. Figure 5-19 shows the test conditions.

5.5 Case Study Summary

This chapter presented the first case study for series elasticity applied to an electro-magnetic motor in series with a transmission. The chapter looks at both the mathematical model of the actuator as well as a physical prototype. These models are used to discuss bandwidth, impedance, error rejection and saturation bandwidth. Where appropriate experimental results are compared to the mathematical models.

Part	mass (g)	% of total
Motor and Magnet	580	51.3%
Ball Screw and Nut	130	11.5%
Thrust Bearing Block	115	10.2%
Springs (4)	60	5.3%
CFRP Pushrods (2)	26	2.3%
CFRP Rails (2)	26	2.3%
Spring Carriage Clamps (2)	44	3.9%
Motor Mount	44	3.9%
End Clamp	33	2.9%
Pushrod End	25	2.2%
Nut Rider	20	1.8%
Sensor	10	0.9%
Bushings (8)	8	0.7%
Screws and Socket Caps	4	0.4%
Simple Support Bearing	5	0.4%
Total	1130	100%

Table 5.2: Itemized mass distribution for EM series elastic actuator. This actuator is used in two dynamically stable robots described in Chapter 2. The table shows that over 50% of the mass is contained in the motor and magnet. In the design of series elastic actuators, it is important to keep the percentage power producing element mass high in comparison to the overall actuator mass.



Figure 5-19: Fully loaded actuator demonstrating small force sensitivity. The actuator is fully loaded with 300 lbs and has a force equal to gravity pull on the load mass. Finger force of approximately 1 lb can get the actuator to move up and down. This shows that the dynamic range of the actuator is 300:1.

Chapter 6

Conclusions

Many of the key characteristics of series elastic actuators are described and demonstrated in this thesis. Three models are used to explain the actuators. A minimal-complexity mathematical model captures the essence of the actuator's properties. This is followed by two case studies of physical actuators with both mathematical models and physical prototypes. The first is a hydro-elastic actuator consisting of a hydraulic piston and servo valve under PI control. The second is an electro-magnetic motor with a linear transmission under PD control. Each of these models help to explain closed-loop bandwidth, large force bandwidth, output impedance, internal error rejection, impact tolerance and inertial load forces.

Closed-loop bandwidth

The fundamental limits in closed-loop force bandwidth for series elastic actuators are *independent* of the spring stiffness that senses the force. The control system gain and the spring stiffness gain each contribute to the loop gain of the closed-loop system. With a lower spring stiffness, the controller gain can be increased a proportional amount to bring the loop gain to the desired phase and gain stability margins. Series elastic actuators take the gain out of the spring and put it into the control system.

Large force bandwidth

The ability of a series elastic actuator to oscillate at a force equal to the maximum steady state force is limited due to force and velocity saturation of the actuator and low stiffness of the spring. The motor in the actuator must move a significant amount in order to compress the spring and generate the maximum force. While, low forces can still be generated to the full controlled closed-loop bandwidth, the large force bandwidth is limited. Large force bandwidth can be increased by using a less compliant spring. Nevertheless, understanding the tradeoff of large force bandwidth is important in designing and using series elastic actuators.

Output impedance

At low frequencies, the output impedance of a series elastic actuator is very small and increases with increased frequency. In the limit at high frequencies, the output impedance is equal to the stiffness of the physical spring in the actuator. The output impedance is significantly lower than if the actuator used a stiff load cell. The low frequency impedance can be considered as a physically equivalent first or second order system depending on the control system. This means that an equivalent mass or damper, defined by the control system parameters, is effectively in series with the actual spring connected to the actuator load. Overall, the lower the spring stiffness the lower the output impedance. Having a very soft spring, and thus low output impedance, needs to be balanced with the actuators requirements for the large force bandwidth.

Internal error rejection

There are internal non-linearities in any physical actuator that hinder closed-loop force control performance. Closed-loop force control with a compliant sensor reduces the magnitude of these errors. The high gain controller provides for a clean force output.

Impact tolerance

Series elastic actuators can successfully handle shock loading. Because of the spring in the system, the actuator can minimize impact power from the environment and effectively spread an impulse load over time to minimize peak forces. This protects the internal actuator components, the robot structure, and the environment from damage.

Inertial load forces

Series elastic actuator behavior is altered when connected to a finite inertial load moving in free space rather than when in contact with an external environment. This deviation from expected performance is a function of the magnitude of the load inertia and actuator output impedance. As the load mass increases, better actuator performance is realized. In the limit as mass becomes infinite, the actuator behaves exactly as predicted in the closed-loop bandwidth case. Regardless, the dynamics of the actuator are significantly decoupled from that of the load.

6.1 Further Work

There are many topics that deserve further investigation that relate to the understanding and design of series elastic actuators.

6.1.1 Actuator Scaling

This thesis has presented several models of actuators. Each of the models have been generalized by reformulating them with non-dimensionless groups. This gives the models flexibility in understanding how to scale a given actuator system to a different situation.

This thesis does not, however, explain when it is beneficial to use one actuator system over another. For example, at low forces it may be that a simple cable drive mechanism, with no elasticity, has the force and power density required to complete the task. Using simple feed-forward current control on the motor may be sufficient for that case. When the force and power requirements increase to a certain level, a series elastic actuator with an EM motor transmission is required. At very high force and power density levels, a hydro-elastic actuator is appropriate.

The above scenario is only a guess at the appropriate use of different embodiments of series elasticity. It would be helpful if there were force and power density models of these actuator system to aid as *rules of thumb* when the actuators are used robot construction.

6.1.2 Springs

Springs are at the core of the series elastic actuators. This thesis focused attention only on linear springs. However, in order to more fully understand the actuators, the springs themselves need to be investigated. Spring hysteresis, materials, nonlinear stiffening springs, space constraints, geometry and life cycle are all important. I briefly elaborate on the first two.

- **Hysteresis and materials** – Most physical springs have some hysteresis. The die compression springs used in this thesis have very little hysteresis and were assumed to be linear in the control. It is suspected that with increased spring hysteresis, the actuator becomes more difficult to control. For example rubber springs are often used for vibration isolation because

of inherent hysteresis and damping properties. Air springs are often used for high force applications. However, they too have thermodynamic hysteresis properties. Quantifying the effects of hysteresis would be an important step to using new materials and springs in the actuators.

- **Non-linear stiffening springs** – Biological springs (tendons) are stiffening. One theory behind this is that at low forces or during contact tasks the low stiffness helps maintain stability. At much higher forces, low stiffness is unnecessary and may be even undesirable.

Some initial theoretical and experimental work has been done previously in applying non-linear stiffening springs to the actuators in fixed base robots [32, 55, 61]. In this thesis, I show that there is a fundamental trade off between large force bandwidth and impedance when choosing a spring stiffness. Low impedance requires a soft spring whereas a soft spring reduces the large force bandwidth. Using a non-linear stiffening spring may be a bridge between these requirements.

Stable control of series elastic actuators with non-linear springs may be as simple as using a scheduling control gain that is a function of spring deflection. As the spring stiffness increases, the control gain decreases proportionally. This keeps the loop gain of the system constant and within stability margins.

6.1.3 EM velocity mode control

The motor of EM series elastic actuator used in this thesis is current controlled. Under current control, it is easy to analytically demonstrate the large force bandwidth limitations of the actuator. Due to space constraint requirements for the actuator, a tachometer and encoder were eliminated from the design which also forced the move to current control.

It is strongly suspected that if the motor were run with velocity control, that the overall actuator performance could potentially improve. Velocity control would make the closed-loop model more similar to that of the hydro-elastic actuator model by partially masking some of the effects of the motor inertia. The same fundamental limits would apply to the large force bandwidth. However, the small force sensitivity and error rejection would get better.

6.1.4 Control system design

This thesis focused attention on *simplicity* of control system design. P, PI and PD control operating on the force error signal adequately demonstrated the properties of the actuators.

There exist many other more complex control systems that could incrementally enhance series elastic actuator performance. Proper use of state feedback could eliminate the zeros in the closed-loop system. The use of feed-forward could help further eliminate internal errors such as stiction. Adaptive control could be used to better understand actuator load conditions and accommodate for load variations.

The use of these and many other control system possibilities, may help to reach closer to the fundamental closed-loop bandwidth limits of the actuator and improve the decoupling of the actuator dynamics from that of the load. However, if using a linear compliant spring, regardless of the simplicity or complexity of control system, the large force bandwidth is constrained by the open-loop characteristics of the actuator.

6.2 Summary

This thesis investigates the closed-loop force control characteristics of series elastic actuators. A minimal mathematical model and two physical case studies help demonstrate and quantify actuator properties.

The ideas of force control and using compliance in actuation are not new. Chapter 2 presented detailed background material on the general ideas of force control and discusses the capabilities of present-day actuator technology to accomplish good force control. This chapter also introduces the

related work on actuators which use compliance including series elastic actuators. It also describes some of the robots that use previous versions of series elastic actuators and robots that use the actuators designed in this thesis.

The principles of series elastic actuators are quite general. Chapter 3 describes a general model of series elastic actuators with minimum complexity. Using this model, I explain all of the key characteristics of using series elasticity as a compliant load sensor for feedback in closed-loop force control. I discuss the ideas of closed-loop bandwidth in conjunction with large force bandwidth. I explain actuator output impedance, internal error rejection and impact tolerance. Finally, I look at the case of the actuator being connected to an inertial load.

The principles of series elastic actuators discussed in Chapter 3 are applied in Chapter 4 to a case study of a hydraulic piston and servo valve with a series elastic force control system, which is called a hydro-elastic actuator. A theoretical model of the actuator is compared with experimental results.

In a second case study, Chapter 5 applies results of chapter 3 to an electro-magnetic motor with a gear reduction. Again, the theoretical model is compared with experimental results. Both case studies demonstrate good closed-loop bandwidth, low output impedance, shock tolerance and large dynamic range.

This thesis has helped to lay a foundation for understanding, characterizing and designing series elastic actuators in both the hydro-mechanical and electro-mechanical power domains. It shows that actuators under closed-loop force control using a compliant sensor can achieve good force bandwidth and have low output impedance. The actuators show great promise in advancing the state-of-the-art of real world robotics.

Bibliography

- [1] Farhad Aghili, Martin buehler, and John M. Hollerbach. Sensing the torque in a robot's joints. *Mechanical Engineering*, pages 66–69, Sept. 1998.
- [2] M. L. Aisen, H. I. Krebs, N. Hogan, F. McDowell, and B. T. Volpe. The effect of robot-assisted therapy and rehabilitative training on motor recovery following stroke. *Archives of Neurology*, 54:443–6, 1997.
- [3] R. McNeill Alexander. *Elastic Mechanisms in Animal Movement*. Cambridge University Press, 1988.
- [4] Andrew Alleyne. Nonlinear force control of an electro-hydraulic actuator. *Japan/USA Symposium on Flexible Automation*, 1:193–200, 1996.
- [5] H. Asada and J.J. Slotine. *Robot Analysis and Control*. John Wiley and Sons, New York, 1985.
- [6] H. Asada and K. Youcef-Toumi. *Direct Drive Robots: Theory and Practice*. MIT Press, Cambridge, 1987.
- [7] Haruhiko Asada. Manufacturing robotics: Basic issues and challenges. *IFAC*, pages 319–330, 1996. San Francisco, CA.
- [8] David Scott Barrett. *Propulsive efficiency of a flexible hull underwater vehicle*. PhD thesis, Massachusetts Institute of Technology, May 1996. Ocean Engineering.
- [9] B. E. Berlinger. Evoloid – a new concept in high ratio gearing. *AGMA Paper*, 5(109.37), Oct. 1975.
- [10] David Brock and Woojin Lee. Dynamic model of a linear actuator based on polymer hydrogel. *Journal of Intelligent Material Systems & Structures*, 5(6):764–771, Nov. 1994.
- [11] Rodney A. Brooks, Cynthia Breazeal, Matthew Marjanovic, Brian Scassellati, and Matthew Williamson. *The Cog Project: Building a Humanoid Robot*. Springer-Verlag, 1999. To appear in a Springer-Verlag Lecture Notes in Computer Science Volume.
- [12] F. Conrad and C. Jensen. Design of hydraulic force control systems with state estimate feedback. *IFAC*, pages 307–312, 1987. Munich, Germany.
- [13] John J. Craig. *Introduction to Robotics: Mechanics and Control*. Addison-Wesley, 1989.
- [14] Samuel Hunt Drake. *Using compliance in lieu of sensory feedback for automatic assembly*. PhD thesis, Massachusetts Institute of Technology, 1978. Mechanical Engineering.
- [15] S.D. Eppinger and W.P. Seering. Understanding bandwidth limitations in robot force control. *IEEE International Conference on Robotics and Automation*, 2:904–909, 1987. Raleigh, NC.
- [16] Steven D. Eppinger. *Modeling Robot Dynamic Performance for Endpoint Force Control*. PhD thesis, Massachusetts Institute of Technology, 1998. Mechanical Engineering.

- [17] Masato Hirose et. al. Legged mobile robot and a system for controlling the same. *United States Patent*, (#5,455497). Issued October 3, 1995.
- [18] James M. Gere and Stephen P. Timoshenko. *Mechanics of Materials*. PWS-KENT Publishing Company, Boston, MA., 1990.
- [19] Layton C. Hale and Alexander H. Slocum. Design of anti-backlash transmissions for precision position control systems. *Precision Engineering*, 16(4):244–258, 1994.
- [20] David Halliday and Robert Resnick. *Fundamentals of Physics*. John Wiley & Sons, New York, 1988.
- [21] H. Hanafusa and H. Asada. A robotic hand with elastic fingers and its application to assembly process. *IFAC Symposium on Information and Control Problems in manufacturing Technology*, pages 127–138, 1977. Tokyo.
- [22] Blake Hannaford and Jack Winters. Actuator properties and movement control: Biological and technological models. In Winters and Woo, editors, *Multiple Muscle Systmes: Biomechanics and Movement Organization*, pages 101–120. Springer-Verlag, 1990.
- [23] B. Heinrichs, N. Sepehri, and A.B. Thornton-Trump. Position-based impedance control of an industrial hydraulic manipulator. *IEEE Control Systems Magazine*, 17(1):46–52, 1997.
- [24] Kazuo Hirai, Masato Hirose, Yuji Haikawa, and Toru Takenaka. The development of honda humanoid robot. *International Conference on Robotics and Automation*, 1998.
- [25] Jessica K. Hodgins and Marc H. Raibert. Biped gymnastics. *International Journal of Robotics Research*, September 13 1989.
- [26] N. Hogan. Impedance control: An approach to manipulation: Part i - theory, part ii - implementation, part iii - applications. *J. of Dynamic Systems, Measurement and Control*, 107:1–24, 1985.
- [27] John Hollerbach, Ian Hunter, and John Ballantyne. A comparative analysis of actuator technologies for robotics. In *Robotics Review 2*, pages 299–342. MIT Press, 1991.
- [28] Won Hong. Robotic catching and manipulation using active vision. Master’s thesis, Massachusetts Institute of Technology, September 1995. Mechanical Engineering.
- [29] Russel D. Howard. *Joint and Actuator Design for Enhanced Stability in Robotic Force Control*. PhD thesis, Massachusetts Institute of Technology, September 1990.
- [30] S.C. Jacobsen, C.C. Smith, D.K. Backman, and E.K. Iversen. High performance, high dexterity, force reflective teleoperator i. *ANS topical meeting on robotics and remote systems*, 2:180–185, 1990. Washington, DC, November.
- [31] S.C. Jacobsen, C.C. Smith, K.B. Biggers, and E.K. Iverson. Behavior based design of robot effectors. *Proc. of the Fourth Int’l Symp. on robotics research*, pages 41–55, 1989.
- [32] Arrin Katz. The design and applicaiton of a nonlinear series compliance actuator for use in robotic arms. Master’s thesis, Massachusetts Institute of Technology, September 1999. Mechanical Engineering.
- [33] Glenn K. Klute, Joseph M. Czerniecki, and Blake Hannaford. Mckibben artificial muscles: Pneumatic actuators with biomechanical intelligence. *IEEE/ASME Conference on Advanced Intelligent Mechatronics*, Sept. 19-22, 1999. Atlanta, GA.
- [34] Benjamin T. Krupp. Design and control of a planar robot to study quadrupedal locomotion. Master’s thesis, Massachusetts Institute of Technology, 2000. Mechanical Engineering.

- [35] Akhil J. Madhani. *Design of teleoperated surgical instruments for minimally invasive surgery*. PhD thesis, Massachusetts Institute of Technology, 1998. Mechanical Engineering.
- [36] Matthew Mason. Compliant motion. In *Robot Motion: Planning and Control*, pages 305–322. MIT Press, 1982.
- [37] Matthew Mason. Compliance and force control for computer controlled manipulators. *IEEE Transactions on Systems, Man, and Cybernetics*, SMC-11(6):419–426, June 1981.
- [38] Thomas H. Massie. Design of a three degree of freedom force-reflecting haptic interface. 1993. Undergraduate Thesis, Massachusetts Institute of Technology.
- [39] John Bryant Morrell. *Parallel coupled micro-macro actuators*. PhD thesis, Massachusetts Institute of Technology, 1996. Mechanical Engineering.
- [40] Charles J. Murray. All-in-one hydraulics. *Design News*, pages 84–89, Nov. 15, 1999.
- [41] Gunter Niemeyer. *Using Wave Variables in Time Delayed Force Reflecting Teleoperation*. PhD thesis, Massachusetts Institute of Technology, 1996. Aeronautics and Astronautics.
- [42] Katsuhiko Ogata. *Modern Control Engineering*. Prentice Hall, 1990.
- [43] Henry M. Paynter. *Analysis and Design of Engineering Systems*. MIT Press, Cambridge, MA, 1960.
- [44] M. Pelletier and M. Doyon. On the implementation and performance on impedance control on position controlled robots. *IEEE Conference on Robotics and Automation*, pages 1228–1233, 1994. Atlanta, GA.
- [45] Ron Pelrine, Roy Kornbluh, Qibing Pei, and Jose Joseph. High-speed electrically actuated elastomers with strain greater than 100%. *Science*, 287:836–839, 4 February 2000.
- [46] Gill A. Pratt and Matthew M. Williamson. Series elastic actuators. *IEEE International Conference on Intelligent Robots and Systems*, 1:399–406, 1995.
- [47] Jerry Pratt. Virtual model control of a biped walking robot. Master’s thesis, Massachusetts Institute of Technology, May 1995. Electrical Engineering and Computer Science.
- [48] Jerry Pratt and Gill Pratt. Intuitive control of a planar bipedal walking robot. *ICRA*, 1998.
- [49] Jerry Pratt, Ann Torres, Peter Dilworth, and Gill Pratt. Virtual actuator control. *IROS*, 1996. Osaka, Japan, Nov. 3-9.
- [50] Jerry E. Pratt. *Exploiting Inherent Robustness and Natural Dynamics in the Control of Bipedal Walking Robots*. PhD thesis, Massachusetts Institute of Technology, June 2000. Electrical Engineering and Computer Science.
- [51] M. H. Raibert and J. J. Craig. Hybrid position/force control of manipulators. *Journal of Dynamic Systems, Measurement, and Control*, 102, 1981.
- [52] Marc. H. Raibert. *Legged Robots That Balance*. MIT Press, Cambridge, MA., 1986.
- [53] David W. Robinson and Gill A. Pratt. Force controllable hydro-elastic actuator. *IEEE International Conference on Robotics and Automation*, April 24-28, 2000. San Francisco, CA.
- [54] David W. Robinson, Jerry E. Pratt, Daniel J. Paluska, and Gill A. Pratt. Series elastic actuator development for a biomimetic walking robot. *IEEE/ASME AIM99*, Sept 20-23, 1999. Atlanta, GA.
- [55] J. Kenneth Salisbury. *Kinematic and force Analysis of Articulated hands*. PhD thesis, Stanford University, May 1982. Department of Mechanical Engineering.

- [56] J. Kenneth Salisbury. Making graphics physically tangible. *Communications of the ACM*, 42(8):75–81, August 1999.
- [57] J. Kenneth Salisbury. The heart of microsurgery. *Mechanical Engineering*, pages 46–51, Dec. 1998.
- [58] J. Kenneth Salisbury and Mandayam A. Srinivasan. *Proceedings of The First PHANToM User’s Group Workshop*. MIT AI Laboratory, 1996.
- [59] J.K. Salisbury, W.T. Townsend, B.S. Eberman, and D.M. DiPietro. Preliminary design of a whole-arm manipulation system (wam). *Proceedings 1988 IEEE International Conference on Robotics and Automation*, 1988. Philadelphia, PA, April 1988.
- [60] K. Salisbury. Active stiffness control of a manipulator in cartesian coordinates. *19th IEEE Conference on Decision and Control*, pages 83–88, Dec. 1980.
- [61] Vinay K. Shah. Design and control of a nonlinearly compliant robotic finger. Master’s thesis, Massachusetts Institute of Technology, September 1997. Mechanical Engineering.
- [62] Thomas B. Sheridan. Telerobotics. *Automatica*, 9(5):487–507, 1989.
- [63] Thomas B. Sheridan. *Telerobotics, Automation, and Human Supervisory Control*. MIT Press, Cambridge, MA, 1992.
- [64] Alexander H. Slocum. *Precision machine design*. Society of Manufacturing Engineers, 1992.
- [65] Jean-Jacques E. Slotine and Weiping Li. *Applied Nonlinear Control*. Prentice-Hall, Cambridge, MA., 1991.
- [66] C.C. Smith, S.C. Jacobsen, L.A. Robins, D.W. Wilcox, and S.J. Bohn. Design and control of electromechanical actuation systems. *ASME DSC Modelling and Control of Compliant and Rigid Motion Systems Winter Annual Meeting*, pages 137–144, 1991. Dec 1-6.
- [67] Mark W. Spong and M. Vidyasagar. *Robot Analysis and Control*. John Wiley & Sons, 1989.
- [68] S. Sugano, S. Tsuto, and I. Kato. Force control of the robot finger joint equipped with mechanical compliance adjuster. *International Conference on Intelligent Robots and Systems*, pages 2005–2012, 1992.
- [69] Thomas Sugar and Vijay Kumar. Design and control of a compliant parallel manipulator for a mobile platform. *ASME Design Engineering Technical Conference*, September 13-16, 1998. Atlanta, GA.
- [70] W.T. Townsend and J.K. Salisbury. Mechanical bandwidth as a guideline to high-performance manipulator design. *IEEE International Conference on Robotics and Automation*, pages 1390–1395, 1989. Scottsdale, AZ.
- [71] M.S. Triantafyllou and G.S. Triantafyllou. An efficient swimming machine. *Scientific American*, 272(3):64–70, March 1995.
- [72] Dieter Vischer and Oussama Khatib. Design and development of high-performance torque-controlled joints. *IEEE Transactions on Robotics and Automation*, 11(4):537–544, 1995.
- [73] D.L. Wells, E.K. Iversen, C.C. Davis, and S.C. Jacobsen. An investigation of hydraulic actuator performance trade-offs using a generic model. *IEEE International Conference on Robotics and Automation*, pages 2168–2173, 1990. May 13-18.
- [74] Daniel E. Whitney. Historical perspective and state of the art in robot force control. *International Journal of Robotics Research*, 6(1), 1987.

- [75] Matthew M. Williamson. Series elastic actuators. Master's thesis, Massachusetts Institute of Technology, June 1995.
- [76] Matthew M. Williamson. *Robot Arm Control Exploiting Natural Dynamics*. PhD thesis, Massachusetts Institute of Technology, June 1999.